Non-isothermal falling film flows with variable viscosity: Stability and non-uniform steady states

a thesis presented for the degree of

Doctor of Philosophy of Imperial College London

and the

Diploma of Imperial College

by

Nikolaos Fyssas

Department of Mathematics

Imperial College

180 Queen's Gate, London SW7 2BZ

October 2019

I certify that this thesis, and the research to which it refers, are the product of my own work, and that any ideas or quotations from the work of other people, published or otherwise, are fully acknowledged in accordance with the standard referencing practices of the discipline.

Signed: _____

Copyright

The copyright of this thesis rests with the author. Unless otherwise indicated, its contents are licensed under a Creative Commons Attribution-Non Commercial-No Derivatives 4.0 International Licence (CC BY-NC-ND).

Under this licence, you may copy and redistribute the material in any medium or format on the condition that; you credit the author, do not use it for commercial purposes and do not distribute modified versions of the work.

When reusing or sharing this work, ensure you make the licence terms clear to others by naming the licence and linking to the licence text.

Please seek permission from the copyright holder for uses of this work that are not included in this licence or permitted under UK Copyright Law.

Abstract

This thesis presents analysis and computations of non-isothermal falling films flowing down an inclined, heated plane. We consider two types of wall heating: uniform and non-uniform. We examine the heat transfer of a viscoelastic liquid film with variable viscosity as it flows over a uniformly heated plane. The polymeric viscosity is modeled using the Oldroyd-B model, and, as the solvent viscosity, is temperature-dependent. The determination of the flow involves the numerical solution of the energy equation and Navier-Stokes. We continue with problems regarding Newtonian fluids and non-uniform heating. The flow and heat transport is modeled with a long-wave theory for small Brinkman numbers, and it leads to reduced systems of ODEs. Analytic solutions of the velocity, temperature, and shape of the surface for the basic flow and the next order are obtained. We carry out extensive numerical experiments and reveal the contribution of each parameter in the velocity and temperature profile, as well as in the deformation of the surface, for various heating conditions. We continue with numerical analysis of non-uniformly weak heated falling film for zero Brinkman number as well as for arbitrary values of it.

The linear stability of a non-isothermal falling film with temperature-dependent viscosity over a uniformly heated, inclined plane is studied. We derive the system of equations: the non-isothermal analogue of the Orr -Sommerfeld equation coupled with the energy equation. We solve analytically the above system for small wavenumber and numerically for arbitrary values. Finally, we verify the model using isothermal and non-isothermal comparisons.

To my family

Acknowledgments

I would like to express my appreciation to my supervisor, professor Demetrious T. Papageorgiou; his expert guidance and support helped me complete this thesis. I gratefully acknowledge the financial support of a Roth Ph.D. scholarship by the Department of Mathematics, Imperial College London.

Also, I would like to thank my colleagues for providing much needed distractions and encouragement, and for making me feel like I was at home. Especially, I want to thank Raquel, Ruben, Fran, Csabi, Max, Emma, Calum, Jordan, and Paul for being my drinking buddies. I want to thank dr Shahid Mughal for his goodwill to help me.

Special thanks go to professors Jonathan Mestel and Jean-Marc Vanden-Broeck for their proof-reading and assistance in guiding the shape of this thesis into an examinable form.

Contents

1 Structure of Thesis **16**

2 Introduction **18**

3 Literature Review **21**

3.1 Falling Films 21

3.2 Viscoelastic Fluid 24

3.2.1 Newtonian Fluid 24

3.2.2 Mechanical Analogies 25

3.2.3 Derivation of Oldroyd-B 27

4 Oldroyd B Model Equations And Non-Isothermal Falling Films **32**

4.0.1 Cartesian Coordinates 33

4.1 Laminar Falling Film 38

4.1.1 Non Dimensionalization 39

5 Non-isothermal Falling Films **44**

5.1 Problem Formulation 44

5.2 Governing Equations 47

5.3 Boundary Conditions 48

5.4 Non-dimensionalization 50

5.4.1 Governing Equations 50
5.4.2 Boundary Conditions 51
5.5 Non-uniformly Heated Falling Film - Long Wave Asymptotic Analysis 53
5.6 Dimensionless surface tension and deformation of the surface . 59
5.7 Numerical Experiments 60
5.8 Weakly Heated Falling Films - Zero Brinkman Number 76
5.9 Numerical Experiments 79

6 Weakly Heated Falling Films - Arbitrary Brinkman Number 95
6.1 Numerical Experiments 99

7 Stability of Falling Film 104
7.1 Introduction 104
7.1.1 Governing Equations 104
7.1.2 Non-dimensionalization 106
7.1.3 Boundary Conditions 107
7.2 Small Amplitude Perturbations And Normal Modes 108
7.3 Long Wave Analysis 112
7.4 Validation Of Model 118
7.5 Arbitrary Wavenumber - Numerical Analysis 120
7.6 Numerical Experiment 122
7.7 Verification of the numerical Methods 124

8 Conclusions 127

9 Future Work 130

Appendix A Appendix **136**

A.1 Introduction 136

A.2 Falling Film 137

A.2.1 Non-dimensionalization 141

A.2.2 Non-uniformly heated Plane - Long wave Analysis . . . 143

A.2.3 Non-uniformly heated plane - Weakly Heating 148

List of Figures

3.1 Representation of Maxwell's Model. 25

3.2 Kelvin-Voigt Element 25

4.1 Schematic Representation of flow down an inclined channel . . 38

4.2 Temperature profile, where:$\beta = 0$ and $\lambda = 0.75$. 42

4.3 Temperature profile, where:$\beta = 0$ and λ ranges. 42

4.4 Temperature over film thickness, where $\beta = 0.7$ and different values of Brinkman number. 43

4.5 Temperature over film thickness, where $\beta = 1$ and different values of Brinkman number. 43

4.6 Temperature over film thickness, where $\beta = 2$ and 3, and $\lambda = 0.75$. 43

5.1 $T_1(X, 0)$, where $\lambda, \beta, \Gamma = 1$. 60

5.2 Isothermal lines of T_1. The dimensionless group is the same as in Fig. 5.1. 61

5.3 u_1 streamlines. The dimensionless group is the same as in Fig. 5.1. 61

5.4 $\Theta_1(0, y)$ regarding different values of Brinkman number. The remaining dimensionless groups are the same as in Fig. 5.1. . . 62

5.5 $u_1(0, y)$ regarding different values of Brinkman number. The remaining dimensionless groups are the same as in Fig. 5.1. . . 63

5.6 Stationary Waves for the free surface regarding different values of exponential constant β. The remaining dimensionless group is the same as in Fig. 5.1. 64

5.7 $\Theta_1(0, y)$ regarding different values of exponential constant β. The remaining dimensionless group is the same as in Fig. 5.1. 64

5.8 $u_1(0, y)$ regarding different values of exponential constant β. The remaining dimensionless group is the same as in Fig. 5.1. 65

5.9 $h_1(X)$ regarding different values of dimensionless surface tension Γ. The remaining dimensionless group is the same as in Fig. 5.1. 66

5.10 $\Theta_1(0, y)$ dimensionless surface tension Γ. The remaining dimensionless group is the same as in Fig. 5.1. 67

5.11 $u_1(0, y)$ dimensionless surface tension Γ. The remaining dimensionless group is the same as in Fig. 5.1. 67

5.12 $T_1(X, 0)$, where $\lambda, \beta, \Gamma = 1$. 68

5.13 Isothermal lines of T1. The dimensionless group is the same as in Fig.5.12. 69

5.14 u_1 Streamlines. The dimensionless group is the same as in Fig.5.12. 69

5.15 $\Theta_1(0, y)$ regarding different values of Brinkman number. The remaining dimensionless groups are the same as in Fig. 5.12. . 70

5.16 u1(0,y) regarding different values of Brinkman number. The remaining dimensionless groups are the same as in Fig. 5.12. . 71

5.17 Stationary waves for the free surface regarding different values of exponential constant β. The remaining dimensionless group is the same as in Fig. 5.12. 72

5.18 $\Theta_1(0, y)$ regarding different values of exponential constant β. The remaining dimensionless group is the same as in Fig. 5.12. 72

5.19 $u_1(0, y)$ regarding different values of exponential constant β. The remaining dimensionless group is the same as in Fig. 5.12. 73

5.20 $h_1(X)$ regarding different values of dimensionless surface tension Γ. The remaining dimensionless group is the same as in Fig. 5.12. 74

5.21 $\Theta_1(0, y)$ dimensionless surface tension Γ. The remaining dimensionless group is the same as in Fig. 5.12. 74

5.22 $u_1(0, y)$ regarding dimensionless surface tension Γ. The remaining dimensionless group is the same as in Fig. 5.12. . . . 75

5.23 2D schematic representation of the heating boundary conditions and computational domain 82

5.24 Base flow velocity and temperature profile 88

5.25 Deformation of the film surface, $R = 1$, $\Gamma = 10$, $b = 0.2$, $\xi = 0.7$, $\theta = 30^o$. 89

5.26 Streamfunction, Velocity and Temperature Profile, $R = 1$, $\Gamma = 10$, $b = 0.2$,$\xi = 0.7$, $\Theta = 30^o$. 89

5.27 Deformation of the film surface regarding different β, where $R = 1$, $\Gamma = 10$, $\xi = 0.7$, $\theta = 30^o$. 90

5.28 Base flow velocity, $O(\epsilon)$ velocity and temperature regarding different β, where $R = 1$, $\Gamma = 10$, $\xi = 0.7$, $\theta = 30^o$. The maximum velocity increases with an increase of β since the viscosity decreases; while at the peak of the deformation there is an increase in the velocity after $y = 0.7$ due to the increase in the film thickness. 91

5.29 Deformation of the film surface regarding different Γ, where $R = 1$, $\xi = 0.7$, $\theta = 30^o$. A decrease of 33% of the dimensionless surface tension refers to an almost double altitude of the surface deformation. 92

5.30 $O(\epsilon)$ velocity and temperature regarding different Γ, where $R = 1$, $\beta = 0.2$, $\xi = 0.7$, $\theta = 30^o$. 92

5.31 $O(\epsilon)$ velocity and temperature regarding different Γ, where $R = 1$, $\beta = 0.2$, $\xi = 0.7$, $\theta = 30^o$. An increase of Grashof results on stronger convention in the fluid. This leads to a rapidly heat transfer along the fluid and hence the lower temperature of the fluid, and increases the velocity profile near the plate but as the distance from the plate increase the velocity profile decreases. 93

5.32 Surface deformation, Temperature and Velocity profile at $x = 0$ and $x = 0.5263$ (peak point). The changes are hardly noticeable. 94

6.1 Base flow velocity and temperature where $\beta = 0.2$, $\Gamma = 10$, $\lambda = 5$, $\xi = 0.7$ and $\theta = 30^o$. 100

6.2 Comparison on Base Velocity and Temperature profiles regarding different Brinkman numbers where $\beta = 0.2$, $\Gamma = 10$, $\xi = 0.7$ and $\theta = 30^o$. An increase on Brinkman number leads to a higher temperature on the fluids, hence lower viscosity and a faster base flow. 100

6.3 Deformation of the film surface regarding different λ, where $R = 1$, $\Gamma = 10$, $\xi = 0.7$, $\theta = 30^o$. The increase in λ increases the velocity and temperature that leads to higher surface deformation and shifts the peak point of the curve towards left. . 101

6.4 Comparison on Velocity, Temperature and Viscosity profiles regarding different β where $\lambda = 5$, $\Gamma = 10$, $\xi = 0.7$ and $\theta = 30^o$. 102

6.5 Deformation of the film surface regarding different Γ, where $R = 1$, $\lambda = 5$, $\xi = 0.7$, $\theta = 30^o$. The decrease in Γ leads to an increase in surface deformation and in the altitude of the oscillations before the heating in comparison with the wavelength which decreases. The Brinkman number magnitude the shift on the right of the surface deformation that the increase in Γ occurs. 103

7.1 The amplification rate increases with the increase in β and ξ, where R=3, and $\theta = 45^o$. The flow is unstable since the critical Reynolds is $R_c = 2.5$ 118

7.2 Growth rate over wavenumber regarding different values of β, where: $\beta = 0.5$, $\xi = 1$, $R = 5$, and $\theta = 45^o$. The dimensionless viscosity parameter β increases the growth rate rapidly. 122

7.3 Growth rate over wavenumber regarding different Reynolds numbers, where: $\beta = 0.5$, $\xi = 1$, $R = 5$, and $\theta = 45^o$. When R increases, the growth rate increases substantially. 123

7.4 Growth rate over wavenumber regarding different values of the dimensioless surface tension, where: $\beta = 0.5$, $\xi = 1$, $R = 5$, and $\theta = 45^o$. The increase in Γ decreases the growth rate. . . . 123

7.5 Comparison between long wave exact solutions and the non-isothermal plots, where: $\beta = 0.01$,$\xi = 1$, $\Gamma = 0.1$, and $\theta = 45^o$. For small values of wavenumber, the analytical and numerical solutions match. 124

7.6 Comparison between isothermal and non-isothermal flow where: $\beta = 0.01$, $\xi = 1$ and $\Gamma = 0.1$. The uniform heating creates a slightly higher growth rate. 125

7.7 Comparison of long wave exact solutions with the non-isothermal plots regarding different value of Grashof number, where: $\beta = 0.01$, $R = 5$, $\Gamma = 0.1$, and $\theta = 45^o$. The numerical solutions match the analytical for small wavenumbers. Increasing β we notice a rapidly increase in the growth rate. 125

7.8 Comparison of long wave exact solutions with the non-isothermal plots regarding different value of Grashof number, where: $\beta = 0.01$, $R = 5$, $\Gamma = 0.1$, and $\theta = 45^o$. The numerical solutions match the analytical for small wavenumbers. An increase in Grashof increase the growth rate which is very noticeable especially in the exact solutions. 126

1

Structure of Thesis

We shall briefly present the structure of the thesis. We started with the introduction of the problem, the motivation for the study, and the gap in the literature that made us researching it. We overviewed the literature, starting with isothermal falling films, proceeding to non-isothermal falling films, and finally to temperature-dependent viscosity flows. Lastly, we presented the derivation of the Oldroyd-B model that we chose to describe the viscoelastic behaviour of the fluid. In chapter 4, we began with the dimension equations and corresponding boundary conditions of an Oldroyd-B viscoelastic fluid, with variable viscosity, flows over a uniformly heated incline plane. We non-dimensionalized equations and conditions and solved numerically the problem. In the next chapter of this dissertation, we turned our attention to steady-states, non-uniformly heated Newtotonian falling films with variable viscosity. We presented the equations of energy and momentum that dictate the system with the corresponding boundary conditions and non-dimensionalized them. We derived the analytical expressions for the long-wave falling film and evaluated the contribution of each parameter (Reynolds and Brinkman number, viscosity parameter, and dimensionless surface tension) to the surface deformation and performed numerical exper-

iments for various heating conditions. In the final section of this chapter, we examined weakly heated falling films with zero Brinkman number. We analyzed in-depth the custom made finite-difference based code, we specifically designed in Matlab®, for the given problem, and performed numerous numerical experiments. In what follows in chapter 6, we extended the work of the previous section and investigated further weakly heated falling films, where the Brinkman number is $O(1)$. We designed again, a finite-difference code and numerically solved the energy and Navier-Stokes equations and performed several numerical experiments revealing the relations between velocity and temperature profiles, surface deformation with the parameters (Reynolds, Brinkman and Grashof numbers, viscosity parameter and dimensionless surface tension). The research shown in the following chapter 7 focuses on the linear stability of non-isothermal falling films with variable viscosity. We non-dimensionalized the energy and Navier-Stokes equations with the corresponding boundary conditions. We derived analytical expressions for the growth rates of disturbances for small wavenumbers by solving the non-isothermal analogue of the Orr-Sommerfeld and energy equations. We validated the model by extracting and comparing the results with the ones of the isothermal problem. We continued with arbitrary wavenumbers and conducted various numerical experiments, following a global approach. We determined the eigenvalues and growth rates. Finally, we finished that chapter with the verification of the numerical method comparing the numerical results with the analytical expressions found in section 7.3 for small wavenumbers. In what follows, chapter 8 showed the conclusions of the thesis. In the final chapter 9 of the thesis, we presented topics and set directions for future work. Finally, we included appendix A where we showed an attempt for mathematical describe and establish the governing equations and boundary conditions for steady-states non-uniformly heated viscoelastic falling films with temperature-depended viscosity (section A.2.2), and weakly heated viscoelastic falling films with temperature-depended viscosity, section A.2.3.

2

Introduction

The study of heat transfer on falling films possesses an important part of fluid dynamics. It has been studied extensively, theoretically and experimentally, due to its engineering and industrial applications, like in tribology -gears lubrication [Dowson and Higginson (1966); Borsoff (1959)], cooling engines and reactors [Khani et al. (2011)], flow and fixed bed reactors design [Tarhan (1983)], glass production, gluing labels on hot bodies [Shortland (2009)], spinning coating [Lawrence (1988)]. The majority of chemical processes, such as in drug manufacturing, contains one or more steps in which a fluid flows over an inclined plate exchanging heat. The flow of a cooler fluid over a hot body increases the temperature of a thin layer of the fluid, which is known as the thermal boundary layer. In this layer, fundamental parameters change, such as viscosity [Makinde (2006)]. These changes have to be taken into consideration during computational modeling, process engineering, and industrial line-production designing. Flow reactor processing is a very complex task especially from the viewpoint of applied mathematics. Despite the importance of viscosity variation on heat transfer, information for linking this to the temperature profile and its effect on surface wave instabilities is still lacking. Our work has been motivated by such a challenge.

Furthermore, process engineering remains at the forefront of modern research. A primary goal is to design new reactors or optimize existing ones. Flow reactors have been in use for several decades now, in applications across all scales with numerous variations, from large scale fabrications to extremely highly exothermic reactions, to miniature laboratories inside medical tools. An example of a flow reactor is the microreactor (MR), a device in which chemical reactions take place in microchannels. The MR is usually a continuous reactor demands specific conditions, depending on the type and speed of the reactions. In a reversible reaction, reactants and products are never fully consumed. They are each constantly reacting and being produced. The reaction will reach an equilibrium point where the concentrations of the reactants and products will no longer change. Applying specific conditions of temperature and pressure, are possible to change the equilibrium point in favour of the products, increasing that way the reaction yield. Enthalpy of reaction may affect the temperature of the fluid significantly and decrease the reaction yield or rate. Knowing how the fluid reacts to those changes, allow us to adjust temperature and pressure or even the mixture distribution simulating a multi-layer flow increasing the speed and efficiency of MR reactors.

Another commonly used type of flow reactor is the coated-wall reactor (CWR). It is a device in which the catalyst is located in a layer attached to the wall. The fluid flows along this wall in which the required reactions are allowed to take place. More recently, the number of applications of coated walls reactors is increasing rapidly, i.e. in the applications of monolith reactors, in which each channel is a CWR, and also a microchannel reactor. The CWR allows much faster heat exchange with the wall than the fixed-bed reactor because of the intimate contact of the catalyst with the wall. The heat-transfer from the catalyst to the reactor wall increases, and fewer heat transfers to the fluid, achieving "near-isothermal" conditions. No much research has been done in that matter and the study of weakly non-uniformly heated falling films may be able to fill the gap. Our thesis is motivated by such a challenge. Finally, transferring fluids through channels, such as petroleum, and spinning coating are other reasons that motivated us to research the stability of

non-isothermal falling films. In many cases, a flat surface is needed. Surface distributions can occur from the properties of the fluid, i.e. low surface tension, or reasons regarding the structure, i.e. small bump on the surface wall. By changing the temperature on the wall is possible to compensate or even cancel any surface distributions.

3

Literature Review

3.1 Falling Films

Falling films are extensively applied in heat and mass transfer processes of industrial equipment, such as vertical condensers, film evaporators, absorption tower, engine coolers, and flow reactors [Zhang et al. (2008); Makinde (2006)]. The mechanism of falling liquid film is closely related to energy efficiency, so there have been many attempts to examine this flow, theoretically and experimentally [Jones and Whitaker (1966); Karapantsios et al. (1989)]. Benjamin (1957) and Yih (1963) studied the stability of isothermal films, using linear stability analysis. Yin extended Benjamin's work by investigating the stability of a liquid layer flowing down an inclined plane not only for small wavenumbers but also for small Reynolds numbers and large wavenumbers. In any case, the vertical uniform film is always unstable. The flat film on an inclined plate is unstable to long-wave disturbances for Reynolds numbers (with $Re = \frac{uL}{\nu}$ where u is the velocity, L the characteristic linear dimension and ν the kinematic viscosity) greater than $R_c = \frac{5}{2}\cot\theta$, where θ is the angle of inclination with the horizontal. Benney (1966) studied the nonlinear behavior of film flows. He applied the lubrication approxi-

mation to the Navier–Stokes equations and suggested a nonlinear evolution equation for two-dimensional flows, which is much simpler than the full dynamic equations. Pumir et al. (1983), predicted the existence of solitary waves for wavenumbers much smaller than the cut-off wavenumber, by using a nonlinear stability analysis for two-dimensional flows. Numerical simulations based on the long-wave approximation provide limiting values of the Reynolds number, beyond which there are no stationary travelling waves and solutions of the evolution equation blow up after a finite time. Salamon et al. (1994), studied surface wave instabilities by direct numerical simulation (DNS) of the full nonlinear equations. Their results are in line with the long-wave theory for small-amplitude waves. They showed no tendency to wave breaking. Instabilities on falling films on a heated plane can occur not only as surface wave instabilities but also as instabilities driven by shear stresses arising from the temperature dependence of the surface tension, due to the well known Marangoni effect. Several authors investigate Bernard-Marangoni's instabilities or thermocapillary instabilities. Firstly, Lin and later Davis studied the hydrodynamic (or surface-wave) and thermocapillary instability of a heated incline and the interaction of these instabilities. Surface tension driven stationary circulation in a thin film flow down a heated incline is studied with the use of linear theory, by Sreenivasan and Lin (1978). They found that the critical Marangoni number of the film on a heated incline is smaller than that of the corresponding horizontal film by an amount $\sin^2\theta F$, where θ is the inclination angle and F, depends on relevant flow parameters. Kelly et al. (1986) also dealt with a similar problem a decade after. They considered the effect of a temperature-dependent surface tension upon the instability of a film flow down a heated inclined plane for long-wavelength disturbances. The two roots of the quadratic equation for the critical Reynolds number, correspond to a hydrodynamic instability as modified by thermocapillary action, and to a thermocapillary instability as modified by shear. Kalliadasis et al. (2003) consider the motion of a liquid film falling down a heated planar substrate, using the integral-boundary-layer approximation of the Navier–Stokes/energy equations and free-surface boundary conditions. The essential spectrum is always stable, while part of the discrete spectrum becomes unstable for values of the Marangoni num-

ber larger than a critical value. Above this critical Marangoni number, the growth rate curve as a function of wavenumber has a finite band of unstable modes which increases as the Marangoni number increases. Further research from Joo et al. (1991), shows the importance of evaporation on the long-wave instabilities. A nonlinear stability theory was applied, and they found that by increasing the slope, the effect of the mean flow became more important, the thermocapillary force amplified the perturbations, the wave steepening, and the surface fingering tended to develop at earlier times. It is worth to note that the terms depending on the Marangoni number are of second order in comparison with those due to gravity and mean flow in the relevant evolution equation. Frank (2006) has investigated, numerically, the possibility of controlling flow stability to prevent the rupture of a film flowing down an inclined plane with a local heater. It is shown that control can flatten the surface and increase the threshold temperature for the film rupture. Finally, Kalliadasis (2007) analyzed, further, the problem of heated thin films. He compared all the models obtained to date in order to improve the approximation and to derive equations that agree completely with the linear results of the Orr-Sommerfeld equation [Davalos-Orozco (2013)].

The thing that has not been studied in detail is the effect of temperature-dependent viscosity. Makinde (2006) investigated a steady-state problem of heat transfer in laminar flows of a variable viscosity liquid film along an inclined heated plate, using perturbation series summation. Later, he extended the results for a gravity-driven variable viscosity liquid film along an inclined heated plate with convective cooling [Makinde (2010)]. Reisfeld and Bankoff (1990) examined a thin liquid layer bounded below by a flat infinite extent substrate with uniform constant temperature, and above by a liquid-vapor interface whose temperature varies according to a boundary condition. They used long-wave theory to derive an evolution equation for a heated film of a linearly temperature-dependent viscosity liquid. The outcome of viscosity's variations is to reduce the timescale for the process leading to more rapid rupture of the film, a reduction that can be significant for a viscous fluid.

3.2 Viscoelastic Fluid

The laminar flow of certain fluids such as polymeric liquids, blood, paints, slurries, metallic melts, and so forth cannot be sufficiently described by the linearly viscous Newtonian model. Therefore, much research has been done to develop several non-Newtonian fluid models over the past several decades. We begin with the Maxwell and Kelvin-Voigt models as a first approach to define the viscoelasticity. Ultimately, we will derive the Oldroyd-B equations to adequately describe the changes of the variable solvent and polymeric viscosities of the fluid.

3.2.1 Newtonian Fluid

We begin with the mass conservation (Equation 3.2.1.1), momentum (Equation 3.2.1.2) and stress equations (Equation 3.2.1.3) in incompressible form of a Newtonian fluid.

$$\nabla \cdot \boldsymbol{u} = 0 \tag{3.2.1.1}$$

$$\rho\Big(\frac{\partial \boldsymbol{u}}{\partial t} + \boldsymbol{u} \cdot \nabla \boldsymbol{u}\Big) = \nabla \cdot \bar{\boldsymbol{\sigma}}^s \tag{3.2.1.2}$$

$$\bar{\boldsymbol{\sigma}}^s = -p\bar{\boldsymbol{I}} + \bar{\boldsymbol{T}}^s, \quad \text{with} \quad \bar{\boldsymbol{\sigma}}^s = (\bar{\boldsymbol{\sigma}}^s)^T \tag{3.2.1.3}$$

where: ρ is the density and we assume that it is constant, $\boldsymbol{u}$ is the flow velocity vector field, p is the pressure, $\bar{\boldsymbol{I}}$ is the identity matrix with $p\bar{\boldsymbol{I}}$ represents the spherical part of the stress due to the constraint of incompressibility, $\bar{\boldsymbol{\sigma}}^s$ is the stress tensor and $\bar{\boldsymbol{T}}^s$ reflects the stress that the fluid develops in response to the deformation. For an incompressible Newtonian viscous fluid:

$$\bar{\boldsymbol{T}}^s = 2\eta_s \bar{\boldsymbol{D}} \tag{3.2.1.4}$$

where: η_s is the solvent viscosity, and $\bar{\boldsymbol{D}}$ is the deformation tensor which is calculated by the following equation:

$$\bar{\boldsymbol{D}} = \frac{1}{2}\Big(\nabla \boldsymbol{u} + (\nabla \boldsymbol{u})^T\Big) \tag{3.2.1.5}$$

3.2.2 Mechanical Analogies

Viscoelastic fluids lie somewhere in between the purely elastic and Newtonian flow characteristics. As a first approach to viscoelasticity, we use mechanical analogies; since viscoelastic fluids consist of elastic and viscous elements, we can use the springs to represent elastic elements of the fluids and dashpots as the viscous. The Maxwell model can be represented by a purely viscous dashpot and a purely elastic spring connected in series, as shown in figure 3.1. In contrast with the above model, the Kelvin-Voigt has the dashpot and spring connected in parallel, figure 3.2.

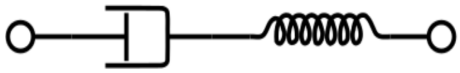


Figure 3.1: Representation of Maxwell's Model.

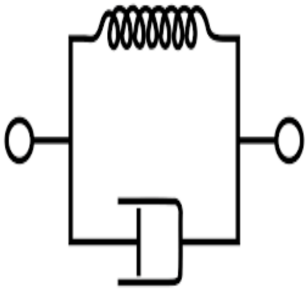


Figure 3.2: Kelvin-Voigt Element

The images 3.1 and 3.2 are downloaded from:
https://commons.wikimedia.org/wiki/File:Maxwell˙diagram.svg, and
.wikimedia.org/wiki/File:Kelvin˙Voigt˙diagram.svg, respectively.

The models describe the dashpot as a Newtonian fluid, equation 3.2.2.2, and model the spring with Hooke's law, equation 3.2.2.1, as follow:

$$\sigma_e = \mathrm{k}\gamma_e, \tag{3.2.2.1}$$

and

$$\sigma_d = \eta_s \gamma_d \tag{3.2.2.2}$$

where: σ_e and σ_d are the stress of the springs and dashpot, respectively, γ_e the strain of the spring, γ_d is the strain of the dashpot, **k** is the spring constant and η_s the viscosity.

In the Maxwell model, the total strain is the sum of the two individual, and the stresses are equals because dashpot and spring are in series. That gives:

$$\gamma_t = \gamma_e + \gamma_d \tag{3.2.2.3}$$

$$\sigma_t = \sigma_e = \sigma_d \tag{3.2.2.4}$$

Differentiating equation 3.2.2.3 with respect to time, we obtain:

$$\sigma_t + \frac{\eta_s}{\mathrm{k}}\dot{\sigma_t} = \eta_s \dot{\gamma_t} \tag{3.2.2.5}$$

where we used the Newton's notation for differentiation. The $\frac{\eta_s}{\mathrm{k}}$ is the relaxation time, the memory of the fluid. We know that the stress is a symmetric tensor field, equation 3.2.1.3. The $\bar{\boldsymbol{T}}^s$ in equation 3.2.1.3 reflects the stress that the fluid develops in response to the deformation. In the Maxwell model that term is the σ_t. and the the $\dot{\gamma_t}$ can be represent by the deformation tensor $\bar{\boldsymbol{D}}$. That means the one-dimensional Maxwell constitutive model can be

generalized and written in tensor form as

$$\bar{\boldsymbol{T}}^s + \frac{\eta_s}{\mathrm{k}}\frac{\partial \bar{\boldsymbol{T}}}{\partial t} = 2\eta_s \bar{\boldsymbol{D}} \tag{3.2.2.6}$$

The Kelvin-Voight has in parallel connected the dashpot and spring, so the total stress is the sum of the individuals and the strains are equal.

$$\gamma_t = \gamma_e = \gamma_d, \tag{3.2.2.7}$$

and

$$\sigma_t = \sigma_e + \sigma_d \tag{3.2.2.8}$$

Differentiating equation 3.2.2.8 with respect to time, we obtain:

$$\sigma_t = \mathrm{k}\gamma_t + \eta_s \dot{\gamma}_t \tag{3.2.2.9}$$

3.2.3 Derivation of Oldroyd-B

The Oldroyd-B model has been designed in order to express not only the viscous behaviour of the fluid but also the polymeric. We need to introduce polymeric stress, $\bar{\boldsymbol{\sigma}}$, and modify the Newtonian equations. To do that, we use the dumbbell model, in which the molecules forming the fluid are represented as spheres connected by Hookean springs. At microscopic level, inertial forces are small compared to viscous forces, and we have Stoke flow:

$$\nabla \cdot \boldsymbol{u} = 0, \quad \eta_s \nabla^2 \boldsymbol{u} = \nabla p \quad ,$$

where: $\boldsymbol{u}$ the velocity vector, η_s the solvent viscosity and p the pressure.

The motion of the sphere will be subjected to: the spring force, the Stokes drag force fro the solvent viscosity, and the Brownian motion due to the random motion and collisions.

The spring force of a Hookean spring is $F_s = \lambda \boldsymbol{r}$, where: λ is the spring constant and $\boldsymbol{r}$ the distance from the equilibrium length. That means a

sphere A will experience force equal to $F_S^A = \lambda \boldsymbol{r}$, while the connected sphere Bwill experience force: $F_S^B = -\lambda \boldsymbol{r}$. The spring constant due to thermal forces is $\lambda = \frac{3K_BT}{\alpha^2}$, where: T is the temperature, α the diameter of the spheres, and K_B the Boltzmann constant [Winkler (2016)]. Assuming now that the sphere A is located at $\boldsymbol{x}$ and moves with velocity $\boldsymbol{U}^A$ relative with the fluid, the drag force is:

$$F_D^A = 6\pi\eta_s\alpha(\boldsymbol{u}(\boldsymbol{x}) - \boldsymbol{U}^A)$$

where $\boldsymbol{u}(\boldsymbol{v})$ the fluid velocity. Similalary, the sphere B located at $\boldsymbol{x}+\boldsymbol{r}$ with velocity $\boldsymbol{U}^B$ experience drag force:

$$F_D^B = 6\pi\eta_s\alpha(\boldsymbol{u}(\boldsymbol{x}+\boldsymbol{r}) - \boldsymbol{U}^B)$$

The total force balance must be zero:

$$F_t^A = F_S^A + F_D^A = 0 \quad \text{and} \quad F_t^B = F_S^B + F_D^B = 0$$

.

$$F_t^A = \lambda \boldsymbol{r} + 6\pi\eta_s\alpha(\boldsymbol{u}(\boldsymbol{x}) - \boldsymbol{U}^A) \Rightarrow \frac{3K_BT}{\alpha^2}\boldsymbol{r} + 6\pi\eta_s\alpha\Big(\boldsymbol{u}(\boldsymbol{x}) - \boldsymbol{U}^A\Big) = 0, \tag{3.2.3.1}$$

and

$$\begin{aligned} F_t^B = -\lambda \boldsymbol{r} + 6\pi\eta_s\alpha\Big(\boldsymbol{u}(\boldsymbol{x}+\boldsymbol{r}) - \boldsymbol{U}^B\Big) = 0 \qquad (3.2.3.2)\\ \Rightarrow -\frac{3K_BT}{\alpha^2}\boldsymbol{r} + 6\pi\eta_s\alpha\Big(\boldsymbol{u}(\boldsymbol{x}+\boldsymbol{r}) - \boldsymbol{U}^B\Big) \end{aligned}$$

Solving equations 3.2.3.1 and 3.2.3.2 for $\boldsymbol{U}^A$ and $\boldsymbol{U}^B$, respectively, we have:

$$\boldsymbol{U}^A = \frac{K_BT}{2\pi\eta_s\alpha^3}\boldsymbol{r} + \boldsymbol{u}(\boldsymbol{x}), \quad \text{and} \tag{3.2.3.3}$$

$$\boldsymbol{U}^B = -\frac{K_B T}{2\pi\eta_s\alpha^3}\boldsymbol{r} + \boldsymbol{u}(\boldsymbol{x}+\boldsymbol{r}) \tag{3.2.3.4}$$

We introduce a new parameter τ the relaxation time, defined as $\tau = \frac{2\pi\eta_s\alpha^3}{K_B T}$. The relaxation time represents the "memory" of the dumbbell. We can write the velocity of sphere A like $\boldsymbol{U}^A = \frac{d\boldsymbol{x}}{dt}$, and similarly, $\boldsymbol{U}^B = \frac{d(\boldsymbol{x}+\boldsymbol{r})}{dt}$. Substratacting the adove equations we derive the evolution equation for $\boldsymbol{r}$:

$$\frac{d\boldsymbol{r}}{dt} = -\frac{1}{2\tau}\boldsymbol{r} + \boldsymbol{u}(\boldsymbol{x}) - \boldsymbol{u}(\boldsymbol{x}+\boldsymbol{r}) \tag{3.2.3.5}$$

The suspenssion $\boldsymbol{r}$ from the equilibrium position is small regarding $\boldsymbol{x}$. That allows us to use the basic Taylor series method for the denominator(i.e. if $\boldsymbol{r} << 1$, then $\boldsymbol{u}(\boldsymbol{x}+\boldsymbol{r}) = \boldsymbol{u}(\boldsymbol{x}) + \boldsymbol{r}\frac{d\boldsymbol{u}(\boldsymbol{x})}{d\boldsymbol{x}} + O(\boldsymbol{r}^2)$) [Fenton (1983),Blyth et al. (2003)]. Applying it into equation 3.2.3.5 we get:

$$\frac{d\boldsymbol{r}}{dt} = -\frac{K_B T}{\pi\eta_s\alpha^3}\boldsymbol{r} + \boldsymbol{r}\cdot\nabla\boldsymbol{u}(\boldsymbol{x}) + O(\boldsymbol{r}^2) \tag{3.2.3.6}$$

Consider now, a suspension that contains lots of dumbbell. It will contribute an extra stress, the polymeric stress $\bar{\boldsymbol{\sigma}}^p$. Stress is defined as force per area. The force from one dumbbell will be $\lambda\boldsymbol{r}$. We assume a finite surface, δS, with a perpendicular to it unit vector $\boldsymbol{n}$. If there are m dumbbells per unit volume, the we expect the number crossing the are to be $m\boldsymbol{r}\cdot\boldsymbol{n}\delta S$. Then the extra stress exerted by the dumbbells is:

$$\bar{\boldsymbol{\sigma}}^p\cdot\boldsymbol{n}\delta S = \lambda\boldsymbol{r}\Big(m\boldsymbol{r}\cdot\boldsymbol{n}\delta S\Big) \Rightarrow \bar{\boldsymbol{\sigma}}^p = m\lambda\boldsymbol{r}\boldsymbol{r}, \quad \text{or} \qquad \bar{\boldsymbol{\sigma}}^p = G\boldsymbol{r}\boldsymbol{r} \tag{3.2.3.7}$$

where: $G = m\lambda$ is the shear modulus. Adding a three dimensional Brownian motion the evolution of $\boldsymbol{r}$ becomes:

$$d\boldsymbol{r} = \Big(-\frac{1}{2\tau}\boldsymbol{r} + \boldsymbol{r}\cdot\nabla\boldsymbol{u}\Big)dt + \tau^{-\frac{1}{2}}d\boldsymbol{B}_t \tag{3.2.3.8}$$

with $d\boldsymbol{B}_t$ is the contribution of the Brownian motion into the evolution of $\boldsymbol{r}$. In order to evaluate the dyadic $\boldsymbol{r}\boldsymbol{r}$, or tensor product $\boldsymbol{r}\otimes\boldsymbol{r}$, we introduce

the conformation tensor $\bar{\boldsymbol{A}}$ such as:

$$\bar{\boldsymbol{A}}(\boldsymbol{x},t) = \boldsymbol{r}\boldsymbol{r} \tag{3.2.3.9}$$

We assume a finite time-step dt. After that $\boldsymbol{r}$ will have changed by $d\boldsymbol{r}$ and $\boldsymbol{x}$ by $d\boldsymbol{x}$ or $\boldsymbol{u}(\boldsymbol{x})dt$. Applying those on equation 3.2.3.9:

$$\bar{\boldsymbol{A}}(\boldsymbol{x}+\boldsymbol{u}(\boldsymbol{x})dt, t+dt) = (\boldsymbol{r}+d\boldsymbol{r})(\boldsymbol{r}+d\boldsymbol{r}) \tag{3.2.3.10}$$
$$\bar{\boldsymbol{A}}(\boldsymbol{x}+\boldsymbol{u}(\boldsymbol{x})dt, t+dt) - \bar{\boldsymbol{A}}(\boldsymbol{x}, t+dt) + \bar{\boldsymbol{A}}(\boldsymbol{x}, t+dt) = \boldsymbol{r}\boldsymbol{r} + \boldsymbol{r}d\boldsymbol{r} + d\boldsymbol{r}\boldsymbol{r} + d\boldsymbol{r}d\boldsymbol{r}$$

Substituting equations 3.2.3.8 and 3.2.3.9 into equation 3.2.3.10 we get:

$$(\boldsymbol{u}(\boldsymbol{x})dt\cdot\nabla)\bar{\boldsymbol{A}}(\boldsymbol{x},t) + \bar{\boldsymbol{A}}(\boldsymbol{x},t+dt) - \bar{\boldsymbol{A}}(\boldsymbol{x},t) + \bar{\boldsymbol{A}}(\boldsymbol{x},t) = \tag{3.2.3.11}$$
$$\boldsymbol{r}\Big((-\frac{1}{2\tau}\boldsymbol{r} + \boldsymbol{r}\cdot\nabla\boldsymbol{u}(\boldsymbol{x}))dt + \tau^{-\frac{1}{2}}d\boldsymbol{B}_t\Big) + \Big((-\frac{1}{2\tau}\boldsymbol{r} + \boldsymbol{r}\cdot\nabla\boldsymbol{u}(\boldsymbol{x}))dt + \tau^{-\frac{1}{2}}d\boldsymbol{B}_t\Big)\boldsymbol{r}$$
$$+\Big((-\frac{1}{2\tau}\boldsymbol{r} + \boldsymbol{r}\cdot\nabla\boldsymbol{u}(\boldsymbol{x}))dt + \tau^{-\frac{1}{2}}d\boldsymbol{B}_t\Big)\Big((-\frac{1}{2\tau}\boldsymbol{r} + \boldsymbol{r}\cdot\nabla\boldsymbol{u}(\boldsymbol{x}))dt + \tau^{-\frac{1}{2}}d\boldsymbol{B}_t\Big) \Rightarrow$$
$$\frac{\partial\bar{\boldsymbol{A}}(\boldsymbol{x},t)}{\partial t} + (\boldsymbol{u}(\boldsymbol{x})\cdot\nabla)\bar{\boldsymbol{A}}(\boldsymbol{x},t) - \bar{\boldsymbol{A}}(\boldsymbol{x},t)\cdot\nabla\boldsymbol{u}(\boldsymbol{x}) - (\nabla\boldsymbol{u}(\boldsymbol{x}))^T\cdot\bar{\boldsymbol{A}}(\boldsymbol{x},t)$$
$$= -\frac{1}{\tau}(\bar{\boldsymbol{A}}(\boldsymbol{x},t) - \bar{\boldsymbol{I}}) + O(dt^2) \tag{3.2.3.12}$$

The equation 3.2.3.11 is used to evaluate the conformation tensor $\bar{\boldsymbol{A}}$. We used some properties of the Brownian vector: $\boldsymbol{r}d\boldsymbol{B}_t$=0, $d\boldsymbol{B}_t\boldsymbol{r} = 0$, and $d\boldsymbol{B}_t d\boldsymbol{B}_t = \bar{\boldsymbol{I}}$. The extra stress, equation 3.2.3.7, can be written like:

$$\bar{\boldsymbol{\sigma}}^p = G\bar{\boldsymbol{A}} \tag{3.2.3.13}$$

The extra polymeric stress acts with the Newtonian stress Assuming that the total stress is $\bar{\boldsymbol{\sigma}}$ then:

$$\bar{\boldsymbol{\sigma}} = \bar{\boldsymbol{\sigma}}^s + \bar{\boldsymbol{\sigma}}^p \tag{3.2.3.14}$$

Adding the polymeric stress into the Newtonian equations 3.2.1.1 and 3.2.1.3

we, finally, acquire the Oldroyd-B model equations.

$$\nabla \cdot \boldsymbol{u} = 0,$$

$$\rho\left(\frac{\partial \boldsymbol{u}}{dt} + \boldsymbol{u} \cdot \nabla \boldsymbol{u}\right) = \nabla \cdot \bar{\boldsymbol{\sigma}},$$

$$\bar{\boldsymbol{\sigma}} = -p\bar{\boldsymbol{I}} + \eta_s\left(\nabla \boldsymbol{u} + (\nabla \boldsymbol{u})^T\right) + G\bar{\boldsymbol{A}},$$

$$\frac{\partial \bar{\boldsymbol{A}}}{\partial t} + (\boldsymbol{u} \cdot \nabla)\bar{\boldsymbol{A}} - \bar{\boldsymbol{A}} \cdot \nabla \boldsymbol{u} - (\nabla \boldsymbol{u})^T \cdot \bar{\boldsymbol{A}} = -\frac{1}{\tau}(\bar{\boldsymbol{A}} - \bar{\boldsymbol{I}})$$

Oldroyd was the first to develop systematically three-dimensional models that can describe stress relaxation and normal stress differences in a simple shear flow. Although it is incapable of describing shear thinning/shear thickening, it can be easily generalized to do that too. [Winkler (2016),Marrucci (1972), Prilutski et al. (1983), and Matthews (1982)]

4

Oldroyd B Model Equations And Non-Isothermal Falling Films

In this chapter we use a different notation for the velocity such as u_x,u_y and u_z for the components of the velocity in x, y and z direction, respectively. We summarize the chapter 3.2.3 and present the governing equations for the Oldroyd B model:

$$\nabla \cdot \boldsymbol{u} = 0 \tag{4.0.0.1}$$

$$\rho\Big(\frac{\partial \boldsymbol{u}}{\partial t} + \boldsymbol{u} \cdot \nabla \boldsymbol{u}\Big) = \nabla \cdot \bar{\boldsymbol{\sigma}} \tag{4.0.0.2}$$

$$\bar{\boldsymbol{\sigma}} = -p\bar{\boldsymbol{I}} + \eta_s\Big(\nabla \boldsymbol{u} + (\nabla \boldsymbol{u})^T\Big) + G\bar{\boldsymbol{A}} \tag{4.0.0.3}$$

$$\frac{\partial \bar{\boldsymbol{A}}}{\partial t} + (\boldsymbol{u} \cdot \nabla)\bar{\boldsymbol{A}} - \bar{\boldsymbol{A}} \cdot \nabla \boldsymbol{u} - (\nabla \boldsymbol{u})^T \cdot \bar{\boldsymbol{A}} = -\frac{1}{\tau}(\bar{\boldsymbol{A}} - \bar{\boldsymbol{I}}) \tag{4.0.0.4}$$

where: $\boldsymbol{u}$ is the velocity vector and $\nabla \boldsymbol{u} = \begin{bmatrix} \frac{\partial u_x}{\partial x} & \frac{\partial u_y}{\partial x} & \frac{\partial u_z}{\partial x} \\ \frac{\partial u_x}{\partial y} & \frac{\partial u_y}{\partial y} & \frac{\partial u_z}{\partial y} \\ \frac{\partial u_x}{\partial z} & \frac{\partial u_y}{\partial z} & \frac{\partial u_z}{\partial z} \end{bmatrix}$, ρ density, $\bar{\boldsymbol{\sigma}}$ the stress tensor, p the pressure, η_s the solvent viscosity, G the shear modulus, τ is the relaxation time, and $\bar{\boldsymbol{A}}$ the conformation tensor. Last but not least, is the conservation of energy:

$$\rho \hat{C_p} \frac{DT}{Dt} = (\nabla \cdot \kappa \nabla T) + \frac{1}{2} \eta_s (\dot{\gamma} : \dot{\gamma}) \quad , \tag{4.0.0.5}$$

where: $\hat{C_p}$ is the specific heat capacity at constant pressure, T the temperature, k is the thermal conductivity, and $\frac{1}{2}(\dot{\gamma} : \dot{\gamma})$ is the deformation tensor.

The stress balance is:

$$\boldsymbol{n} \cdot \bar{\boldsymbol{T}} + \hat{\boldsymbol{n}} \cdot \bar{\hat{\boldsymbol{T}}} = \sigma \boldsymbol{n} (\nabla \cdot \boldsymbol{n}) - \nabla \sigma \quad , \tag{4.0.0.6}$$

where: σ is the surface tension, $\sigma \boldsymbol{n}(\nabla \cdot \boldsymbol{n})$ is the normal curvature force per unit area associated with local curvature of interface, $\nabla \sigma$ is the tangential stress associated with gradients in surface tension, $\boldsymbol{n}$ is the unit inward normal to the surface and $\hat{\boldsymbol{n}}$ the unit outward normal ($\hat{\boldsymbol{n}} = -\boldsymbol{n}$), $\bar{\boldsymbol{T}}$ and $\bar{\hat{\boldsymbol{T}}}$ are the stress tensors.

4.0.1 Cartesian Coordinates

The governing equations may be written in analytical form as follow:

Continuity Equation

$$\frac{\partial u_x}{\partial x} + \frac{\partial u_y}{\partial y} + \frac{\partial u_z}{\partial z} = 0$$

where: u_x, u_y and u_z are the components of velocity in x, y and z direction respectively.

Momentum Equation

And equation 4.0.0.2 becomes:

$$\rho\Bigg(\begin{bmatrix} \frac{\partial u_x}{\partial t} & \frac{\partial u_y}{\partial t} & \frac{\partial u_z}{\partial t} \end{bmatrix} \tag{4.0.1.1}$$

$$+ \begin{bmatrix} u_x\frac{\partial u_x}{\partial x} + u_y\frac{\partial u_x}{\partial y} + u_z\frac{\partial u_x}{\partial z} & u_x\frac{\partial u_y}{\partial x} + u_y\frac{\partial u_y}{\partial y} + u_z\frac{\partial u_y}{\partial z} & u_x\frac{\partial u_z}{\partial x} + u_y\frac{\partial u_z}{\partial y} + u_z\frac{\partial u_z}{\partial z} \end{bmatrix} \Bigg)$$

$$= \begin{bmatrix} \frac{\partial \sigma_{xx}}{\partial x} + \frac{\partial \sigma_{yx}}{\partial y} + \frac{\partial \sigma_{zx}}{\partial z} & \frac{\partial \sigma_{xy}}{\partial x} + \frac{\partial \sigma_{yy}}{\partial y} + \frac{\partial \sigma_{zy}}{\partial z} & \frac{\partial \sigma_{zx}}{\partial x} + \frac{\partial \sigma_{zy}}{\partial y} + \frac{\partial \sigma_{zz}}{\partial z} \end{bmatrix}$$

Equation 4.0.0.3 becomes:

$$\begin{bmatrix} \sigma_{xx} & \sigma_{xy} & \sigma_{xz} \\ \sigma_{yx} & \sigma_{yy} & \sigma_{yz} \\ \sigma_{zx} & \sigma_{zy} & \sigma_{zz} \end{bmatrix} = -\begin{bmatrix} p & 0 & 0 \\ 0 & p & 0 \\ 0 & 0 & p \end{bmatrix} + \eta\Bigg(\begin{bmatrix} \frac{\partial u_x}{\partial x} & \frac{\partial u_y}{\partial x} & \frac{\partial u_z}{\partial x} \\ \frac{\partial u_x}{\partial y} & \frac{\partial u_y}{\partial y} & \frac{\partial u_z}{\partial y} \\ \frac{\partial u_x}{\partial z} & \frac{\partial u_y}{\partial z} & \frac{\partial u_z}{\partial z} \end{bmatrix} + \begin{bmatrix} \frac{\partial u_x}{\partial x} & \frac{\partial u_x}{\partial y} & \frac{\partial u_x}{\partial z} \\ \frac{\partial u_y}{\partial x} & \frac{\partial u_y}{\partial y} & \frac{\partial u_y}{\partial z} \\ \frac{\partial u_z}{\partial x} & \frac{\partial u_z}{\partial y} & \frac{\partial u_z}{\partial z} \end{bmatrix} \Bigg)$$

$$+ G\begin{bmatrix} A_{xx} & A_{xy} & A_{xz} \\ A_{yx} & A_{yy} & A_{yz} \\ A_{zx} & A_{zy} & A_{zz} \end{bmatrix} \tag{4.0.1.2}$$

And finally equation 4.0.0.4:

$$
\begin{bmatrix}
\frac{\partial A_{xx}}{\partial t} & \frac{\partial A_{xy}}{\partial t} & \frac{\partial A_{xz}}{\partial t} \\
\frac{\partial A_{yx}}{\partial t} & \frac{\partial A_{yy}}{\partial t} & \frac{\partial A_{yx}}{\partial t} \\
\frac{\partial A_{zx}}{\partial t} & \frac{\partial A_{zy}}{\partial t} & \frac{\partial A_{zz}}{\partial t}
\end{bmatrix}
$$

$$
+ \begin{bmatrix}
u_x \frac{\partial A_{xx}}{\partial x} + u_y \frac{\partial A_{xx}}{\partial y} + u_z \frac{\partial A_{xx}}{\partial z} & u_x \frac{\partial A_{xy}}{\partial x} + u_y \frac{\partial A_{xy}}{\partial y} + u_z \frac{\partial A_{xy}}{\partial z} & u_x \frac{\partial A_{xz}}{\partial x} + u_y \frac{\partial A_{xz}}{\partial y} + u_z \frac{\partial A_{xz}}{\partial z} \\
u_x \frac{\partial A_{yx}}{\partial x} + u_y \frac{\partial A_{yx}}{\partial y} + u_z \frac{\partial A_{yx}}{\partial z} & u_x \frac{\partial A_{yy}}{\partial x} + u_y \frac{\partial A_{yy}}{\partial y} + u_z \frac{\partial A_{yy}}{\partial z} & u_x \frac{\partial A_{yz}}{\partial x} + u_y \frac{\partial A_{yz}}{\partial y} + u_z \frac{\partial A_{yz}}{\partial z} \\
u_x \frac{\partial A_{zx}}{\partial x} + u_y \frac{\partial A_{zx}}{\partial y} + u_z \frac{\partial A_{zx}}{\partial z} & u_x \frac{\partial A_{zy}}{\partial x} + u_y \frac{\partial A_{zy}}{\partial y} + u_z \frac{\partial A_{zy}}{\partial z} & u_x \frac{\partial A_{zz}}{\partial x} + u_y \frac{\partial A_{zz}}{\partial y} + u_z \frac{\partial A_{zz}}{\partial z}
\end{bmatrix}
$$

$$
- \begin{bmatrix}
A_{xx} \frac{\partial u_x}{\partial x} + A_{xy} \frac{\partial u_x}{\partial y} + Axz \frac{\partial u_x}{\partial z} & A_{xx} \frac{\partial u_y}{\partial x} + A_{xy} \frac{\partial u_y}{\partial y} + Axz \frac{\partial u_y}{\partial z} & A_{xx} \frac{\partial u_z}{\partial x} + A_{xy} \frac{\partial u_z}{\partial y} + Axz \frac{\partial u_z}{\partial z} \\
A_{yx} \frac{\partial u_x}{\partial x} + A_{yy} \frac{\partial u_x}{\partial y} + Ayz \frac{\partial u_x}{\partial z} & A_{yx} \frac{\partial u_y}{\partial x} + A_{yy} \frac{\partial u_y}{\partial y} + Ayz \frac{\partial u_y}{\partial z} & A_{yx} \frac{\partial u_z}{\partial x} + A_{yy} \frac{\partial u_z}{\partial y} + Ayz \frac{\partial u_z}{\partial z} \\
A_{zx} \frac{\partial u_x}{\partial x} + A_{zy} \frac{\partial u_x}{\partial y} + Azz \frac{\partial u_x}{\partial z} & A_{zx} \frac{\partial u_y}{\partial x} + A_{zy} \frac{\partial u_y}{\partial y} + Azz \frac{\partial u_y}{\partial z} & A_{zx} \frac{\partial u_z}{\partial x} + A_{zy} \frac{\partial u_z}{\partial y} + Azz \frac{\partial u_z}{\partial z}
\end{bmatrix}
$$

$$
- \begin{bmatrix}
A_{xx} \frac{\partial u_x}{\partial x} + A_{yx} \frac{\partial u_x}{\partial y} + Azx \frac{\partial u_x}{\partial z} & A_{xy} \frac{\partial u_x}{\partial x} + A_{yy} \frac{\partial u_x}{\partial y} + Azy \frac{\partial u_x}{\partial z} & A_{xz} \frac{\partial u_x}{\partial x} + A_{yz} \frac{\partial u_x}{\partial y} + Azz \frac{\partial u_x}{\partial z} \\
A_{xx} \frac{\partial u_y}{\partial x} + A_{yx} \frac{\partial u_y}{\partial y} + Azx \frac{\partial u_y}{\partial z} & A_{xy} \frac{\partial u_y}{\partial x} + A_{yy} \frac{\partial u_y}{\partial y} + Azy \frac{\partial u_y}{\partial z} & A_{xz} \frac{\partial u_y}{\partial x} + A_{yz} \frac{\partial u_y}{\partial y} + Azz \frac{\partial u_y}{\partial z} \\
A_{xx} \frac{\partial u_z}{\partial x} + A_{yx} \frac{\partial u_z}{\partial y} + Azx \frac{\partial u_z}{\partial z} & A_{xy} \frac{\partial u_z}{\partial x} + A_{yy} \frac{\partial u_z}{\partial y} + Azy \frac{\partial u_z}{\partial z} & A_{xz} \frac{\partial u_z}{\partial x} + A_{yz} \frac{\partial u_z}{\partial y} + Azz \frac{\partial u_z}{\partial z}
\end{bmatrix}
$$

$$
= -\frac{1}{\tau} \begin{bmatrix}
A_{xx} - 1 & A_{xy} & A_{xz} \\
A_{yx} & A_{yy} - 1 & A_{yz} \\
A_{zx} & A_{zy} & A_{zz} - 1
\end{bmatrix} \qquad (4.0.1.3)
$$

Normal Stress Balance:

$$\boldsymbol{n}\cdot\bar{\boldsymbol{T}}\boldsymbol{n}-\boldsymbol{n}\cdot\bar{\hat{\boldsymbol{T}}}\cdot\boldsymbol{n}=\sigma(\nabla\cdot\boldsymbol{n})\Rightarrow$$
$$n_1\Big(T_{11}\cdot n_1+T_{21}\cdot n_2\Big)+n_2\Big(T_{12}\cdot n_1+T_{22}\cdot n_2\Big)-n_1\Big(\hat{T_{11}}\cdot n_1+\hat{T_{21}}\cdot n_2\Big)$$
$$-n_2\Big(\hat{T_{12}}\cdot n_1+\hat{T_{22}}\cdot n_2\Big)=\sigma\nabla\cdot\boldsymbol{n}\Rightarrow$$
$$\frac{-h'}{\Big(1+(h')^2\Big)^{\frac{1}{2}}}\Bigg(\Big(-p+2\eta_s\frac{\partial u_x}{\partial x}+GA_{xx}\Big)\cdot\frac{-h'}{\Big(1+(h')^2\Big)^{\frac{1}{2}}}+\Big(\eta_s(\frac{\partial u_x}{\partial y}+\frac{\partial u_y}{\partial x})$$
$$+GA_{xy}\Big)\cdot\frac{1}{\Big(1+(h')^2\Big)^{\frac{1}{2}}}\Bigg)+\frac{1}{\Big(1+(h')^2\Big)^{\frac{1}{2}}}\Bigg(\Big(\eta_s(\frac{\partial u_x}{\partial y}+\frac{\partial u_y}{\partial x})+GA_{xy}\Big)\cdot\frac{-h'}{\Big(1+(h')^2\Big)^{\frac{1}{2}}}$$
$$+\Big(-p+2\eta_s\frac{\partial u_y}{\partial y}+GA_{yy}\Big)\cdot\frac{1}{\Big(1+(h')^2\Big)^{\frac{1}{2}}}\Bigg)-\frac{-h'}{\Big(1+(h')^2\Big)^{\frac{1}{2}}}\Bigg(\bar{\hat{\boldsymbol{T}}}_{\boldsymbol{11}}\cdot\frac{-h'}{\Big(1+(h')^2\Big)^{\frac{1}{2}}}$$
$$+\bar{\hat{\boldsymbol{T}}}_{\boldsymbol{12}}\cdot\frac{1}{\Big(1+(h')^2\Big)^{\frac{1}{2}}}\Bigg)-\frac{1}{\Big(1+(h')^2\Big)^{\frac{1}{2}}}\Bigg(\bar{\hat{\boldsymbol{T}}}_{\boldsymbol{21}}\cdot\frac{-h'}{\Big(1+(h')^2\Big)^{\frac{1}{2}}}+\bar{\hat{\boldsymbol{T}}}_{\boldsymbol{22}}\cdot\frac{1}{\Big(1+(h')^2\Big)^{\frac{1}{2}}}\Bigg)=$$
$$-\sigma\frac{h"}{\Big(1+(h')^2\Big)^{\frac{3}{2}}}\qquad(4.0.1.4)$$

where: $\boldsymbol{n}=[n_1\quad n_2]=\left[\frac{-h'}{\Big(1+(h')^2\Big)^{\frac{1}{2}}}\quad\frac{1}{\Big(1+(h')^2\Big)^{\frac{1}{2}}}\right]$ is a unit vector perpendicular to the interface which is located at $y=h(x)$.

Tangential force balance equation:

$$\boldsymbol{n}\cdot\bar{\boldsymbol{T}}\cdot\boldsymbol{t}-\boldsymbol{n}\cdot\bar{\hat{\boldsymbol{T}}}\cdot\boldsymbol{t}=-\nabla\sigma\cdot\boldsymbol{t}\qquad(4.0.1.5)$$

We only consider flows with constant surface tension, so $\nabla\sigma=0$.

That leads to:

$$
\begin{aligned}
&n_1\Big(T_{11}\cdot t_1+T_{21}\cdot t_2\Big)+n_2\Big(T_{12}\cdot t_1+T_{22}\cdot t_2\Big)-n_1\Big(\hat{T}_{11}\cdot t_1+\hat{T}_{21}\cdot t_2\Big)\\
&-n_2\Big(\hat{T}_{12}\cdot t_1+\hat{T}_{22}\cdot t_2\Big)=0\Rightarrow\\
&\frac{-h'}{\Big(1+(h')^2\Big)^{\frac{1}{2}}}\Bigg(\Big(-p+2\eta_s\frac{\partial u_x}{\partial x}+GA_{xx}\Big)\frac{1}{\Big(1+(h')^2\Big)^{\frac{1}{2}}}\\
&+\Big(\eta_s(\frac{\partial u_x}{\partial y}+\frac{\partial u_y}{\partial x})+GA_{xy}\Big)\frac{h'}{\Big(1+(h')^2\Big)^{\frac{1}{2}}}\Bigg)+\frac{1}{\Big(1+(h')^2\Big)^{\frac{1}{2}}}\Bigg(\Big(\eta_s(\frac{\partial u_x}{\partial y}+\frac{\partial u_y}{\partial x})\\
&+GA_{xy}\Big)\frac{1}{\Big(1+(h')^2\Big)^{\frac{1}{2}}}+\Big(-p+2\eta_s\frac{\partial u_y}{\partial y}+GA_{yy}\Big)\frac{h'}{\Big(1+(h')^2\Big)^{\frac{1}{2}}}\Bigg)\\
&-\frac{-h'}{\Big(1+(h')^2\Big)^{\frac{1}{2}}}\Bigg(\hat{T}_{11}\frac{1}{\Big(1+(h')^2\Big)^{\frac{1}{2}}}+\hat{T}_{12}\frac{h'}{\Big(1+(h')^2\Big)^{\frac{1}{2}}}\Bigg)\\
&-\frac{1}{\Big(1+(h')^2\Big)^{\frac{1}{2}}}\Bigg(\hat{T}_{12}\frac{1}{\Big(1+(h')^2\Big)^{\frac{1}{2}}}+\hat{T}_{22}\frac{h'}{\Big(1+(h')^2\Big)^{\frac{1}{2}}}\Bigg)=0 \qquad (4.0.1.6)
\end{aligned}
$$

where: $\boldsymbol{t}=[t_1 \quad t_2]=\left[\frac{1}{\Big(1+(h')^2\Big)^{\frac{1}{2}}} \quad \frac{h'}{\Big(1+(h')^2\Big)^{\frac{1}{2}}}\right]$ is a unit vector tangent to the interface

For the free surface scenario: $\overset{\bar{\wedge}}{\boldsymbol{T}}=0$.

4.1 Laminar Falling Film

Imagine a two dimensional flow driven by gravity along an inclined plate. An incompressible viscoelastic fluid of density ρ and variable total viscosity η_t flows in the plate which is inclined at an angle θ to the horizontal. A Cartesian frame (x, y) is chosen with x and y measuring distances down a perpendicular to the wall, respectively. The Oldroyd-B model is used to describe the polymeric stress. The wall is smooth and coated with a catalyst. The reaction rate is not taken under consideration, as the reagent reacts immediately, and it is irreversible. As a result of this, the wall has a uniform temperature of T_0. We assume no differences in physical properties between reagents and products. The upper surface of the liquid film is located at $y = h(x)$, considered free with uniform temperature (T_f) and parallel to x-direction so $h(x) = 1$. In this case we assume that $T_0 > T_f$.

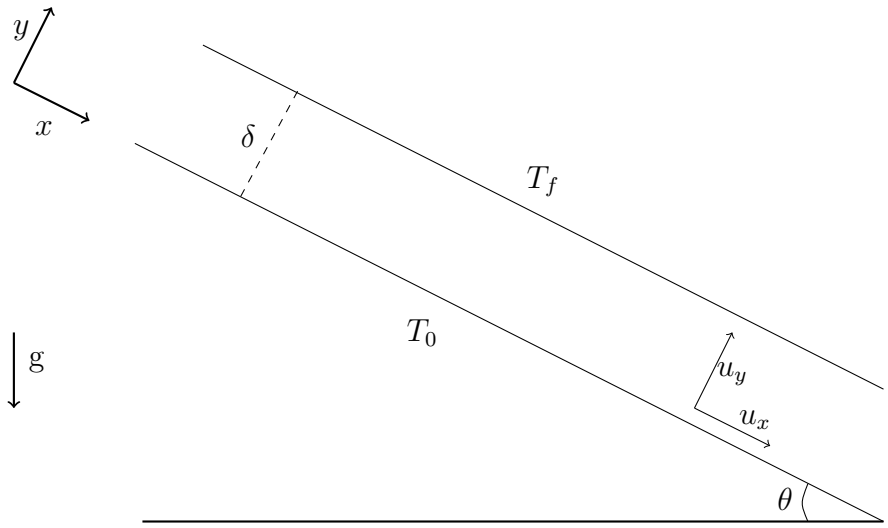


Figure 4.1: Schematic Representation of flow down an inclined channel

We begin with the governing equations, 4.0.0.1, 4.0.0.2, 4.0.0.3, 4.0.0.4 and 4.0.0.5.

X-DIRECTION

$$\frac{\partial \sigma_{xx}}{\partial x}+\frac{\partial \sigma_{xy}}{\partial y}=0 \Rightarrow \Big(\frac{\partial \eta_s}{\partial y}+\tau\frac{\partial G}{\partial y}+G\frac{\partial \tau}{\partial y}\Big)\frac{\partial u_x}{\partial y}+\Big(\eta_s+G\tau\Big)\frac{\partial^2 u_x}{\partial y^2}=0$$
$$\Rightarrow \quad \eta_t\frac{\partial^2 u_x}{\partial y^2}+\frac{\partial \eta_t}{\partial y}\frac{\partial u_x}{\partial y}+\rho g\sin\theta=0$$

Y-DIRECTION

$$\frac{\partial \sigma_{xy}}{\partial x}+\frac{\partial \sigma_{yy}}{\partial y}=0 \overset{4.0.1.2}{\Rightarrow} -\frac{\partial p}{\partial y}+\frac{\partial G}{\partial y}+\rho g\cos\theta=0$$

4.1.1 Non Dimensionalization

We assume that solvent viscosity obeys an Arrhenius type equation like, $\eta=\mu_o e^{\alpha(T-T_f)}$, where α is a positive constant. That means the solovent viscosity is $\eta_s=\mu_s e^{\alpha(T-T_f)}$ and the polymeric viscosity is $\eta_p=G\tau$. We shall nondimensionalize the governing equations. For this reason we introduce the dimensionless variables and parameters as follow:

Dimensionless Variables

$$x=\delta x^*, \qquad y=\delta y^*, \qquad u_x=\frac{\delta^2\rho g\sin\theta}{\mu_t}u_x^* \qquad p=p^*\delta\rho g\sin\theta,$$
$$\Theta=\frac{T-T_f}{T_0-T_f}, \qquad G=G^*\delta\rho g\sin\theta, \qquad \tau=e^{-\beta\Theta}\frac{\mu_p}{\delta\rho g\sin\theta}$$

Dimensionless Parameters

$$\lambda=\frac{(\delta^2\rho g\sin\theta)^2}{\mu_t\kappa(T_0-T_f)} \qquad \beta=\alpha(T_0-T_f)$$

where: λ is the Brinkman number. Note that this time β is a positive constant.

So after dropping asterisks, the energy equation (4.0.0.5) becomes:

$$\frac{d^2\Theta}{dy^2} + \lambda e^{-\beta\Theta}\Big(\frac{\partial u_x}{\partial y}\Big)^2 = 0 \tag{4.1.1.1}$$

Cauchy x-direction becomes:

$$\begin{aligned} & e^{-\beta\Theta}\frac{\partial^2 u_x}{\partial y^2} + \frac{\partial e^{-\beta\Theta}}{\partial y}\frac{\partial u_x}{\partial y} + 1 = 0 \Rightarrow \frac{\partial u_x}{\partial y} = \Big(c_1 - y\Big)e^{\beta\Theta} \\ & \Rightarrow u_x = -\int_0^y e^{\beta\Theta} y' dy' + \int_0^y c_1 e^{\beta\Theta} dy' \end{aligned} \tag{4.1.1.2}$$

Determine the constant of integration c_1 using the tangential force balance equation 4.0.1.6 :

$$\begin{aligned} & \boldsymbol{n}\cdot\bar{\boldsymbol{T}}\cdot\boldsymbol{t} - \boldsymbol{n}\cdot\bar{\bar{\boldsymbol{T}}}\cdot\boldsymbol{t} = 0 \Rightarrow \\ & \frac{-h'}{\Big(1+(h')^2\Big)^{\frac{1}{2}}}\Bigg(\Big(-p + 2\eta_s\frac{\partial u_x}{\partial x} + GA_{xx}\Big)\frac{1}{\Big(1+(h')^2\Big)^{\frac{1}{2}}} \\ & + \Big(\eta_s(\frac{\partial u_x}{\partial y} + \frac{\partial u_y}{\partial x}) + GA_{xy}\Big)\frac{h'}{\Big(1+(h')^2\Big)^{\frac{1}{2}}}\Bigg) + \frac{1}{\Big(1+(h')^2\Big)^{\frac{1}{2}}}\Bigg(\Big(\eta_s(\frac{\partial u_x}{\partial y} + \frac{\partial u_y}{\partial x}) \\ & + GA_{xy}\Big)\frac{1}{\Big(1+(h')^2\Big)^{\frac{1}{2}}} + \Big(-p + 2\eta_s\frac{\partial u_y}{\partial y} + GA_{yy}\Big)\frac{h'}{\Big(1+(h')^2\Big)^{\frac{1}{2}}}\Bigg) = 0 \\ & \Rightarrow \eta_s\frac{\partial u_x}{\partial y} = -G\tau\frac{\partial u_x}{\partial y}, \end{aligned}$$

where $\bar{\bar{\boldsymbol{T}}}$ is zero due to the free surface; so :

$$\frac{\partial u_x}{\partial y}\Big|_{y=1} = 0 \Rightarrow -e^{\beta\Theta}y + c_1 e^{\beta\Theta}\Big|_{y=1} = 0 \Rightarrow c_1 = 1 \tag{4.1.1.3}$$

Cauchy y-direction

$$-\frac{\partial p}{\partial y}+\frac{\partial G}{\partial y}+\cot\theta=0\Rightarrow p=y\cot\theta+G+c(x) \tag{4.1.1.4}$$

with $\frac{dc(x)}{dx}=\frac{\partial p}{\partial x}=const$

Finally, equations 4.1.1.1, 4.1.1.2 and 4.1.1.3 give:

$$\frac{d^2\Theta}{dy^2}+\lambda e^{-\beta\Theta}\left((1-y)e^{\beta\Theta}\right)^2=0\Rightarrow\frac{\partial^2\Theta}{\partial y^2}+\lambda e^{\beta\Theta}(1-y)^2=0 \tag{4.1.1.5}$$

Boundary Conditions:
At $y=0$ $\Theta\Big|_{y=0}=1$ and at $y=1$ $\Theta\Big|_{y=1}=0$.

The above equation is solved numerically for a variety of λ and β. Makinde has solved a similar problem for a Newtonian fluid with $T_0<T_f$, see [Makinde (2006)]. We design a code based on the finite-difference method in the Matlab® environment. We are mainly using two built-in routines the bvp4c and the ode45. The bvp4c-routine which implements the three-stage Lobatto IIIa formula Kierzenka and Shampine (2001) and ode45-routine a six-stage fifth-order Runge-Kutta method.

In absence of variable viscosity, plot 4.2 shows a classical inclined heated film. The fig. 4.3a presents the case of instantaneous heat transfer. We observe that by increasing of Brinkman number with constant β, a peak point appears at 0.2-0.3. Indeed, the higher the Brinkman-value is, the slower the conduction of heat produced by viscous dissipation and hence the larger the temperature rise. As expected, that can also be observed in plots 4.3b and 4.3c where β was increasing more and more up to 2.5. It is very important to note that an increase in the value of variable viscosity parameter β, signifies an increase in the fluid viscosity, and an increase in the value of the Brinkman number, λ, shows the viscous heating effect. From the application point of view, a realistic case of a polymer melt, where λ is 0.75 and variable viscosity parameter β is 0.7, is represented in 4.4a which shows us a rapid

decrease in temperature which appears an almost linear behavior.

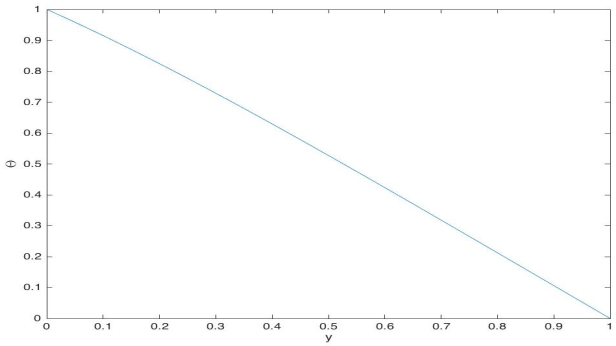
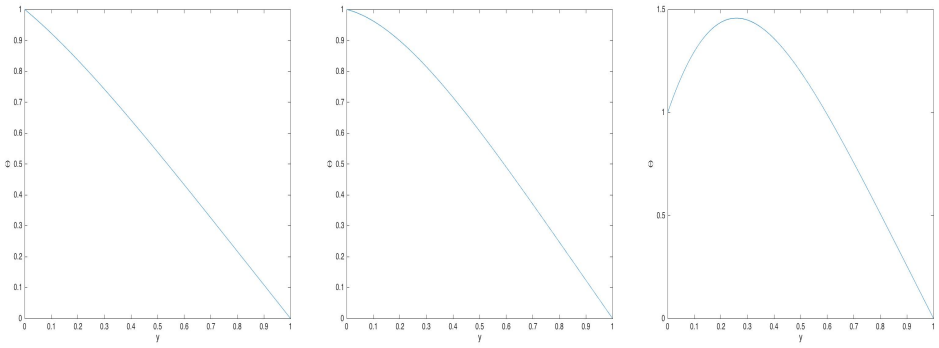
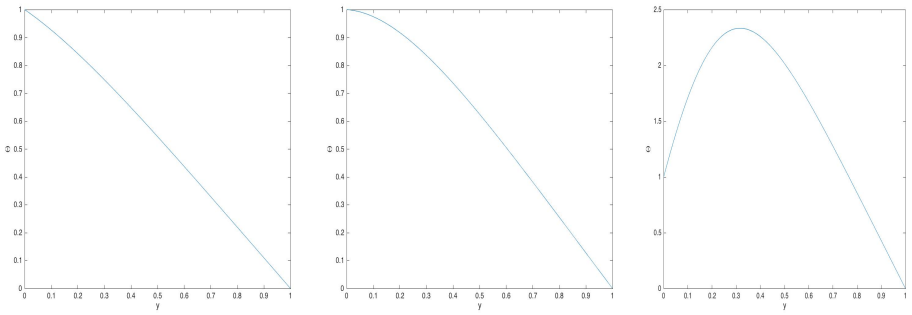


Figure 4.2: Temperature profile, where:$\beta = 0$ and $\lambda = 0.75$.



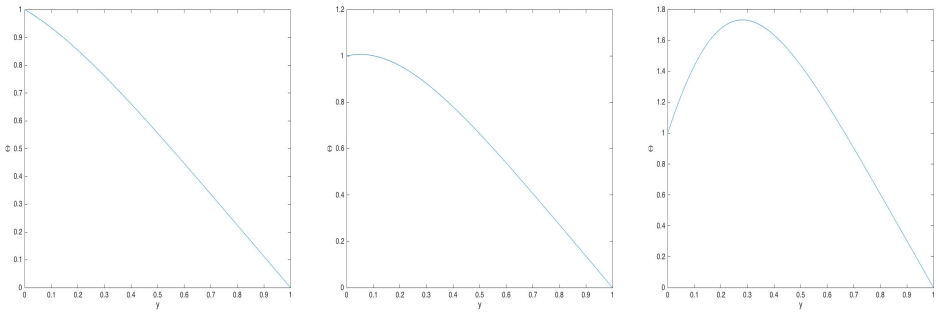
(a) $\lambda = 0.75$. **(b)** $\lambda = 2$ **(c)** $\lambda = 10$

Figure 4.3: Temperature profile, where:$\beta = 0$ and λ ranges.



(a) $\lambda = 0.75$ **(b)** $\lambda = 10$ **(c)** $\lambda = 10$

Figure 4.4: Temperature over film thickness, where $\beta = 0.7$ and different values of Brinkman number.

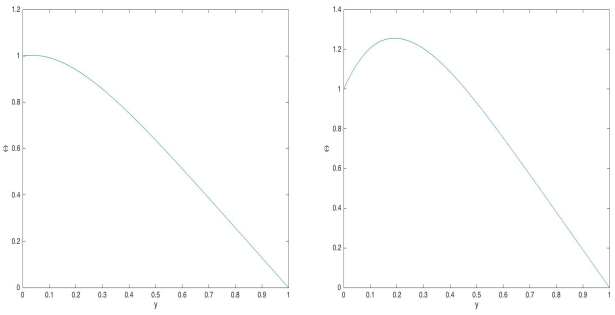


(a) Diagram 8
$\beta = 1 \qquad \lambda = 0.75$

(b) Diagram 3
$\beta = 1 \qquad \lambda = 2$

(c) Diagram 10
$\beta = 1 \qquad \lambda = 10$

Figure 4.5: Temperature over film thickness, where $\beta = 1$ and different values of Brinkman number.



(a) Diagram 11
$\beta = 2 \qquad \lambda = 0.75$

(b) Diagram 12
$\beta = 3 \qquad \lambda = 0.75$

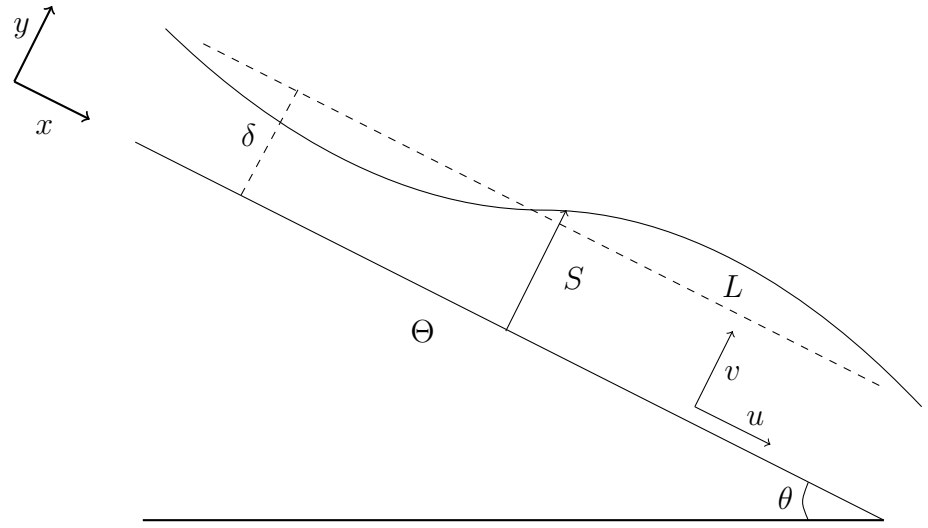
Figure 4.6: Temperature over film thickness, where $\beta = 2$ and 3, and $\lambda = 0.75$.

5

Non-isothermal Falling Films

5.1 Problem Formulation

In the previous chapter (chpt.4) we considered viscoelastic fluid flows.. However, this chapter examines only Newtonian fluids.
A two-dimensional flow with a free surface is the system for study. The fluid flows down an infinite wide plate, inclined at an angle, θ, and the dominant driving force for the flow is gravity, g. The channel has a typical length scale, L, in the x-direction and height, δ, in the y-direction. The fluid density, ρ, is constant and the viscosity, η, will vary exponentially with temperature, T, obeying the Reynolds or Nahme's law [Tanner (2000)]. The temperature at the bottom surface is T_0, the temperature at the free surface, T_f, is equal to the ambient temperature, and the fluid temperature is T. It is assumed that the wall is completely wetted, and that the liquid flows in the form of a thin continuous film. The surface is located at $y = S(x)$. The coefficient of surface tension across the air/liquid interface is σ. For a sketch of the assumed configuration see Figure 5.1.



In developing the mathematical model for the fluid flow the following assumptions will be made:

- Consider flow with small Rayleigh number, so any change in density is negligible,
- Steady States,
- the wall at the bottom is smooth ,
- the free surface has a uniform temperature T_f equal to the ambient temperature,
- viscosity is temperature-dependent obeying Reynold's law, $\eta = \mu e^{-\alpha(T-T_f)}$, where α and μ are positive constants,
- the height δ is small in comparison to the length L,
- Consider flow with small Marangoni number, so any change in surface tension is negligible.

An example that can be made is water. Water at 25^oC has the following properties, according to [Green and Perry (1973), Keenan et al. (1969) and Bejan (2016)]:

- Viscosity $\mu = 0.889\frac{mNs}{m^2}$,
- Density $\rho = 0.997\frac{kg}{m^3}$,
- Surface Tension $\sigma = 72\frac{mN}{m}$,
- Thermal Conductivity $\kappa = 0.608\frac{W}{mK}$,
- Heat Capacity $c_p = 4.186\frac{J}{gr^oC}$,
- Thermal Expansion Coefficient $\beta' = 214 * 10^{-6}\frac{1}{K}$.

Assuming a film where the characteristic height is $\delta < 10mm$ and a temperature difference $\Delta T = 15K$, the Marangoni and Rayleigh number can written as follow: $Ma = \frac{d\sigma}{dT}\frac{L\Delta T}{\mu\alpha'}$ and $Ray = \frac{g\beta'}{\nu\alpha'}\Delta T L^3$, where ν is the kinematic viscosity and α' is the thermal diffusivity. Those give thermal diffusivity $\alpha' \approxeq 0.04\frac{m^2}{s}$. With rate of change of surface tension with temperature $\frac{d\sigma}{dT} \approxeq 0.1\frac{mN}{m^oC}$, we get a Marangoni number $Ma \approxeq 0.42$ and Rayleigh number $Ray \approxeq 0.90{\cdot}10^{-3}$.Those mean that both Marangoni and Rayleigh number can be negligible since are smaller than the critical values ($Ma << 80$). Lastly, in some points across this project, we assume that the Brinkamn number (λ) is small ($\lambda = O(\epsilon)$, where $\epsilon = \frac{\delta}{L} << 1$).

5.2 Governing Equations

Taking into account these assumptions, the energy (5.2.0.1), continuity (5.2.0.2), and Navier-Stokes (5.2.0.3,5.2.0.4) equations, for a Newtonian fluid, are written as follows:

$$\rho\hat{C_p}\Big(uT_x + vT_y\Big) = \kappa\Big(T_{xx} + T_{yy}\Big) + \eta\Big(2u_x^2 + (u_y + v_x)^2 + 2v_y^2\Big) \quad (5.2.0.1)$$

$$u_x + v_y = 0 \quad (5.2.0.2)$$

$$\rho\Big(uu_x + vu_y\Big) = -P_x + 2\eta_x u_x + 2\eta u_{xx} + \eta_y\Big(v_x + u_y\Big) + \eta\Big(v_{xy} + u_{yy}\Big) + \rho g \sin\theta \quad (5.2.0.3)$$

$$\rho\Big(uv_x + vv_y\Big) = \eta_x\Big(v_x + u_y\Big) + \eta\Big(v_{xx} + u_{xy}\Big) - P_y + 2\eta_y v_y + 2\eta v_{yy} - \rho g \cos\theta \quad (5.2.0.4)$$

where: $\hat{C_p}$ is the specific heat capacity at constant pressure, T the temperature, k is the thermal conductivity, η is the viscosity, ρ density, and u and v the velocity in the x and y direction, respectively.

5.3 Boundary Conditions

The corresponding boundary conditions to the system (5.2.0.1 to 5.2.0.4) are the temperature and the 2 no slip conditions on the bottom, and the kinematic, temperature, normal and tangential stress balance at the interface.

No-slip condition at the wall

This boundary condition says that the fluid on contact with the wall will have the same velocity as the velocity of the wall, which in that case is zero.

$$u\Big|_{y=0} = v\Big|_{y=0} = 0 \tag{5.3.0.1}$$

Temperature Conditions

We assume that the temperature on the interface is equal to the ambient temperature T_f. At the lower wall we investigate two scenarios,
$T\Big|_{y=0} = \epsilon f(X)$ (chapter 5.5), where$X$ is slowly varying valuable (long wave assumption) and $T\Big|_{y=0} = \epsilon f(x)$ (chapter 5.8).

Kinematic Condition

The fluid particles on the free surface always remain part of the free surface, therefore we must have

$$v\Big|_{y=S} = uS_x \tag{5.3.0.2}$$

Stress Balance Conditions

If two viscous fluids meet and form a flow boundary, this same boundary condition would require that the stress in one fluid equals the stress in the

other at the boundary. The stress balance is:

$$\boldsymbol{n}\cdot\bar{\boldsymbol{T}}+\hat{\boldsymbol{n}}\cdot\bar{\hat{\boldsymbol{T}}}=\sigma\boldsymbol{n}(\nabla\cdot\boldsymbol{n})-\nabla\sigma \quad , \tag{5.3.0.3}$$

where: σ is the interfacial tension which is constant (see section 5.1 Problem Formulation), $\sigma\boldsymbol{n}(\nabla\cdot\boldsymbol{n})$ is the normal curvature force per unit area associated with local curvature of interface, $\nabla\sigma$ is the tangential stress associated with gradients in surface tension,

$\boldsymbol{n}=\dfrac{\Big(-S_x,1\Big)}{\Big(1+(S_x)^2\Big)^{\frac{1}{2}}}$ the unit inward normal to the surface and $\hat{\boldsymbol{n}}$ the unit outward normal ($\hat{\boldsymbol{n}}=-\boldsymbol{n}$), $\boldsymbol{t}=\dfrac{\Big(1,S_x\Big)}{\Big(1+(S_x)^2\Big)^{\frac{1}{2}}}$ the tangential vector, and $\bar{\boldsymbol{T}}$ and $\bar{\hat{\boldsymbol{T}}}$ are the stress tensors. These lead to

Normal Stress Balance

$$\begin{aligned}
&\boldsymbol{n}\cdot\bar{\boldsymbol{T}}\cdot\boldsymbol{n}-\boldsymbol{n}\cdot\bar{\hat{\boldsymbol{T}}}\cdot\boldsymbol{n}=\sigma(\nabla\cdot\boldsymbol{n})\Rightarrow\\
&n_1\Big(T_{11}\cdot n_1+T_{21}\cdot n_2\Big)+n_2\Big(T_{12}\cdot n_1+T_{22}\cdot n_2\Big)=\sigma\nabla\cdot\boldsymbol{n}\\
&-S_x\Bigg(\Big(-P+2\eta u_x\Big)(-S_x)+\eta(u_y+v_x)\Bigg)+\eta(u_y+v_x)(-S_x)\\
&-P+2\eta v_y=\sigma\frac{S_{xx}}{\Big(1+(S_x)^2\Big)^{\frac{1}{2}}}
\end{aligned} \tag{5.3.0.4}$$

Tangential Stress Balance

$$\begin{aligned}
&\boldsymbol{n}\cdot\bar{\boldsymbol{T}}\cdot\boldsymbol{t}+\hat{\boldsymbol{n}}\cdot\bar{\hat{\boldsymbol{T}}}\cdot\boldsymbol{t}=0\Rightarrow\\
&n_1\Big(T_{11}\cdot t_1+T_{21}\cdot t_2\Big)+n_2\Big(T_{12}\cdot t_1+T_{22}\cdot t_2\Big)=0\\
&-S_x\Bigg(\eta u_x+\eta\Big(u_y+v_x\Big)S_x\Bigg)+\eta(u_y+v_x)+2\eta v_yS_x=0
\end{aligned} \tag{5.3.0.5}$$

where: $\boldsymbol{t}=[t_1 \quad t_2]$ is a unit vector tangent to the interface. Note that on

the free surface is $\bar{\hat{\boldsymbol{T}}} = 0$. In the following section we will scale the above equations and boundary conditions.

5.4 Non-dimensionalization

We shall convert the governing equations (5.2.0.1 to 5.2.0.4) into dimensionless form. For this purpose, we use the characteristic thickness, δ. The non-dimensional independent and dependent variables are

$$x = \delta x^*, \quad y = \delta y^*, \quad u = \frac{\delta^2 \rho g \sin\theta}{\mu} u^*, \quad P = P^* \delta \rho g \sin\theta,$$
$$\Theta = \frac{T - T_f}{T_0 - T_f}, \quad \beta = \alpha(T_0 - T_f) \tag{5.4.0.1}$$

Note that for the scaling, we assumed that the lower surface has an average temperature T_0. This may seem odd, but it is a simplification that can be made as we will explain in the next two sections. Substitution of (5.4.0.1) into (5.2.0.1)-(5.2.0.4) and after dropping asterisks forthwith for convenience:

5.4.1 Governing Equations

Energy Equation:

$$\Theta_{xx} + \Theta_{yy} + \lambda e^{-\beta\Theta}\Big(2u_x^2 + (u_y + v_x)^2 + 2v_y^2\Big) = \xi\Big(u\Theta_x + v\Theta_y\Big) \tag{5.4.1.1}$$

Continuity

$$u_x + v_y = 0 \tag{5.4.1.2}$$

Cauchy x-direction:

$$R\Big(uu_x + vu_y\Big) = -P_x + 2(e^{-\beta\Theta})_x u_x + e^{-\beta\Theta}u_{xx} + (e^{-\beta\Theta})_y\Big(v_x + u_y\Big) + e^{-\beta\Theta}u_{yy} + 1 \tag{5.4.1.3}$$

Cauchy y-direction:

$$R\Big(uv_x + vv_y\Big) = (e^{-\beta\Theta})_x\Big(u_y + v_x\Big) + e^{-\beta\Theta}v_{xx} - P_y + 2(e^{-\beta\Theta})_y v_y + e^{-\beta\Theta}v_{yy} - \cot\theta \tag{5.4.1.4}$$

where: $\lambda = \frac{(\delta^2\rho g\sin\theta)^2}{\mu\kappa(T_0 - T_f)}$ is the Brinkman number which is the ratio between heat produced by viscous dissipation and heat transported by molecular conduction, $R = \frac{\delta^3\rho^2 g\sin\theta}{\mu^2}$ is the Reynolds which is the ratio between inertial forces in a fluid over viscous forces, and $\xi = \frac{\hat{C_p}\delta^3 g\rho^2\sin\theta}{\mu\kappa}$ is the Grashof number which is the Reynolds number times the ratio of the force due to differences in density and the viscous force. More specific, it is defined as the ratio of the buoyant to viscous force acting on the fluid. In other worlds, that ratio predicts the dominant effect of the heat transfer, the natural convection or the forced conviction

5.4.2 Boundary Conditions

We non-dimensionalize the corresponding boundary (5.3.0.1-5.3.0.5) using the 5.4.0.1 and after dropping the asterisks:

No-Slip:

$$u\Big|_{y=0} = v\Big|_{y=0} = 0 \tag{5.4.2.1}$$

Kinematic Condition

$$v\Big|_{y=S} = uS_x \tag{5.4.2.2}$$

Normal Stress Balance

$$-S'\Big(\Big(-P+2e^{-\beta\Theta}u_x\Big)(-S')+e^{-\beta\Theta}(u_y+v_x)\Big)+e^{-\beta\Theta}(u_y+v_x)(-S')$$
$$-P+2e^{-\beta\Theta}v_y=\gamma\frac{S''}{\Big(1+(S')^2\Big)^{\frac{1}{2}}} \tag{5.4.2.3}$$

Tangential Stress Balance

$$-S'\left(e^{-\beta\Theta}u_x+e^{-\beta\Theta}\Big(u_y+v_x\Big)S'\right)+e^{-\beta\Theta}(u_y+v_x)+2e^{-\beta\Theta}v_yS'=0 \tag{5.4.2.4}$$

where γ is the dimensionless surface tension, $\gamma=\frac{\sigma}{\delta^2\rho g\sin\theta}$.

Temperature Conditions

The dimensionless temperature on the interface is zero (5.4.2.5)and on the wall has small distributions (5.4.2.6),see section 5.5), or it's slowly varying (5.4.2.7), see section 5.8).

$$\Theta\Big|_{y=S}=0, \tag{5.4.2.5}$$

$$\Theta\Big|_{y=0}=1+\epsilon f(X), \tag{5.4.2.6}$$

$$\Theta\Big|_{y=0}=1+\epsilon f(x) \tag{5.4.2.7}$$

5.5 Non-uniformly Heated Falling Film - Long Wave Asymptotic Analysis

Imagine a two-dimensional flow of an incompressible Newtonian fluid of density ρ and variable viscosity η_t driven by gravity along an inclined, at an angle θ to the horizontal, plate, as shown in figure 5.1 (previous chapter). The angle θ is smooth and does not impose any instabilities. The temperature at the bottom surface varies, the temperature at the free surface (T_f) is constant and equals the ambient temperature, and the fluid temperature is T. At the lower wall, no slip boundary condition is applied and the dimensionless temperature is $\Theta_{y=0} = 1 + \epsilon f(X)$ (for more see 5.4.2). In order to go beyond linear theory without using any numerical simulations of the Navier-Stokes equations, we proceed asymptotically and seek a system of nonlinear evolution equations. The surface deformations are long compared with the channel height. More precisely we assume that the typical interfacial deformation wavelength λ' is large compared with the channel height δ, i.e. $\epsilon = \delta/\lambda' << 1$, providing scale separation (which means that $\epsilon x \to X$) [Sibgatullin and Sibgatullina (2003)]. As a result of the complexity of this problems, perturbation theory is used. That leads to an expression for the desired solution in terms of a formal power series (perturbation series) in some small parameter (ϵ) Henry (2005). As a result the dimensionless variables are:

$$\begin{aligned}
\Theta &= \Theta_0(y) + \epsilon\Theta_1(X,y) + \cdots + \epsilon^\nu\Theta_\nu(X,y) + \cdots \\
u &= u_0(y) + \epsilon u_1(X,y) + \cdots + \epsilon^\nu u_\nu(X,y) + \cdots \\
v &= \epsilon u_1(X,y) + \cdots + \epsilon^\nu u_\nu(X,y) + \cdots \\
S(X) &= 1 + \epsilon h_1(X) + \cdot\cdot + \epsilon^\nu h_\nu(X) + \cdots \\
P &= P_0(X,y) + \epsilon P_1(X,y) + \cdots + \epsilon^\nu P_\nu(X,y) + \cdots
\end{aligned} \tag{5.5.0.1}$$

Finally, we assume that the Grashof number is zero, Brinkman number is small ($\lambda = \epsilon\Lambda$), and the dimensionless surface tension is big ($\Gamma = \epsilon^3\gamma$). Substituting the above expansions (5.5.0.1) in the dimensionless governing equations (5.4.1.1-5.4.1.4) and the corresponding boundary conditions (5.4.2.1-

5.3.0.5) the leading and $O(\epsilon)$ terms are

Leading Order

$$\Theta_{0yy} = 0 \tag{5.5.0.2}$$

$$-\beta e^{-\beta\Theta_0}\Theta_{0y}u_{0y} + e^{-\beta\Theta_0}u_{0yy} + 1 = 0 \Rightarrow \tag{5.5.0.3}$$
$$u_0 = -\int_0^y y' e^{\beta\Theta_0} dy' + \int_0^y c_1 e^{\beta\Theta_0} dy'$$

$$-P_{0y} - \cot\theta = 0 \tag{5.5.0.4}$$

O(ϵ)

$$\Theta_{1yy} + \Lambda e^{-\beta\Theta_0}\Big(u_{0y}\Big)^2 = 0 \tag{5.5.0.5}$$

$$\begin{aligned} Rv_1 u_{0y} = &- P_{0X} - \beta e^{-\beta\Theta_0}\Theta_{1y}u_{0y} - \beta e^{-\beta\Theta_0}\Theta_{0y}u_{1y} \\ &+ \beta^2 e^{-\beta\Theta_0}\Theta_1\Theta_{0y}u_{0y} + e^{-\beta\Theta_0}u_{1yy} - \beta e^{-\beta\Theta_0}\Theta_1 u_{0yy} \end{aligned} \tag{5.5.0.6}$$

$$-P_{1y} - 2\beta e^{-\beta\Theta_0}\Theta_{0y}v_{1y} + 2e^{-\beta\Theta_0}v_{1yy} = 0 \tag{5.5.0.7}$$

The **continuity equation** (5.4.1.2) becomes:

$$u_x + v_y = 0 \rightarrow \quad O(\epsilon): \quad v_{1y} = 0$$
$$O(\epsilon^2): \quad v_{2y} = -u_{1X}$$

Boundary Conditions

On the wall we have the no-slip conditions (5.4.2.1) and the temperature conditions (5.4.2.6). The free surface requires the following boundary conditions to be applied: the kinematic condition (5.4.2.2), which relates the motion of the free surface to the fluid velocities at the free surface and the dynamic conditions, which are the normal (5.4.2.3) and tangential (5.4.2.4) stress balance. The surface is located at $y = S$ where $S = 1 + \epsilon h_1$ (5.5.0.1)with $\epsilon h_1 << 1$. To square the domain we use the basic Taylor series method for the denominator($u(x, 1 + \epsilon h_1) = u(x, 1) + \epsilon h_1 \frac{\partial u(x,1)}{\partial y} + \frac{(\epsilon h_1)^2}{2!} \frac{\partial^2 u(x,1)}{\partial y^2} + \cdots$). [Fenton (1983),Blyth et al. (2003)]. Substituting the previous expansions (5.5.0.1) we get:

On the wall

$$\text{No slip:} \quad u_0\Big|_{y=0} = u_1\Big|_{y=0} = v_1\Big|_{y=0} = v_2\Big|_{y=0} = 0 \tag{5.5.0.8}$$

$$\text{Temperature:} \quad \Theta_0 = 1\Big|_0 \quad and \quad \Theta_1\Big|_{y=0} = f(X) \tag{5.5.0.9}$$

On the surface

$$\text{Temperature:} \quad \Theta = 0\Big|_{y=S} \Rightarrow \quad \Theta_0\Big|_{y=1} = 0 \quad \text{and} \quad h_1\Theta_{0y} + \Theta_1\Big|_{y=1} = 0 \tag{5.5.0.10}$$

$$\text{Normal Stress Balance:} \quad -P_0 = -\gamma\epsilon^3 h_1''\Big|_{y=1+\epsilon h_1} \Rightarrow$$

$$P_0\Big|_{y=1} = \Gamma h_1'', \text{and} \tag{5.5.0.11}$$

$$-P_1 - P_{0y}h_1\Big|_{y=1} = \Gamma h_2'' \tag{5.5.0.12}$$

Note that we assumed $\gamma = O(\frac{1}{\epsilon^3})$ and so $\gamma = \frac{1}{\epsilon^3}\Gamma$ .Furthermore, from equation (5.5.0.4) we know that $P_0 = y\cot\theta + c_5(X)$, where $c_5(X)$ is a function of X. This yields to $c_5(X) = -\cot\theta + \Gamma h_1''$, and finally:

$$P_0 = \cot\theta(1-y) + \Gamma h_1'' \tag{5.5.0.13}$$

$$\text{Tangential Stress Balance :} \quad u_{0y}\Big|_{y=1} = 0, \quad \text{and} \tag{5.5.0.14}$$

$$h_1 u_{0yy} + u_{1y}\Big|_{y=1} = 0 \tag{5.5.0.15}$$

$$\text{Kinematic Condition:} \quad v_1\Big|_{y=1} = 0 \tag{5.5.0.16}$$

$$v_2\Big|_{y=1} = u_0 h_1' \tag{5.5.0.17}$$

Using the conditions (5.5.0.9-5.5.0.17)with the assumption of the Brinkman number is $O(\epsilon)$, $\lambda = \epsilon\Lambda$ we can solve the base flow analytically; the leading and $O(\epsilon)$ parts of the governing equations (5.5.0.2) to (5.5.0.7).

$$\Theta_{0yy} = 0 \Rightarrow \Theta_0 = c_1 y + c_2 \tag{5.5.0.18}$$

But eq. (5.5.0.9) gives $c_2 = 1$ and (5.5.0.10) $c_1 = -c_2 = -1$. So:

$$\Theta_0 = 1 - y \tag{5.5.0.19}$$

Substituting the equation (5.5.0.2) and the boundary conditions (5.5.0.13-5.5.0.16) into the (5.5.0.3), we get

$$u_0 = \frac{e^{-\beta(y-1)}}{\beta^2}(1 - \beta + y\beta) - \frac{(1-\beta)e^{\beta}}{\beta^2}$$

And eq. (5.5.0.13) gives:

$$P_0 = \cot\theta(1-y) + \Gamma h_1''.$$

Dealing with $O(\epsilon)$ terms, eq. (5.5.0.18) gives

$$\Theta_{1yy} + \Lambda e^{-\beta\Theta_0}\Big(u_{0y}\Big)^2 = 0$$

$$\Theta_1 = c_7(X) + c_6(X)y - \frac{\Lambda e^{-\beta(y-1)}}{\beta^2}\Big(\frac{6}{\beta^2} + (y-1)^2 + \frac{4(y-1)}{\beta}\Big)$$

where: $c_7(X) = f(X) + \frac{\Lambda e^{\beta}}{\beta^4}\Big(6 - 4\beta + \beta^2\Big)$ from eq.(5.5.0.9) and $c_6(X) = -f(X) - \frac{\Lambda e^{\beta}}{\beta^4}\Big(6 - 4\beta + \beta^2\Big) + \frac{6\Lambda}{\beta^4} + h_1$ from eq.(5.5.0.10)

And eq. (5.5.0.6) becomes:

$$-P_{0X} - \beta e^{-\beta\Theta_0}\Theta_{0y}u_{1y} - \beta e^{-\beta\Theta_0}\Big(\Theta_{1y} - \beta\Theta_1\Theta_{0y}\Big)u_{0y} + e^{-\beta\Theta_0}\Big(u_{1yy} - \beta\Theta_1 u_{0yy}\Big) = 0$$

$$\Rightarrow -P_{0X} + \Big(e^{-\beta\Theta_0}u_{1y}\Big)_y - \Big(\beta e^{-\beta\Theta_0}u_{0y}\Theta_1\Big)_y = 0$$

$$u_1 = c_9(X) - \frac{e^{-\beta(y-1)}}{\beta}c_8(X) - \frac{e^{-2\beta(y-1)}}{8\beta^5}\Big(23\Lambda - 46\beta\Lambda + 22\beta^2\Lambda - 4\beta^3\Lambda$$
$$- 44\beta^2\Lambda y + 12\beta^3\Lambda y + 22\beta^2\Lambda y^2 - 12\beta^3\Lambda y^2 + 4\beta^3\Lambda y^3 + 8\beta^4\Lambda y e^{\beta(y-1)}c_{5X}(X)$$
$$- 16\beta^4 y e^{\beta(y-1)}c_6(X) + 8\beta^5 y e^{\beta(y-1)}c_6(X) - 8\beta^5 y e^{\beta(y-1)}c_7(X)$$
$$- 8\beta^5 y^2 e^{\beta(y-1)}c_6(X)\Big),$$

with boundary conditions: $u_1(X,0) = 0$ and $u_1(X,1)_y = h_1 u_{0yy}$. These yield to:
$c_9(X) = \frac{e^\beta}{\beta^2}c_8 + \frac{e^{2\beta}}{8\beta^5}\Big(23\Lambda - 46\beta\Lambda + 22\beta^2\Lambda - 4\beta^3\Lambda\Big)$ and $c_8(X) = -P_{0x} + h_1$. The continuity equation is $u_{1X} + v_{2y} = 0$ with boundary conditions: $v_2(X,0) = 0$ and $v_2(X,1) = u_0(1)h_1'$ These give:

$$v_2 = c_{10}(X) \Rightarrow -c_{9X}(X)y - \frac{e^{-\beta(y-1)}}{\beta^3}\Big(2\beta c_{6X}(X) - 2\beta c_{7X}(X) + \beta c_{8X}(X)$$
$$- 6c_{6X}(X) + 2c_{5XX}(X) + \beta^2 y c_{6X}(X) - \beta^2 y c_{7X}(X) + \beta y c_{5XX}(X)$$
$$- \beta^2 y^2 c_{6X}(X) - 4\beta y c_{6X}(X)\Big),$$

where: $c_{10}(X) = \frac{e^\beta}{\beta^3}\Big(2\beta c_{6X}(X) - 2\beta c_{7X}(X) + \beta c_{8X}(X) - 6c_{6X}(X) + 2c_{5XX}(X)\Big)$ and $c_{5XX}(X)(\beta - 2(e^\beta - 1)) = -h_1'\beta + 2c_{6X}(X)(\beta(e^\beta + 1) + 3(1 - e^\beta)) + \beta c_{7X}(X)(2(1 - e^\beta) + \beta) - c_{9X}(X)\beta + c_{8X}(X)(e^\beta - 1)\beta$

Finally substituting everything into the last equation we get:

$$\Gamma h_1^{(4)}\Big(e^\beta\beta^2 - 2\beta e^\beta + 2e^\beta - 2\Big) + h_1'\Big(-6e^\beta + 5e^\beta\beta + \beta + 6 - \beta^2 - \beta^2 e^\beta - \beta^3 e^\beta\Big)$$
$$+ f'(X)\Big(6e^\beta(1 - \beta) + 3e^\beta\beta^2 - e^\beta\beta^3 - 6\Big) = 0 \qquad (5.5.0.20)$$

This fourth order ODE (5.5.0.20) is the final solution to our problem. The h_1 term reveals the relationship between temperature conditions with the velocity profile. The above equation can be solved numerically. As a result, we carried out extensive numerical experiments where the parameters vary. Note that $f(x)$ should be bounded at $\pm\infty$ ($\lim_{x\to\pm\infty} f(x) = 0$), and for this particular problem we set two possible types, an even function, $f(X) = e^{-X^2}$,

and an odd $f(X) = Xe^{-X^2}$.

5.6 Dimensionless surface tension and deformation of the surface

Before we present the numerical experiments, we explore the properties of the above ODE in a try to predict the behaviour of the shape of the interface after the parameters β and Γ change. When $x \to \pm\infty$ then $f(x) \to 0$. If we set $A = \frac{-6e^{\beta}+5e^{\beta}\beta+\beta+6-\beta^2-\beta^2e^{\beta}-\beta^3e^{\beta}}{\Gamma\left(e^{\beta}\beta^2-2\beta e^{\beta}+2e^{\beta}-2\right)}$ then the limit of the ODE 5.5.0.20 is $lim_{x\to\infty}\left(\Gamma h_1^{(4)} + Ah_1'\right)$.
The three solutions of a third order ODE like $h_1(x)''' + Ah_1(x) = 0$, with $A > 0$, are $h_1 = \begin{cases} e^{\left(A^{\frac{1}{3}}e^{\frac{i\pi}{3}}x\right)} = e^{\left(xA^{\frac{1}{3}}(\frac{1}{2}+i\frac{\sqrt{3}}{2})\right)}, \\ e^{\left(xA^{\frac{1}{3}}e^{i\pi}\right)} = e^{-A^{\frac{1}{3}}x} \quad \text{and} \\ e^{\left(A^{\frac{1}{3}}e^{\frac{5i\pi}{3}}x\right)} = e^{\left(xA^{\frac{1}{3}}(\frac{1}{2}-i\frac{\sqrt{3}}{2})\right)}. \end{cases}$
When $x \to -\infty$ the second solution is not acceptable since the wave has infinite amplitude, while it's accepted when $x \to \infty$ since the others produce waves with infinite amplitude.

What the above means are that the frequency of the stationary wave λ' is analogue to Γ^3 and more specific $\lambda' = \frac{4\pi}{A^{\frac{1}{3}}\sqrt{3}}$, when $x \to -\infty$, and an increase of Γ yields to an increase of the wavelength. When $x \to \infty$, the solution of the ODE is $e^{-A^{\frac{1}{3}}x}$, and that leads to an exponential decay to zero where an increase on Γ gives a faster decrease on the deformation of the surface.

5.7 Numerical Experiments

The numerical method for solving the 5.5.0.20 that we use in that section is a build-in routine on MatLab® specific used on ODE boundary value problems (bvp4c). This routine is a finite difference code that implements the three-stage Lobatto IIIa formula [Kierzenka and Shampine (2001),Shampine et al. (2000)]. We investigate two temperature wall conditions and evaluate the effect of different parameters on the stationary waves of the surface.

Wall Condition: $f(X) = e^{-X^2}$

We shall begin with the even function $f(X) = e^{-X^2}$. The dimensionless group parameters are as follow:

- Brinkman Number $\Lambda = 1$,
- Viscosity parameter $\beta = 1$,
- Dimensionless Surface tension $\Gamma = 1$.

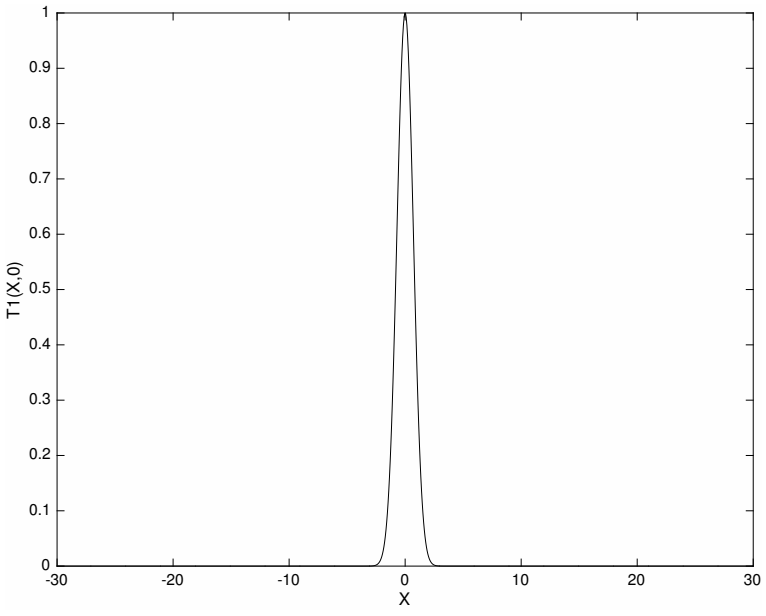


Figure 5.1: $T_1(X, 0)$, where $\lambda, \beta, \Gamma = 1$.

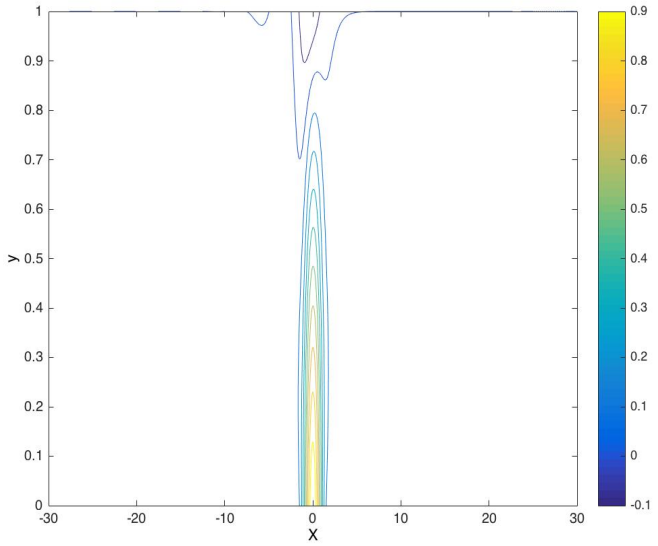


Figure 5.2: Isothermal lines of T_1. The dimensionless group is the same as in Fig. 5.1.

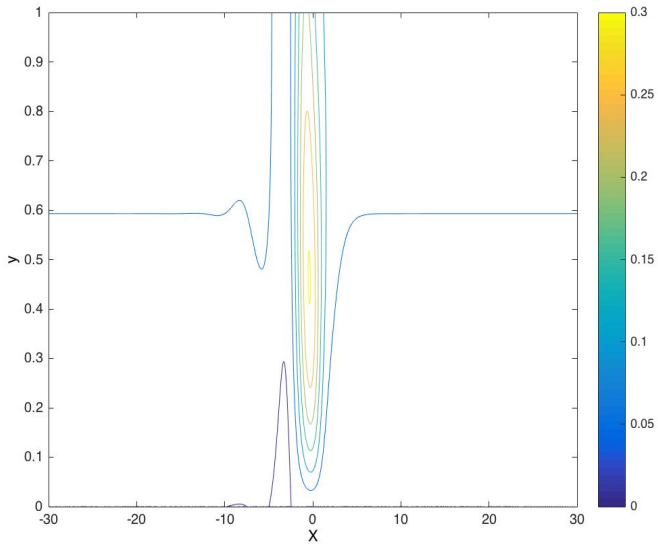


Figure 5.3: u_1 streamlines. The dimensionless group is the same as in Fig. 5.1.

Fig.5.2 illustrates the isothermal lines of T_1, with dimensionless parameters

as stated above. As expected, the isothermal lines are symmetrical, that points they follow the surface shape. That means fig.5.2 and fig.5.6 are in good agreement.

Contribution of Brinkman to Velocity And Temperature Profile

Fig5.4 shows how the Brinkman number influences the velocity distribution in a symmetrically heated plate, for fixed values of surface tension and viscosity parameter. As the Brinkman number increases, it implies higher viscous dissipation in the flow, which in turn implies steeper velocities gradients at the plane. In fact, for Brinkman number $\Lambda = 0.1$ the velocity increases through y-direction, for $\Lambda = 1$ it still accelerates but slower, and finally for $\Lambda = 10$ it slows down, meaning more energy is consumed by viscous dissipation. This behaviour is clearly manifested in fig.5.5.

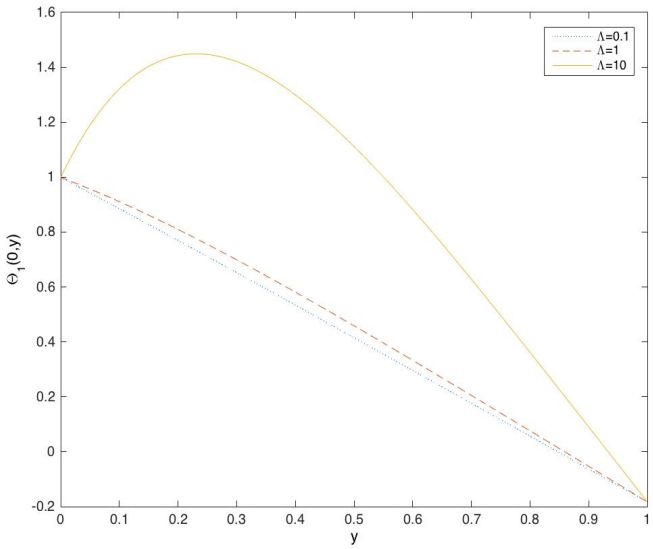


Figure 5.4: $\Theta_1(0, y)$ regarding different values of Brinkman number. The remaining dimensionless groups are the same as in Fig. 5.1.

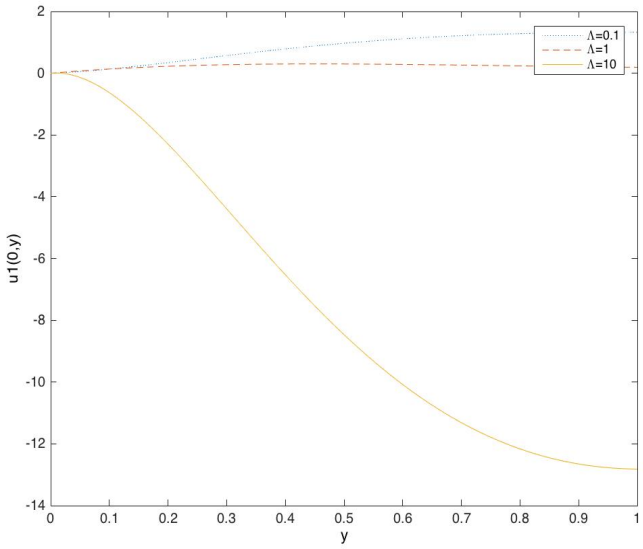


Figure 5.5: $u_1(0, y)$ regarding different values of Brinkman number. The remaining dimensionless groups are the same as in Fig. 5.1.

Contribution of β to Surface, Velocity And Temperature Profile

Stationary waves for the free surface for different values of the viscosity parameter β. By decreasing β, increasing viscosity and so decreasing the amplitude of distribution, but also oscillations start sooner. That is also illustrated in fig.5.8, where big values of β give higher peak velocity. Fig.5.8 shows that as viscosity parameter increases, the $u_1(0, y)$ increases, although the effects are small at $\beta = 0.1$. As noted earlier, a increase in β, decreases the fluid viscosity, which in turn increases the velocity, and less energy is consumed by viscous dissipation as is better shown in fig.5.7.

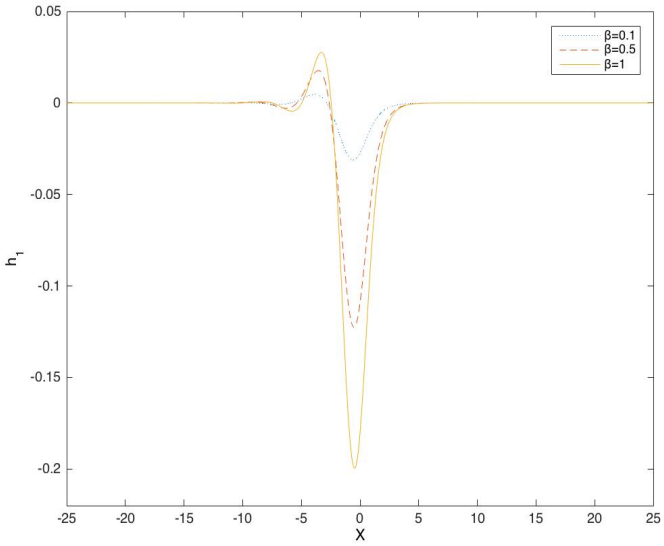


Figure 5.6: Stationary Waves for the free surface regarding different values of exponential constant β. The remaining dimensionless group is the same as in Fig. 5.1.

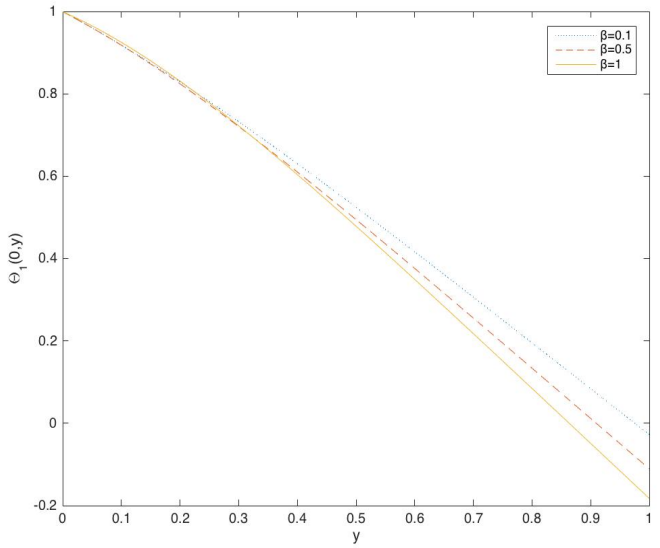


Figure 5.7: $\Theta_1(0, y)$ regarding different values of exponential constant β. The remaining dimensionless group is the same as in Fig. 5.1.

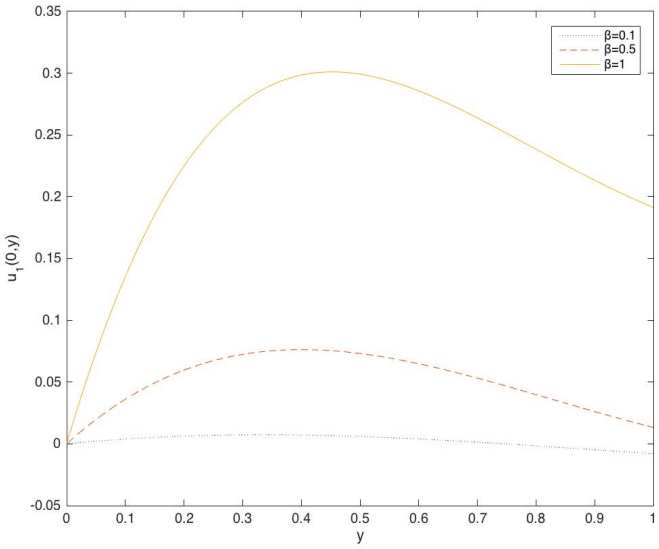


Figure 5.8: $u_1(0, y)$ regarding different values of exponential constant β. The remaining dimensionless group is the same as in Fig. 5.1.

Contribution of Dimensionless Surface Tension to Surface, Velocity and Temperature Profile

Stationary waves are plotted in fig.5.9. As dimensionless surface tension decreases, the amplitude of perturbation increases. However, the decrease in amplitude of h_1, makes oscillations start earlier. A 10 times decrease of surface tension, is translated to an average 46.5% decrease to the start point of perturbation.

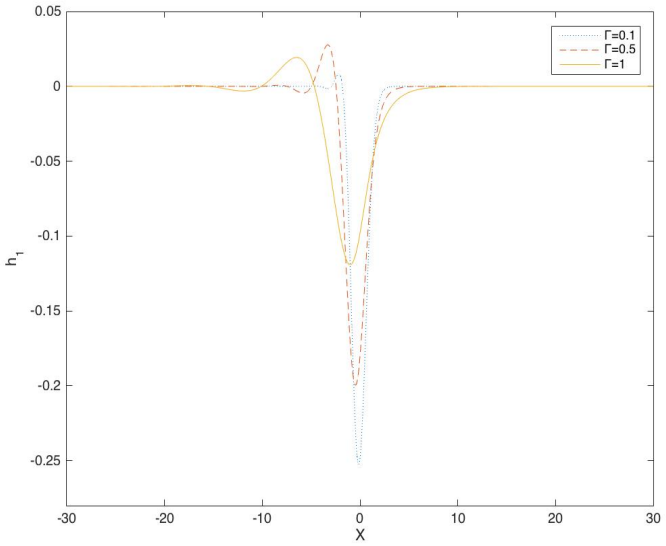


Figure 5.9: $h_1(X)$ regarding different values of dimensionless surface tension Γ. The remaining dimensionless group is the same as in Fig. 5.1.

The temperature distribution profile of fig.5.10 shows the decrease of temperature $T_1(0, y)$ regardless the surface tension, although the effect is small at $\Gamma = 0.1$ and $\Gamma = 1$. However, there is an intersection point around $y = 0.34$ between $\Gamma = 0.1$ and $\Gamma = 1$. Fig.5.11 represents the effect of dimensionless surface tension on the velocity distribution for fixed values of exponential viscosity parameter and Brinkman number. As expected, the peak velocity occurs before the centreline and closer to the wall and its location is slightly affected by the surface tension.

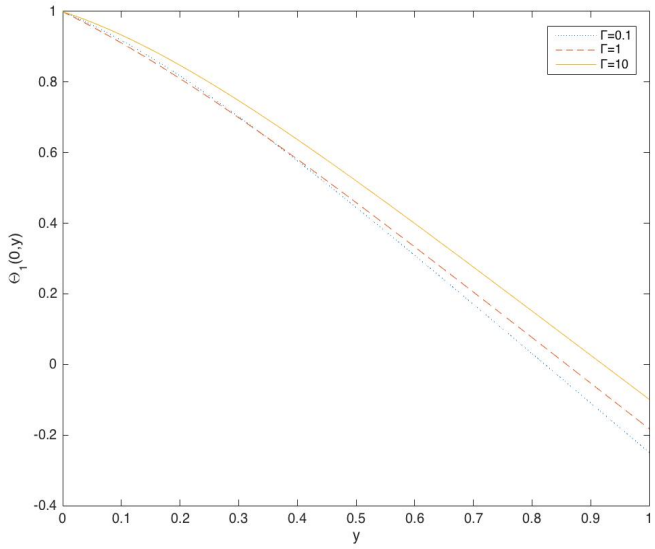


Figure 5.10: $\Theta_1(0, y)$ dimensionless surface tension Γ. The remaining dimensionless group is the same as in Fig. 5.1.

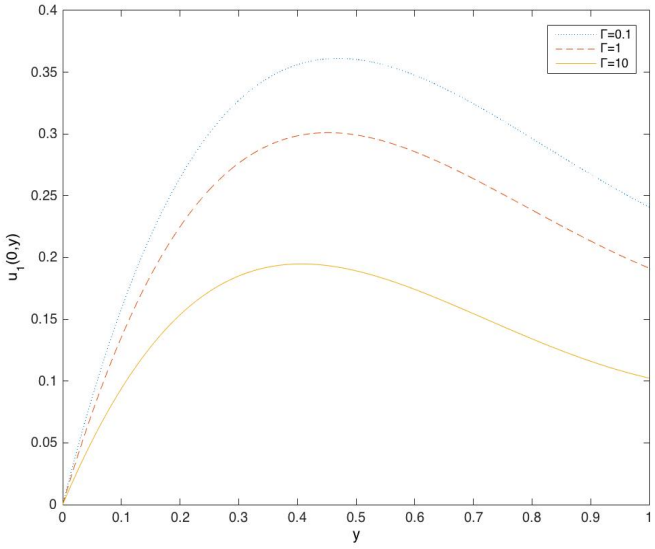


Figure 5.11: $u_1(0, y)$ dimensionless surface tension Γ. The remaining dimensionless group is the same as in Fig. 5.1.

WALL CONDITION: $f(X) = X * e^{-X^2}$

We shall continue with the odd function $f(X) = Xe^{-X^2}$, fig.5.12. The dimensionless group parameters are as follow unless otherwise stated:

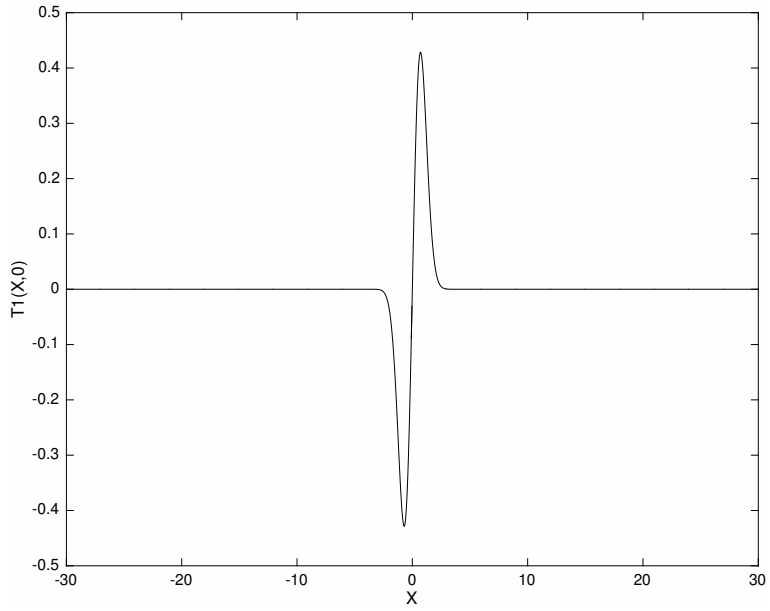


Figure 5.12: $T_1(X, 0)$, where $\lambda, \beta, \Gamma = 1$.

It is interesting to note the double peaks in figs.5.13 and 5.14 that agrees with fig.5.17.

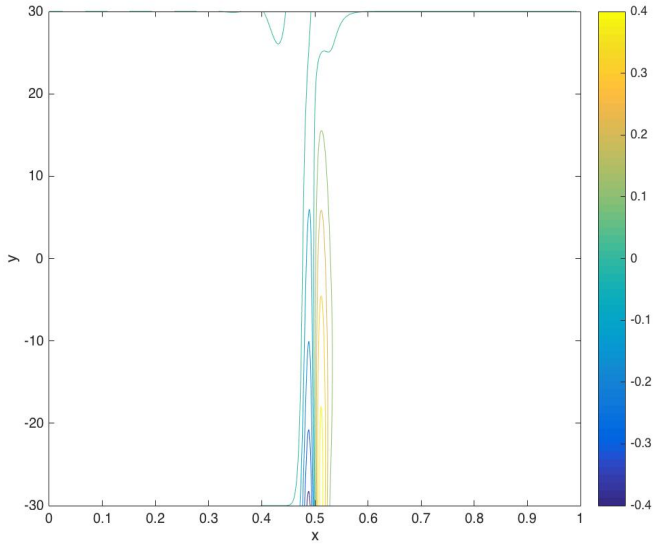


Figure 5.13: Isothermal lines of T1. The dimensionless group is the same as in Fig.5.12.

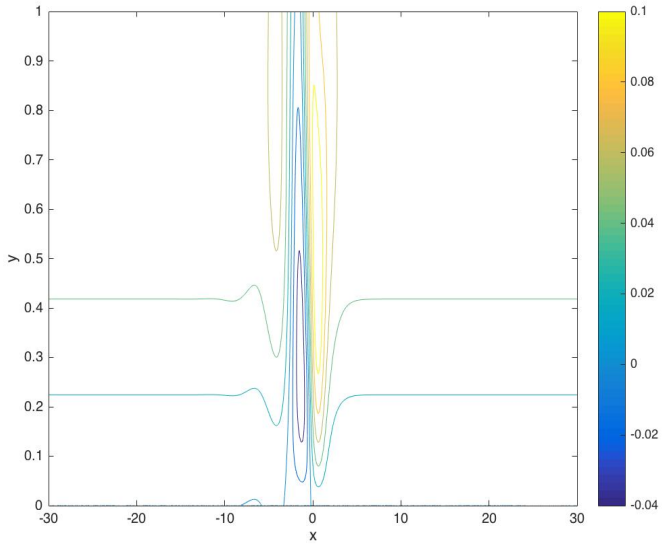


Figure 5.14: u_1 Streamlines. The dimensionless group is the same as in Fig.5.12.

Contribution of Brinkman Number

The heat generation increases sharply as Brinkman number increases (fig.5.15), like before, and the velocity profile, fig.5.16 is identical with the even case.

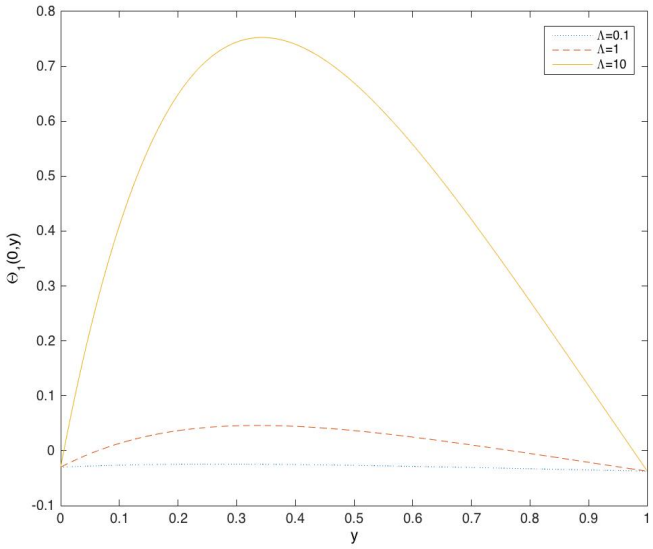


Figure 5.15: $\Theta_1(0, y)$ regarding different values of Brinkman number. The remaining dimensionless groups are the same as in Fig. 5.12.

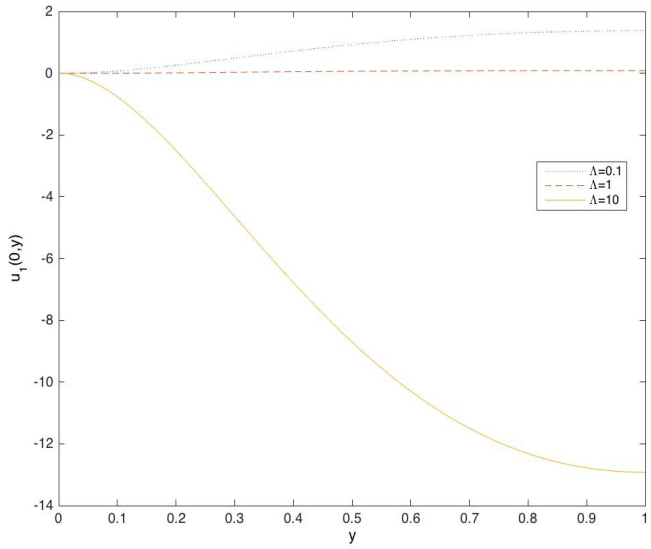


Figure 5.16: u1(0,y) regarding different values of Brinkman number. The remaining dimensionless groups are the same as in Fig. 5.12.

Contribution of Viscosity Exponential Parameter

Fig.5.17 represents the solitary pulses for the free surface for different values of the viscosity parameter β; by decreasing β , increasing viscosity and so decreasing the amplitude of distribution. Fig.5.19 shows that as viscosity parameter increases, the $u_1(0, y)$ increases, although the effects are small at $\beta = 0.1$. As noted earlier, an increase in β, decreases the fluid viscosity, which in turn increases the velocity, and less energy is consumed by viscous dissipation as is better shown in fig.5.18.

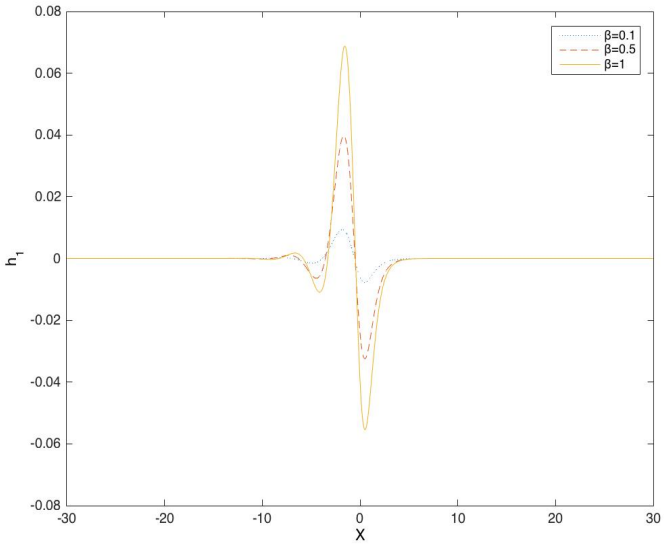


Figure 5.17: Stationary waves for the free surface regarding different values of exponential constant β. The remaining dimensionless group is the same as in Fig. 5.12.

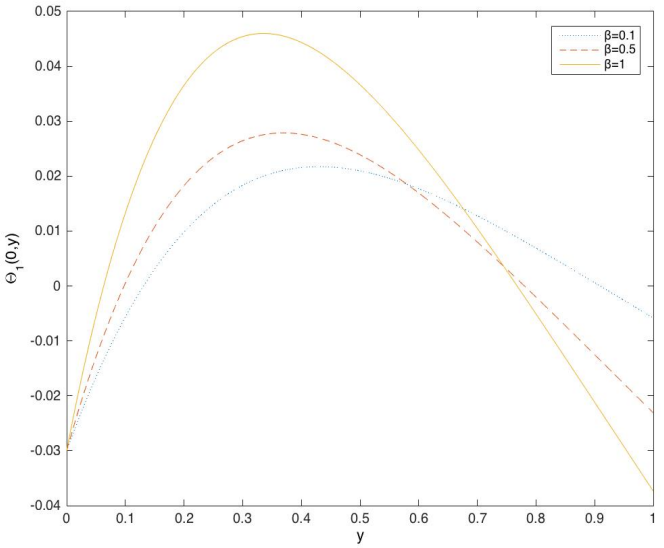


Figure 5.18: $\Theta_1(0, y)$ regarding different values of exponential constant β. The remaining dimensionless group is the same as in Fig. 5.12.

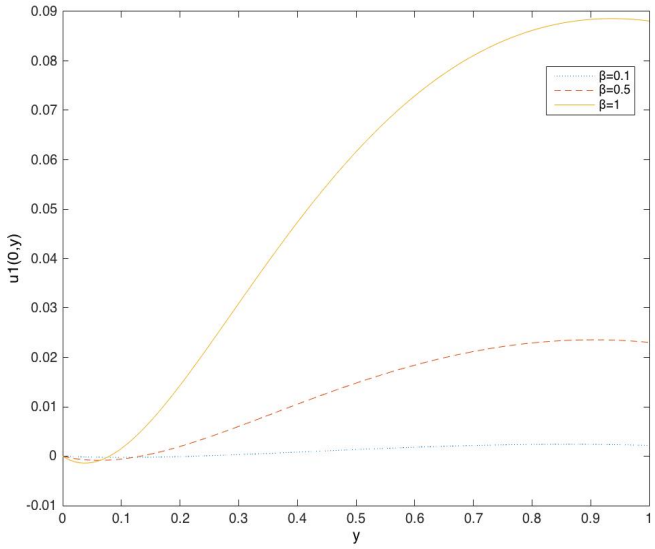


Figure 5.19: $u_1(0, y)$ regarding different values of exponential constant β. The remaining dimensionless group is the same as in Fig. 5.12.

Contribution of Dimensionless Surface Tension

Stationary waves are plotted in fig.5.20. As dimensionless surface tension decreases, the amplitude of perturbation increases. However, the decrease in amplitude of h_1, makes any perturbation appears earlier.

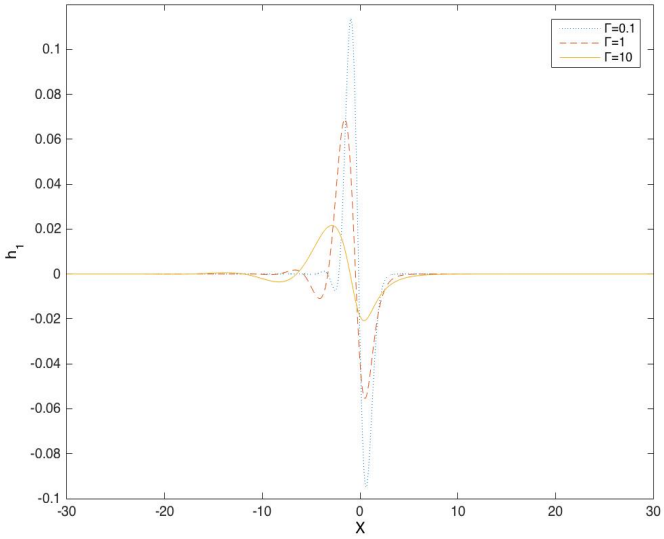


Figure 5.20: $h_1(X)$ regarding different values of dimensionless surface tension Γ. The remaining dimensionless group is the same as in Fig. 5.12.

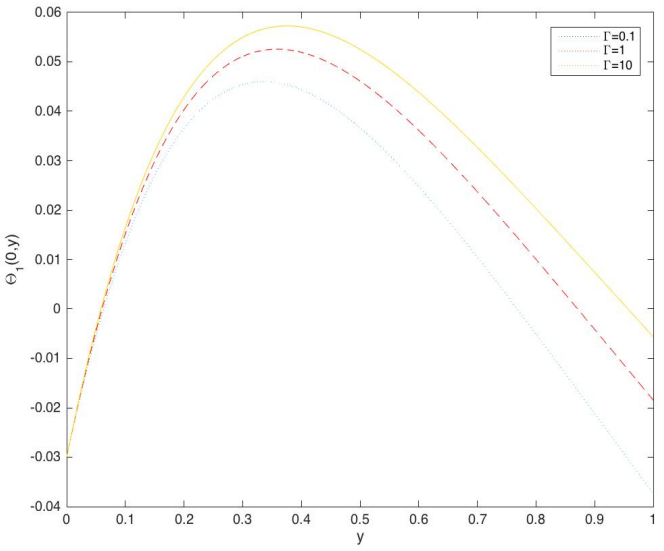


Figure 5.21: $\Theta_1(0, y)$ dimensionless surface tension Γ. The remaining dimensionless group is the same as in Fig. 5.12.

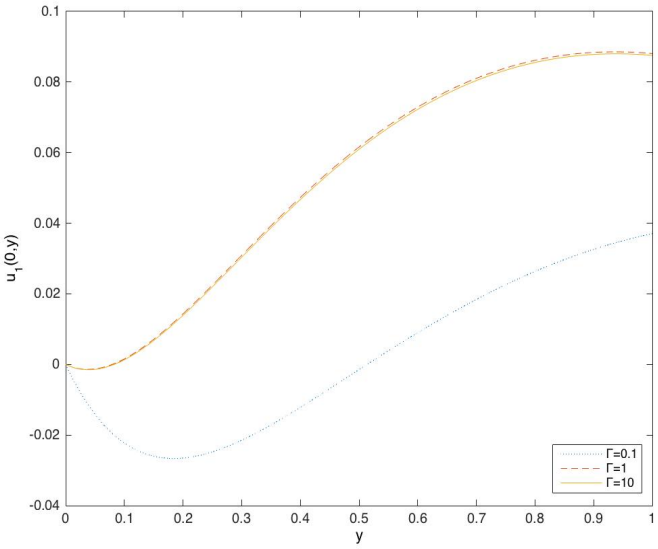


Figure 5.22: $u_1(0, y)$ regarding dimensionless surface tension Γ. The remaining dimensionless group is the same as in Fig. 5.12.

5.8 Weakly Heated Falling Films - Zero Brinkman Number

The problem as shown in Fig.5.1 concerns a fully developed Newtonian, gravity-driven film of thickness δ flowing along an inclined heated plate. The temperature on the lower wall varies ($\Theta_{y=0} = 1 + \epsilon f(x)$). We assume that Brinkamn number is zero ($\lambda = 0$), because that gives us the opportunity to solve the base flow analytically. Once again, we linearize the governing equations (5.4.1.1 -5.4.1.4), and the corresponding boundary conditions (5.4.2.1-5.3.0.5), using expansions (5.8.0.1), since this boundary value problem can only be solved numerically.

$$\begin{aligned} &\boldsymbol{\Theta} = \bar{\Theta}(y) + \epsilon\Theta(x,y), \quad \boldsymbol{u} = \bar{u}(y) + \epsilon u(x,y), \quad \boldsymbol{v} = \epsilon v(x,y) \\ &S(x) = 1 + \epsilon h(x), \quad \boldsymbol{P} = \bar{P}(y) + \epsilon P(x,y) \end{aligned} \tag{5.8.0.1}$$

The governing equations with the corresponding boundary conditions leading and $O(\epsilon)$ are written as follow

$$\bar{\Theta}_{yy} = 0 \Rightarrow \bar{\Theta} = c_1 y + c_2 \tag{5.8.0.2}$$

But $\boldsymbol{\Theta}\Big|_{y=0} = 1+\epsilon f(x) \Rightarrow \Theta\Big|_{y=0} = 1$ and so $c_2 = 1$ and $\boldsymbol{\Theta}\Big|_{y=1} = 0 \Rightarrow \bar{\Theta}\Big|_{y=1} = 0$ that leads $c_1 = -c_2 = -1$.
So:

$$\bar{\Theta} = -y + 1 \tag{5.8.0.3}$$

$$-\beta e^{-\beta\bar{\Theta}}\bar{\Theta}_y\bar{u}_y + e^{-\beta\bar{\Theta}}\bar{u}_{yy} = -1 \rightarrow \bar{u} = c_3 e^{-\beta y} - \frac{e^{-\beta y}}{\beta}\Big(c_4 e^{\beta} - e^{\beta} y\Big)$$

But equations (5.4.2.1) and (5.8.0.8) give:

$$c_3 = \frac{1-\beta}{\beta^2}e^{\beta}, \qquad c_4 = \frac{1-\beta}{\beta}e^{\beta}$$

And finally we have:

$$\bar{u} = \frac{e^{-\beta(y-1)}}{\beta^2}(1-\beta+y\beta) - \frac{(1-\beta)e^{\beta}}{\beta^2}, \tag{5.8.0.4}$$

$$\bar{P}_y + \cot\theta = 0 \overset{(5.8.0.6)}{\Rightarrow} \quad \bar{P} = \cot\theta(1-y)$$

And

$$\bar{u}_x + \bar{v}_y = 0 \rightarrow \qquad v_y = -u_x$$

Boundary Conditions

No-slip condition at the wall

$$\bar{u}\Big|_{y=0} = u\Big|_{y=0} = v\Big|_{y=0} = 0 \tag{5.8.0.5}$$

On the interface Normal Force Balance

$$\text{Leading Order:} \quad \bar{P}\Big|_{y=1} = 0 \tag{5.8.0.6}$$

$$\mathrm{O}(\epsilon): \quad -P + 2e^{-\beta\bar{\Theta}}v_y - \bar{P}_y h\Big|_{y=1} = -\Gamma h'' \tag{5.8.0.7}$$

Tangential Force Balance

$$\text{Leading Order:} \quad \bar{u}_y\Big|_{y=1} = 0 \tag{5.8.0.8}$$

$$\mathrm{O}(\epsilon): \quad h\bar{u}_{yy} + u_y + v_x\Big|_{y=1} = 0 \tag{5.8.0.9}$$

Kinematic Condition

$$\mathrm{O}(\epsilon): \quad v\Big|_{y=1} = \bar{u}h' \tag{5.8.0.10}$$

Temperature Conditions:
On the lower wall we have,

$$\mathbf{\Theta}\Big|_0 = 1 + \epsilon f(x) \rightarrow \quad \bar{\Theta} = 1\Big|_0, \quad \textbf{and} \quad \Theta\Big|_0 = f(x), \tag{5.8.0.11}$$

On the interface S(x) we have:

$$\mathbf{\Theta} = 0\Big|_{y=1+\epsilon h_1} \rightarrow \quad \bar{\Theta}\Big|_{y=1} = 0, \quad \text{and} \quad \Theta + h\bar{\Theta}_y = 0\Big|_{y=1} \tag{5.8.0.12}$$

To sum up the PDEs and the corresponding boundary conditions are:

$$\Theta_{xx} + \Theta_{yy} = \xi\Big(\bar{u}\Theta_x + v\bar{\Theta}_y\Big) \tag{5.8.0.13}$$

$$\begin{aligned} R\Big(\bar{u}u_x + v\bar{u}_y\Big) = -P_x + e^{-\beta\bar{\Theta}}\Big(u_{xx} - \beta\bar{\Theta}_y(u_y + v_x) \\ + \bar{u}_y(\beta^2\bar{\Theta}_y\Theta - \beta\Theta_y) + u_{yy} - \beta\Theta\bar{u}_{yy}\Big) \end{aligned} \tag{5.8.0.14}$$

$$R\bar{u}v_x = e^{-\beta\bar{\Theta}}\Big(- \beta\Theta\bar{u}_y + v_{yy} + v_{xx}\Big) - P_y - 2e^{-\beta\bar{\Theta}}\beta\bar{\Theta}_y v_y \tag{5.8.0.15}$$

In what follows we solve the problem numerically in order to describe the effect of the dimensionless parameters ($R, \beta, \Gamma,$ and ξ) on the system dynamics.

5.9 Numerical Experiments

The above PDEs (5.8.0.13-5.8.0.15) are solved numerically with a Finite Differences-based code for a variety of different heating scenarios. In contrast with the section 5.7 where a built-in Matlab® routine was used, in this sections we use a Finite Differences-based code specifically written for that system. Central finite difference method is selected, where second order approximations are preferred. Generally, the approximations for a function

$f(x)$ are as follow:

$$f'(x) \approx \frac{f(x+h) - f(x-h))}{2h} \tag{5.9.0.1}$$

$$f''(x) \approx \frac{f(x+h) - 2f(x) + f(x-h)}{h^2} \tag{5.9.0.2}$$

$$f'''(x) \approx \frac{f(x+2h) - 2f(x+h) + 2f(x-h) - f(x-2h)}{2h^3}, \text{ and} \tag{5.9.0.3}$$

$$f^{(4)} \approx \frac{f(x+2h) - 4f(x+h) + 6f(x) - 4f(x-h) + f(x-2h)}{h^4} \tag{5.9.0.4}$$

Due to the nature of the problem we have to eliminate the pressure, P, from those PDEs; we differentiate the 5.8.0.15 with respect to x and substitute it into the 5.8.0.14 after differentiating it with respect to y. In addition, we introduce a stream-function ϕ such as $u = \phi_y$ and $v = -\phi_x$. Those changes lead as to the following system (5.9.0.5-5.9.0.6) with the corresponding boundary conditions (5.9.0.7-5.9.0.11):

$$\Theta_{xx} + \Theta_{yy} = \xi(\bar{u}\Theta_x + \phi_x) \tag{5.9.0.5}$$

$$\begin{aligned} &R\Big(\bar{u}(\phi_{xyy} + \phi_{xxx}) - \bar{u}_{yy}\phi_x\Big)e^{\beta\bar{\Theta}} = \phi_{xxxx} + \phi_{yyyy} + 2\phi_{xxyy} + -2\beta\bar{\Theta}_y\phi_{yyy} \\ &- 2\beta\bar{\Theta}_y\phi_{xxy} + \phi_{yy}\Big((\beta\bar{\Theta}_y)^2 - \beta\bar{\Theta}_{yy}\Big) - \phi_{xx}\Big((\beta\bar{\Theta}_y)^2 - \beta\bar{\Theta}_{yy}\Big) \\ &+ \Theta_{yy}(-\beta\bar{\Theta}_y) + \beta\Theta_{xx}\bar{u}_y + \Theta_y\Big(2\beta^2\bar{\Theta}_y\bar{u}_y - 2\beta\bar{u}_{yy}\Big) \\ &+ \Theta\Big(-\beta^3\bar{\Theta}_y^2\bar{u}_y + 2\beta^2\bar{\Theta}_y\bar{u}_{yy} + \beta^3\bar{\Theta}_{yy}\bar{u}_y - \beta\bar{u}_{yyy}\Big) \end{aligned} \tag{5.9.0.6}$$

and

$$h\bar{u}_{yy} + \phi_{yy} - \phi_{xx} = 0\Big|_{y=1} \tag{5.9.0.7}$$

$$\begin{aligned} -h_x\bar{P}_y + R\bar{u}\phi_{xy} - \phi_{yyy} + \beta\bar{\Theta}_y(\phi_{yy} - \beta\phi_{xx}) + \beta\Theta\bar{u}_{yy} - 3\phi_{xxy} = \\ - \Gamma h_{xxx}\Big|_{y=1} \end{aligned} \tag{5.9.0.8}$$

$$\phi_x = -\bar{u}h_x\Big|_{y=1} \tag{5.9.0.9}$$

$$\Theta\Big|_{y=1} = -\frac{h}{\bar{\Theta}_y} \tag{5.9.0.10}$$

$$\phi\Big|_{y=0} = \phi_x\Big|_{y=0} = \phi_y\Big|_{y=0} = 0 \tag{5.9.0.11}$$

We assume that the uneven heating is located between x_{min} (left border), and x_{max} (right border). Outside of that section, only the base flow is present. Using five-point stencil, we need ghost points, for the streamfunction, at all four borders, since momentum equation is a fourth order PDE and the normal stress balance is third order. To create and evaluate the ghost points we are using the boundary conditions(5.9.0.7 and 5.9.0.10). We also assume that on the borders the stream function ϕ and surface h are zero as well as the first derivatives of those (with respect to x). That means the boundary conditions left and right are as follow:

$$\begin{aligned}\Theta\Big|_{x=x_{min}} = \Theta\Big|_{x=x_{max}} = 0, \qquad \phi\Big|_{x=x_{min}} = \phi\Big|_{x=x_{max}} = \phi_x\Big|_{x=x_{min}} = \phi_x\Big|_{x=x_{max}} = 0,\\ h\Big|_{x=x_{min}} = h\Big|_{x=x_{max}} = h_x\Big|_{x=x_{min}} = h_x\Big|_{x=x_{max}} = 0 \qquad (5.9.0.12)\end{aligned}$$

The kinematic condition and tangential stress balance are used to evaluate the ghost points above the surface for the temperature and stream-function, respectively. To reduce the ghost lines, we substituting the eq. 5.9.0.6, at $y = 1$ into eq. 5.9.0.8, achieving to eliminate the second ghost line above the surface. Since we used the eq.5.9.0.6 evaluated at $y = 0$, we use the condition 5.9.0.7 to eliminate the ghost points of temperature above the surface (eq.5.9.0.18). Using the $\phi_y\Big|_{y=0} = 0$, we eliminate the ghost line below the wall, by replacing it with the first line above the wall, ϕ(wall-1) = ϕ(wall + 1). Following the same technique, we eliminate the ghost lines from the left and right boundaries, using the conditions 5.9.0.12. After all of these, we end up with a domain $nx(k+1)$, where n and k: is the number of points

on x, and y-direction, respectively.

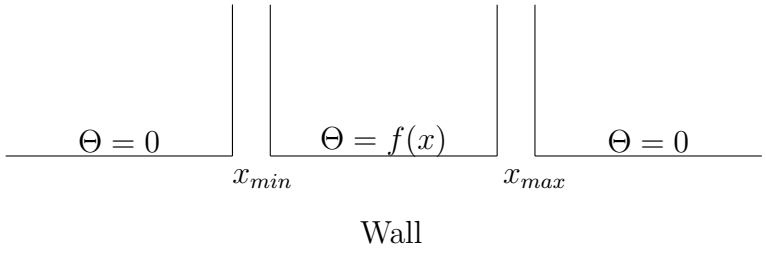


Figure 5.23: 2D schematic representation of the heating boundary conditions and computational domain

The distance between two adjacent points in x-direction is $Dx = \frac{x_{max}-x_{min}}{n-1}$, and $Dy = \frac{y_{max}-y_{min}}{k-1} = \frac{1}{k-1}$ in the y.

Substituting the approximations 5.9.0.1 into the eq.5.9.0.5 at the random point (i,j) where i and j is the coordinates at x and y directions, respectively, we have:

$$\Theta(i+1,j)\Big(\frac{1}{Dx^2} - \frac{\xi\bar{u}}{2Dx}\Big) + \Theta(i-1,j)\Big(\frac{1}{Dx^2} + \frac{\xi\bar{u}}{2Dx}\Big) + \Theta(i,j+1)\frac{1}{Dy^2}$$
$$\Theta(i,j-1)\frac{1}{Dy^2} + \Theta(i,j)\Big(-\frac{2}{Dx^2} - \frac{2}{Dy^2}\Big) + \phi(i+1,j)\frac{\xi\bar{\Theta}_y}{2Dx}$$
$$+ \phi(i-1,j)\frac{-\xi\bar{\Theta}_y}{2Dx} = 0 \qquad (5.9.0.13)$$

Doing the same, the streamfunction at the random point (i,j) we get:

$$B_1(j)\phi(i+2,j) + B_2(j)\phi(i-2,j) + B_3(j)\phi(i,j+2) + B_4(j)\phi(i,j-2)$$
$$+ B_5(j)\phi(i+1,j) + B_6(j)\phi(i-1,j) + B_7(j)\phi(i,j+1) + B_8(j)\phi(i,j-1)$$
$$+ B_9(j)\phi(i+1,j+1) + B_{10}(j)\phi(i-1,j-1) + B_{11}(j)\phi(i+1,j-1)$$
$$+ B_{12}(j)\phi(i-1,j+1) + B_{13}(j)\Theta(i+1,j) + B_{14}(j)\Theta(i-1,j) + B_{15}(j)\Theta(i,j+1)$$
$$+ B_{16}(j)\Theta(i,j-1) + B_{17}(j)\Theta(i,j) + B_{18}(j)\phi(i,j) = 0 \qquad (5.9.0.14)$$

where:

$$B_1(j) = \frac{1}{Dx^4} + \frac{A_3(j)}{2Dx^2}, \quad B_2(j) = \frac{1}{Dx^4} - \frac{A_3(j)}{2Dx^2}, \quad B_3(j) = \frac{1}{Dy^4} + \frac{A_4(j)}{2Dy^2},$$
$$B_4(j) = \frac{1}{Dy^4} - \frac{A_4(j)}{2Dy^2}, \quad B_9(j) = \frac{A_0(j)}{Dx^2Dy^2} + \frac{A_1(j)}{2Dx^2Dy} + \frac{A_2(j)}{2DxDy^2},$$
$$B_5(j) = \frac{-4}{Dx^4} - \frac{2A_0(j)}{Dx^2Dy^2} - \frac{A_2(j)}{Dx * Dy^2} - \frac{A_3(j)}{Dx^2} + \frac{A_5(j)}{Dx^2} + \frac{A_7(j)}{2Dx},$$
$$B_6(j) = \frac{-4}{Dx^4} - \frac{2A_0(j)}{Dx^2Dy^2} + \frac{A_2(j)}{DxDy^2} + \frac{A_3(j)}{Dx^2} + \frac{A_5(j)}{Dx^2} - \frac{A_7(j)}{2Dx},$$
$$B_7(j) = \frac{-4}{Dy^4} - \frac{2A_0(j)}{Dx^2Dy^2} - \frac{A_1(j)}{Dx^2Dy} - \frac{A_4(j)}{Dy^2} + \frac{A_6(j)}{Dy^2},$$
$$B_8(j) = \frac{-4}{Dy^4} - \frac{2A_0(j)}{Dx^2Dy^2} + \frac{A_1(j)}{Dx^2Dy} + \frac{A_4(j)}{Dy^2} + \frac{A_6(j)}{Dy^2},$$
$$B_{10}(j) = \frac{A_0(j)}{Dx^2Dy^2} - \frac{A_1(j)}{2Dx^2Dy} - \frac{A_2(j)}{2 * DxDy^2},$$
$$B_{11}(j) = \frac{A_0(j)}{Dx^2Dy^2} - \frac{A_1(j)}{2Dx^2Dy} + \frac{A_2(j)}{2 * DxDy^2},$$
$$B_{12}(j) = \frac{A_0(j)}{Dx^2Dy^2} + \frac{A_1(j)}{2Dx^2Dy} - \frac{A_2(j)}{2 * DxDy^2},$$
$$B_{13}(j) = \frac{A_8(j)}{Dx^2}, \quad B14(j) = B13(j), \quad B_{15}(j) = \frac{A_9(j)}{Dy^2} + \frac{A_10(j)}{2Dy}$$
$$B_{16}(j) = \frac{A_9(j)}{Dy^2} - \frac{A_10(j)}{2Dy}, B_{17}(j) = -\frac{2A_8(j)}{Dx^2} - \frac{2A_9(j)}{Dy^2} + A_{11}(j),$$
$$B_{18}(j) = \frac{6}{Dx^4} + \frac{6}{Dy^4} + \frac{4A_0(j)}{Dx^2Dy^2} - \frac{2A_5(j)}{Dx^2} - \frac{2A_6(j)}{Dy^2}$$

and

$$A_1(j) = -2\beta\bar{\Theta}_y(j), \quad A_2(j) = -R\bar{u}(j), \quad A_3(j) = A_2(j) \quad A_4(j) = A_1(j),$$
$$A_5(j) = \beta\bar{\Theta}_y(j) - \beta^2\bar{\Theta}_y^2(j), \quad A_6(j) = -A_5(j) \quad A_7(j) = R\bar{u}_{yy}(j)$$
$$A_8(j) = \beta\bar{u}_y(j), \quad A_9(j) = -A_8(j); A_{10}(j) = 2\beta^2\bar{\Theta}_y(j)\bar{u}_y(j) - \beta\bar{u}_{yy}(j),$$
$$A_{11}(j) = 2\beta^2\bar{\Theta}_y(j)\bar{u}_{yy}(j) - \beta^2\bar{\Theta}_y(j)^2\bar{u}_y(j) + \beta^2\bar{\Theta}_{yy}(j)\bar{u}_y(j) - \beta\bar{u}_{yyy}(j),$$
$$A_0(j) = 3;$$

The tangential stress balance (5.9.0.7) becomes:

$$h(i)\bar{u}_{yy} + \Big(\phi(i,k+1) + \phi(i,k-1)\Big)\frac{1}{Dy^2} + \Big(\phi(i-1,k) + \phi(i+1,k)\Big)\frac{-1}{Dx^2} + \phi(i,k)\Big(-\frac{2}{Dy^2} + \frac{2}{Dx^2}\Big) = 0 \tag{5.9.0.15}$$

and the modified normal stress balance (5.9.0.8) is:

$$\begin{aligned} &G_1\phi(i+1,k+1) + G_2\phi(i-1,k+1) + G_3\phi(i+1,k-1) + G_4\phi(i-1,k-1) \\ &+ G_5\phi(i,k+1) + G_6\phi(i,k-1) + G_7\phi(i+1,k) + G_8\phi(i-1,k) + G_9\phi(i,k+2) \\ &+ G_{10}\phi(i,k-2) + G_{11}\phi(i,k) + G_{12}\Theta(i,k) + G_{13}h(i+1) + G_{14}h(i-1) \\ &+ G_{15}h(i+2) + G_{16}h(i-2) = 0 \end{aligned} \tag{5.9.0.16}$$

where:

$$\begin{aligned} &G_1 = \frac{Ru(\bar{k})}{4DxDy} - \frac{3}{2Dx^2Dy}, \quad G_= - \frac{R\bar{u}(k)}{4DxDy} - \frac{3}{2Dx^2Dy}, \quad G_3 = -G_1, \\ &G_4 = -G_2, \quad G_5 = \frac{3}{Dx^2Dy} + \frac{\beta\bar{\Theta}_y(k)}{Dy^2} + \frac{4}{Dy^2}, \quad G_6 = -\frac{3}{Dx^2Dy} + \frac{\beta\bar{\Theta}_y(k)}{Dy^2} + \frac{4}{Dy^2}, \\ &G_7 = -\frac{1}{Dx^2}, \quad G_8 = G_7, \quad G_9 = -\frac{1}{Dy^2}, \quad G_{10} = G_9, \quad G_{12} = \beta\bar{u}_{yy}(k) \\ &G_{11} = -\frac{2\beta\bar{\Theta}_y(k)}{Dy^2} + \frac{2}{Dxx^2} - \frac{6}{Dy^4}, \quad G_{13} = -\frac{\bar{P}_y(k)}{2Dx} - \frac{\Gamma}{Dx^3}, \quad G_{14} = -G_{13}, \\ &G_{15} = \frac{\Gamma}{2Dx^3}, \quad G_{16} = -G_{15} \end{aligned}$$

The above (5.9.0.16) condition include the ghost line of $\phi(i, k+2)$, where $i \in [1, n]$. Since we want to eliminate that line we substitute the momentum equation (5.9.0.14) evaluated on the surface into equation 5.9.0.16.

The result is:

$$\phi(i+1,k+1)\Big(G_1 - G_9\frac{B_9}{B_3}\Big) + \phi(i-1,k+1)\Big(G_2 - G_9\frac{B_{12}}{B_3}\Big)$$
$$+ \phi(i+1,k-1)\Big(G_3 - G_9\frac{B_{11}}{B_3}\Big) + \phi(i-1,k-1)\Big(G_4 - G_9\frac{B_{10}}{B_3}\Big)$$
$$+ \phi(i,k+1)\Big(G_5 - G_9\frac{B_7}{B_3}\Big) + \phi(i,k-1)\Big(G_6 - G_9\frac{B_8}{B_3}\Big) + \phi(i+1,k)\Big(G_7 - G_9\frac{B_5}{B_3}\Big)$$
$$+ \phi(i-1,k)\Big(G_8 - G_9\frac{B_6}{B_3}\Big) + \phi(i,k-2)\Big(G_{10} - G_9\frac{B_4}{B_3}\Big) + \phi(i,k)\Big(G_{11} - G_9\frac{B_{18}}{B_3}\Big)$$
$$+ \Theta(i,k)\Big(G_{12} - G_9\frac{B_{17}}{B_3}\Big) + \Theta(i+1,k)\Big(-G_9\frac{B_{13}}{B_3}\Big) + \Theta(i-1,k)\Big(-G_9\frac{B_{14}}{B_3}\Big)$$
$$+ \Theta(i,k+1)\Big(-G_9\frac{B_{15}}{B_3}\Big) + \Theta(i,k-1)\Big(-G_9\frac{B_{16}}{B_3}\Big) + h(i+1)G_{13} + h(i-1)G_{14}$$
$$+ h(i+2)G_{15} + h(i-2)G_{16} = 0 \qquad (5.9.0.17)$$

Despite the fact that we eliminated $\phi(i,k+2)$ from the above equation, we couldn't use it since we introduced the ghost points of $\Theta(i,k+1)$. For that reason we substitute eq. 5.9.0.13, evaluated on the surface, into equation

5.9.0.17. The final condition that we can use is:

$$\phi(i+1,k+1)\Big(G_1 - G_9\frac{B_9}{B_3}\Big) + \phi(i-1,k+1)\Big(G_2 - G_9\frac{B_{12}}{B_3}\Big)$$
$$+ \phi(i+1,k-1)\Big(G_3 - G_9\frac{B_{11}}{B_3}\Big) + \phi(i-1,k-1)\Big(G_4 - G_9\frac{B_{10}}{B_3}\Big)$$
$$+ \phi(i,k+1)\Big(G_5 - G_9\frac{B_7}{B_3}\Big) + \phi(i,k-1)\Big(G_6 - G_9\frac{B_8}{B_3}\Big)$$
$$+ \phi(i+1,k)\Big(G_7 - G_9\frac{B_5}{B_3} + G_9\frac{B_{15}}{B_3}Dy^2\frac{\xi\bar{\Theta}_y}{2Dx}\Big)$$
$$+ \phi(i-1,k)\Big(G_8 - G_9\frac{B_6}{B_3} + G_9\frac{B_{15}}{B_3}Dy^2\Big(-\frac{\xi\bar{\Theta}_y}{2Dx}\Big)\Big) + \phi(i,k-2)\Big(G_{10} - G_9\frac{B_4}{B_3}\Big)$$
$$+ \phi(i,k)\Big(G_{11} - G_9\frac{B_{18}}{B_3}\Big) + \Theta(i,k)\Big(G_{12} - G_9\frac{B_{17}}{B_3} + G_9\frac{B_{15}}{B_3}Dy^2\Big(-\frac{2}{Dx^2} - \frac{2}{Dy^2}\Big)\Big)$$
$$+ \Theta(i+1,k)\Big(-G_9\frac{B_{13}}{B_3} + G_9\frac{B_{15}}{B_3}Dy^2(\frac{1}{Dx^2} - \frac{\xi\bar{u}}{2Dx})\Big)$$
$$+ \Theta(i-1,k)\Big(-G_9\frac{B_{14}}{B_3} + G_9\frac{B_{15}}{B_3}Dy^2(\frac{1}{Dx^2} + \frac{\xi\bar{u}}{2Dx})\Big)$$
$$+ \Theta(i,k-1)\Big(-G_9\frac{B_{16}}{B_3} + G_9\frac{B_{15}}{B_3}\Big) + h(i+1)G_{13} + h(i-1)G_{14}$$
$$+ h(i+2)G_{15} + h(i-2)G_{16} = 0 \qquad (5.9.0.18)$$

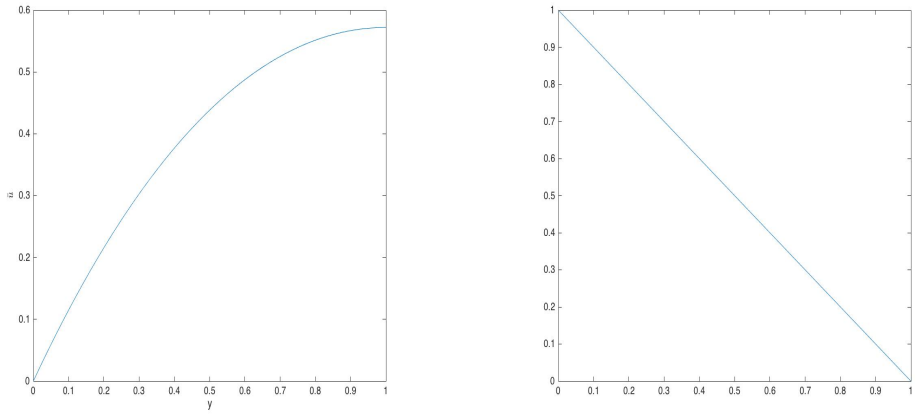
The vector of unknown has $2n(k+1)$ elements. The first is the streamfunction ϕ, at $x = x_{min}$ and $y = 0$, and it's notated as $\psi(1)$, and the counting continues horizontally for the rest of the streamfunctions elements. The temperature Θ at $x = x_{min}$ and $y = 0$ is notated like $\psi(n(k+1)+1)$. For the random point located at (i, j), where i and j is the coordinates at x and y directions, respectively, the streamfunction $\phi(i, j)$ and temperature, $\Theta(i, j)$ are: $\phi(i, j) = \psi(n(j-1)+i)$ and $\Theta(i, j) = \psi(n(k+1)+n(j-1)+i)$. The shape of the deformation is a n-points vector, that we insert after the temperature unknowns. Applying this for the whole domain we end up with

layers of the unknowns:

$$
\begin{array}{ll}
stream function & \left[\begin{array}{c} \psi(1) \\ \psi(2) \\ \ldots \\ \psi(n(j-1)+i) \\ \ldots \\ \psi(n(k+1)) \end{array}\right. \\
Temperature & \left[\begin{array}{c} \psi(n(k+1)+1) \\ \psi(n(k+1)+2) \\ \ldots \\ \psi(n(k+1)+n(j-1)+i) \\ \ldots \\ \psi(2nk+n) \end{array}\right. \\
Surface & \left[\begin{array}{c} \psi(n(k+1)+nk+1) \\ \ldots \\ \psi(n(k+1)+nk+i) \\ \ldots \\ \psi(2n(k+1)) \end{array}\right.
\end{array}
\tag{5.9.0.19}
$$

In what follows, we carried out extensive numerical experiments where the parameters vary for different heating scenarios.

We shall use the even faction $f(x) = e^{x^2}$. The dimensionless viscosity parameter, b, is 0.2 and the dimensionless surface tension, Γ is 1. The base flow that was solved analytically, due to the zero-Brinkman assumption, is displayed by the plots 5.24a and 5.24b. The base flow velocity (eq. 5.8.0.4)is a function of β, unlike the temperature (eq. 5.8.0.3).



(a) $\bar{u}$, where $\beta = 0.2$, and $\Gamma = 10$.

(b) $\bar{\Theta}$, where $\beta = 0.2$, and $\Gamma = 1$.

Figure 5.24: Base flow velocity and temperature profile

Let the liquid occupy a domain $\{(x, y) : x_{min} < x < x_{max}, 0 < y < S(x)\}$. Then the motion of the liquid is described by the 5.9.0.5 and 5.9.0.6 equations. After extensively experiments we found that the best set of computational power-memory space and resolution is a domain where $x_{min} = -30$ and $x_{max} = 30.$, as shown in Fig. 5.23.

After solving the (5.9.0.5-5.9.0.6) with the corresponding boundary conditions (5.9.0.7-5.9.0.11) and the dimensionless parameters are $R = 1$, $\beta = 0.2$, $\Gamma = 10$, $\xi = 0.7$ and $\theta = \pi/6$, the deformation of the surface,h, the velocity, u, and the temperature Θ profile are as follow

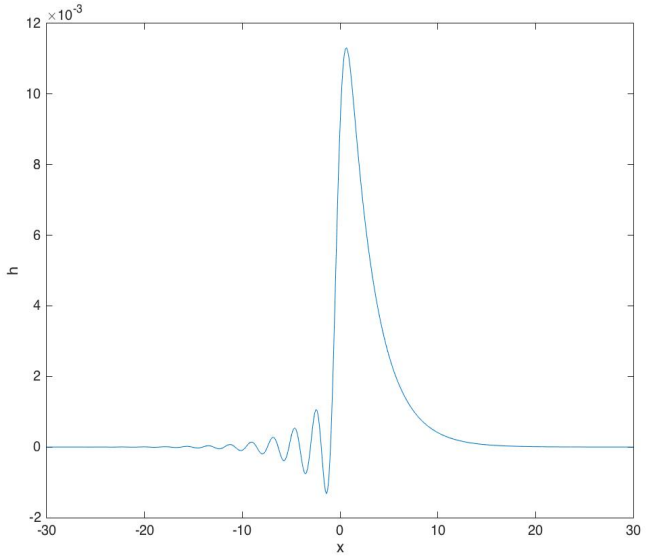


Figure 5.25: Deformation of the film surface, $R = 1$, $\Gamma = 10$, $b = 0.2$, $\xi = 0.7$, $\theta = 30^o$.

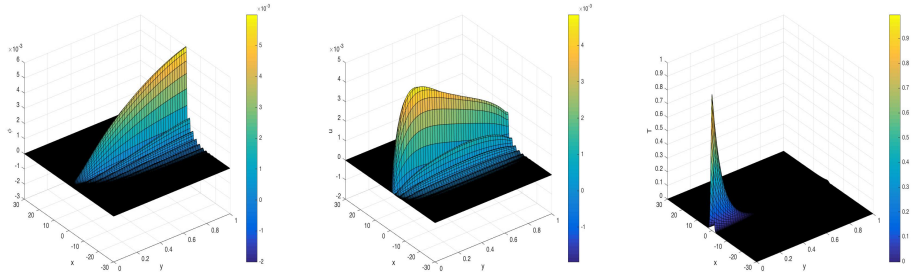


Figure 5.26: Streamfunction, Velocity and Temperature Profile, $R = 1$, $\Gamma = 10$, $b = 0.2$,$\xi = 0.7$, $\Theta = 30^o$.

At this point, in a quest to identify and explain the role of each dimensionless parameter on the above system, we carry out the appropriate simulations. As shown in section (5.5), we expect the dimensionless surface tension will have a dominant role on the deformation of the surface, the Reynolds and Grashof numbers will affect primarily the velocity and temperature profile, much more than the stationary waves of the surface, and the viscosity parameter will affect all the above.

The viscosity parameter β poses a dominant role in the deformation of the surface. An increase in β yields a decrease in viscosity, and hence, an increase in the altitude of the distraction and an higher mean velocity. However, this parameter has a minor effect on the $O(\epsilon)$ temperature.

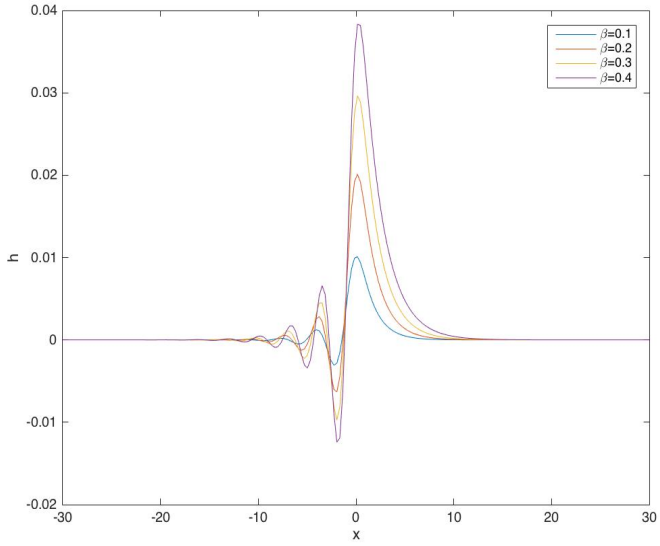
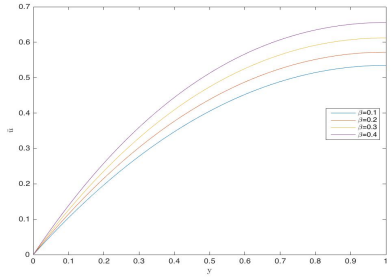
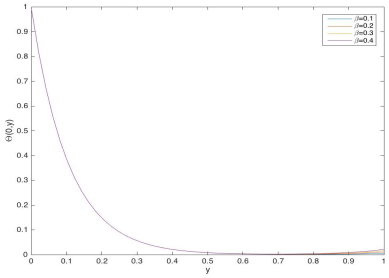


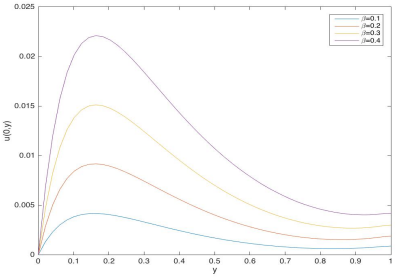
Figure 5.27: Deformation of the film surface regarding different β, where $R = 1$, $\Gamma = 10$, $\xi = 0.7$, $\theta = 30^o$.



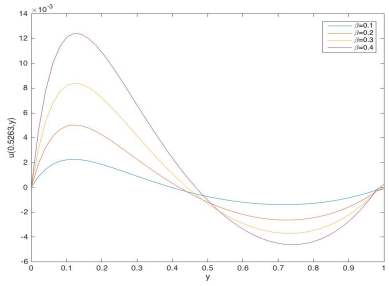
(a) Base Flow Velocity



(b) $O(\epsilon)$ Temperature



(c) $O(\epsilon)$ Velocity



(d) $O(\epsilon)$ Velocity

Figure 5.28: Base flow velocity, $O(\epsilon)$ velocity and temperature regarding different β, where $R = 1$, $\Gamma = 10$, $\xi = 0.7$, $\theta = 30^o$. The maximum velocity increases with an increase of β since the viscosity decreases; while at the peak of the deformation there is an increase in the velocity after $y = 0.7$ due to the increase in the film thickness.

The dimensionless surface tension affects, hugely, the deformation of the free surface. A raise of γ produces a decrease in the deformation. However, as we showed at the end of paragraph 5.5, the bigger the values, the larger the wavelength of the stationary waves. As far as the velocity and temperature profiles, a change in γ effects them slightly.

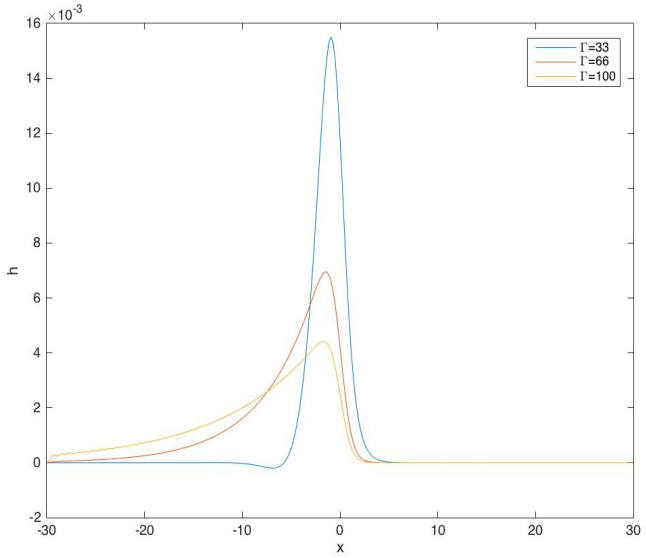
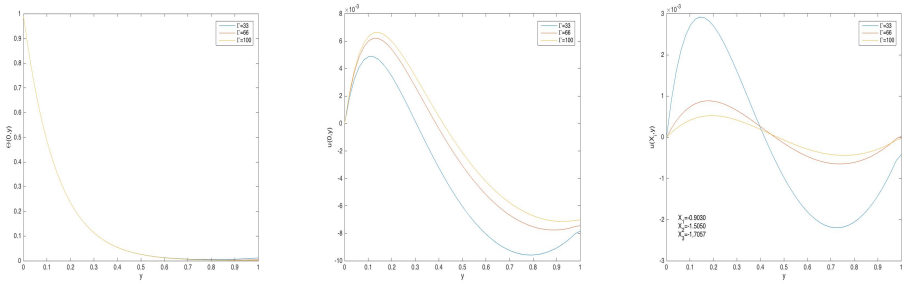


Figure 5.29: Deformation of the film surface regarding different Γ, where $R = 1$, $\xi = 0.7$, $\theta = 30^o$. A decrease of 33% of the dimensionless surface tension refers to an almost double altitude of the surface deformation.

Like before, we present the changes in the velocity ($O(\epsilon)$ that the increase in Γ results, at $x = 0$ and $x = 0.5263$ the peak of the deformation.

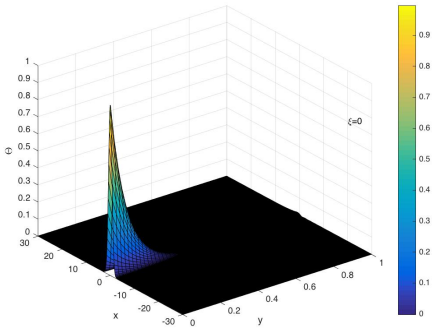


(a) $O(\epsilon)$ Temperature **(b)** $O(\epsilon)$ Velocity **(c)** $O(\epsilon)$ Velocity

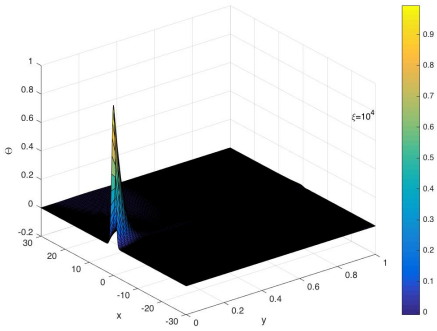
Figure 5.30: $O(\epsilon)$ velocity and temperature regarding different Γ, where $R = 1$, $\beta = 0.2$, $\xi = 0.7$, $\theta = 30^o$.

The Grashof number poses a dominant role on the temperature of the film .For a laminar flow it can value up to 10^6 which is the transition point to turbulence. Figure 5.31 shows that an increase of Grashof results on stronger

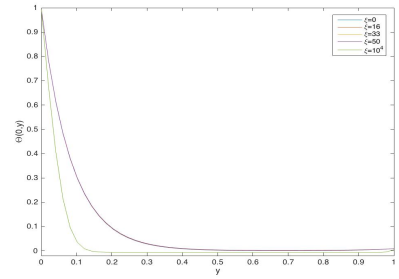
convention in the fluid that leads to a rapidly heat transfer along the fluid and hence the lower temperature of the fluid, and increases the velocity profile near the plate but as the distance from the plate increase the velocity profile decreases.



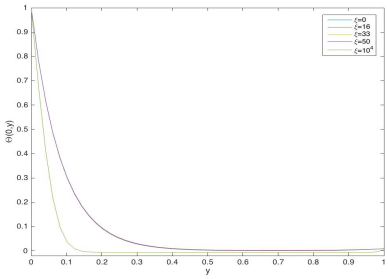
(a) $O(\epsilon)$ Temperature



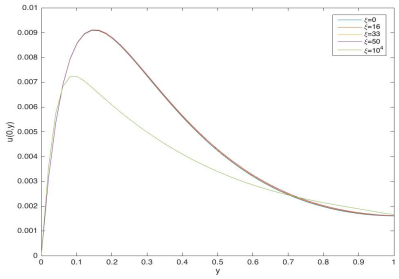
(b) $O(\epsilon)$ Temperature



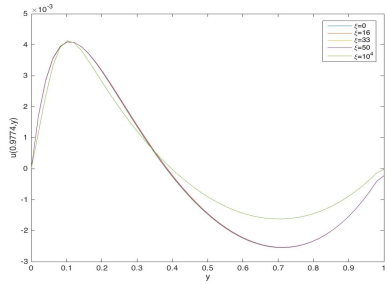
(c) $O(\epsilon)$ Temperature



(d) $O(\epsilon)$ Temperature



(e) $O(\epsilon)$ Velocity

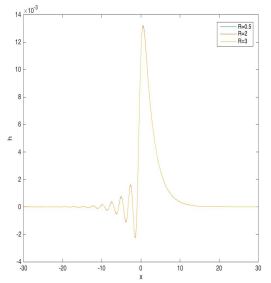


(f) $O(\epsilon)$ Velocity

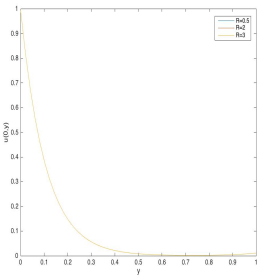
Figure 5.31: $O(\epsilon)$ velocity and temperature regarding different Γ, where $R = 1$, $\beta = 0.2$, $\xi = 0.7$, $\theta = 30^o$. An increase of Grashof results on stronger convention in the fluid. This leads to a rapidly heat transfer along the fluid and hence the lower temperature of the fluid, and increases the velocity profile near the plate but as the distance from the plate increase the velocity profile decreases.

A better way to explain the above plots is by introduce the Richardson number Ri. It is defined as the ratio of Grashof number over the Reynolds square ($Ri = \frac{\xi}{R^2}$). When Ri is much greater than 1 the forced convection may be ignored, while when it is much smaller than 1 the natural convection may be ignored. By increasing the Grashof number and keeping the Reynolds constant we observe the effect of the heating to fade quicker.

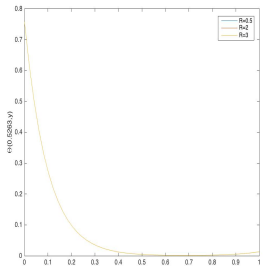
It's well known that a falling film is unstable for Reynolds numbers greater than $R_c = \frac{5}{2}\cot\theta$, where θ is the angle of inclination. Since the angle here is $\frac{\pi}{6}$ the critical Reynolds number is approximately 4.33. We tested a range from 0.5 to 3 and as expected the changes in the deformation of the surface and the temperature profile are almost negligible, while on the velocity profiles are sightly noticeable.



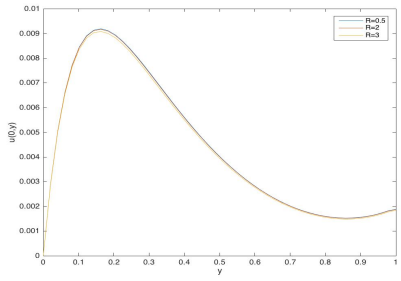
(a) $O(\epsilon)$ Temperature



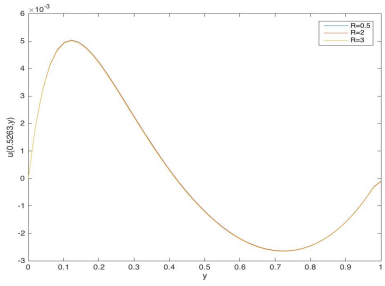
(b) $O(\epsilon)$ Temperature



(c) $O(\epsilon)$ Temperature



(d) $O(\epsilon)$ Temperature



(e) $O(\epsilon)$ Temperature

Figure 5.32: Surface deformation, Temperature and Velocity profile at $x = 0$ and $x = 0.5263$ (peak point). The changes are hardly noticeable.

Due to the symmetry of the system 5.9.0.5-5.9.0.6, there is no need to include cooling scenarios.

6

Weakly Heated Falling Films - Arbitrary Brinkman Number

This section aims to manifest the contributions of the Brinkman number on weakly heated falling films. We examine the same problem with section 5.8. The only difference now is that the Brinkman number is not zero. This assumption yields a coupled ODE system for the base flow, which we will solve numerically, more complicated matrices, and challenges the available computational power in order to converge the results of the numerical solutions.

The two-dimensional steady-state deformations are studied for a non-isothermal thin film of viscous incompressible liquid, falling down a plate inclined at an angle θ. Geometry of the problem is shown in Fig. 5.1. The Cartesian coordinate system (x, y) is chosen again in order that the axis Oy is orthogonal to the substrate, and the axis Ox is directed along the liquid flow.

We shall linearize the governing equations (5.4.1.1 -5.4.1.4), and the corresponding boundary conditions (5.4.2.1-5.4.2.5 and 5.4.2.7), using the following expansions (6.0.0.1). Like section 5.5, we have to solve the base flow numerically since the energy equation and momentum equations are coupled.

$$\boldsymbol{\Theta} = \bar{\Theta}(y) + \epsilon\Theta(x,y), \quad \boldsymbol{u} = \bar{u}(y) + \epsilon u(x,y), \quad \boldsymbol{v} = \epsilon v(x,y)$$
$$S(x) = 1 + \epsilon h(x), \quad \boldsymbol{P} = \bar{P}(y) + \epsilon P(x,y) \tag{6.0.0.1}$$

The energy (6.0.0.2) and momentum equations (6.0.0.3 and 6.0.0.4) for the base flow and the corresponding boundary conditions (6.0.0.5-6.0.0.8) are:

Governing Equations

$$\bar{\Theta}_{yy} + \lambda e^{-\beta\bar{\Theta}}\bar{u}_y^2 = 0 \tag{6.0.0.2}$$

$$e^{-\beta\bar{\Theta}}\Big(- \beta\bar{\Theta}_y\bar{u}_y + \bar{u}_{yy}\Big) + 1 = 0 \tag{6.0.0.3}$$

$$\bar{P}_y + \cot\theta = 0 \tag{6.0.0.4}$$

Boundary Conditions

$$\bar{u}\Big|_{y=0} = 0, \tag{6.0.0.5}$$

$$\Theta\Big|_{y=0} = 1, \tag{6.0.0.6}$$

$$\bar{u}_y\Big|_{y=1} = 0, \text{ and} \tag{6.0.0.7}$$

$$\bar{P}\Big|_{y=1} = 0 \tag{6.0.0.8}$$

The non-isothermal part of the system ($O(\epsilon)$ terms of equations 5.4.1.1-

5.4.1.4) is:

$$\Theta_{xx} + \Theta_{yy} + \lambda e^{-\beta\bar{\Theta}}\Big(2\bar{u}_y(u_y + v_x) - \beta\Theta\bar{u}_y^2\Big) = \xi\Big(\bar{u}\Theta_x + v\bar{\Theta}_y\Big) \tag{6.0.0.9}$$

$$\begin{aligned} &R\Big(\bar{u}u_x + v\bar{u}_y\Big) = -P_x + 2e^{-\beta\bar{\Theta}}u_{xx} \\ &+ e^{-\beta\bar{\Theta}}\Big(- \beta\bar{\Theta}_y(u_x + v_x) + \bar{u}_y(\beta^2\Theta\bar{\Theta}_y - \beta\Theta_y) + v_{xy} + u_{yy} - \beta\Theta\bar{u}_{yy}\Big) \end{aligned} \tag{6.0.0.10}$$

$$R\bar{u}v_x = e^{-\beta\bar{\Theta}}\Big(u_{xy} + v_{xx} - 2\beta\bar{\Theta}_y v_y + 2v_{yy}\Big) - P_y \tag{6.0.0.11}$$

The above PDEs (6.0.0.9-6.0.0.11) are solved numerically in the same way as in section 5.8. A Finite Differences-based code, in Matlab®, specifically written for that system, is selected. Central finite difference method is preferred.

Due to the nature of the problem we have to eliminate the pressure, P, from those PDEs by differentiating the 6.0.0.11 with respect to x and substitute it into the 6.0.0.10 after differentiating it with respect to y. Finally, yet again, we introduce a stream-function ϕ such as $u = \phi_y$ and $v = -\phi_x$. Those changes lead to the following system (6.0.0.12-6.0.0.13) with the corresponding boundary conditions. (6.0.0.14-6.0.0.18):

$$\Theta_{xx} + \Theta_{yy} + \lambda e^{-\beta\bar{\Theta}}\Big(2\bar{u}_y(\phi_{yy} - \phi_{xx}) - \beta\Theta\bar{u}_y^2\Big) = \xi(\bar{u}\Theta_x + \phi_x) \tag{6.0.0.12}$$

$$\begin{aligned} &R\Big(\bar{u}(\phi_{xyy} + \phi_{xxx}) - \bar{u}_{yy}\phi_x\Big)e^{\beta\bar{\Theta}} = \phi_{xxxx} + \phi_{yyyy} + 2\phi_{xxyy} + -2\beta\bar{\Theta}_y\phi_{yyy} \\ &- 2\beta\bar{\Theta}_y\phi_{xxy} + \phi_{yy}\Big((\beta\bar{\Theta}_y)^2 - \beta\bar{\Theta}_{yy}\Big) - \phi_{xx}\Big((\beta\bar{\Theta}_y)^2 - \beta\bar{\Theta}_{yy}\Big) \\ &+ \Theta_{yy}(-\beta\bar{\Theta}_y) + \beta\Theta_{xx}\bar{u}_y + \Theta_y\Big(2\beta^2\bar{\Theta}_y\bar{u}_y - 2\beta\bar{u}_{yy}\Big) \\ &+ \Theta\Big(- \beta^3\bar{\Theta}_y^2\bar{u}_y + 2\beta^2\bar{\Theta}_y\bar{u}_{yy} + \beta^3\bar{\Theta}_{yy}\bar{u}_y - \beta\bar{u}_{yyy}\Big) \end{aligned} \tag{6.0.0.13}$$

and

$$h\bar{u}_{yy} + \phi_{yy} - \phi_{xx} = 0\Big|_{y=1} \tag{6.0.0.14}$$

$$-h_x\bar{P}_y + R\bar{u}\phi_{xy} - \phi_{yyy} - \beta\phi_{yy} + \beta\phi_{xx} + \beta\Theta\bar{u}_{yy} - \phi_{xxy} = - \gamma h_{xxx}\Big|_{y=1} \tag{6.0.0.15}$$

$$\phi_x = -\bar{u}h_x\Big|_{y=1} \tag{6.0.0.16}$$

$$\Theta\Big|_{y=1} = -\frac{h}{\bar{\Theta}_y} \tag{6.0.0.17}$$

$$\phi\Big|_{y=0} = \phi_x\Big|_{y=0} = \phi_y\Big|_{y=0} = 0 \tag{6.0.0.18}$$

We assume that the uneven heating is located between x_{min} (left border), and x_{max} (right border). Outside of that section, only the base flow is present. Using five-point stencil, we need ghost points at all four borders, since momentum equation is a fourth order PDE and the normal stress balance is third order. To create and evaluate the ghost points we are using the boundary conditions(6.0.0.14 and 6.0.0.17). We also assume that on the borders the stream function ϕ and surface h are zero as well as the first derivatives of those, with respect of x. That means the boundary conditions left and right are as follow:

$$\Theta\Big|_{x=x_{min}} = \Theta\Big|_{x=x_{max}} = 0, \qquad \phi\Big|_{x=x_{min}} = \phi\Big|_{x=x_{max}} = \phi_x\Big|_{x=x_{min}} = \phi_x\Big|_{x=x_{max}} = 0,$$
$$h\Big|_{x=x_{min}} = h\Big|_{x=x_{max}} = h_x\Big|_{x=x_{min}} = h_x\Big|_{x=x_{max}} = 0$$

We treat the ghost points in the same way as in section 5.8. The vector of unknowns remain the same as before eq.5.9.0.19. The same is true for the momentum equation (5.9.0.14), in contrast with the energy equation. The

presence of Brinkman term changes the equation as follows:

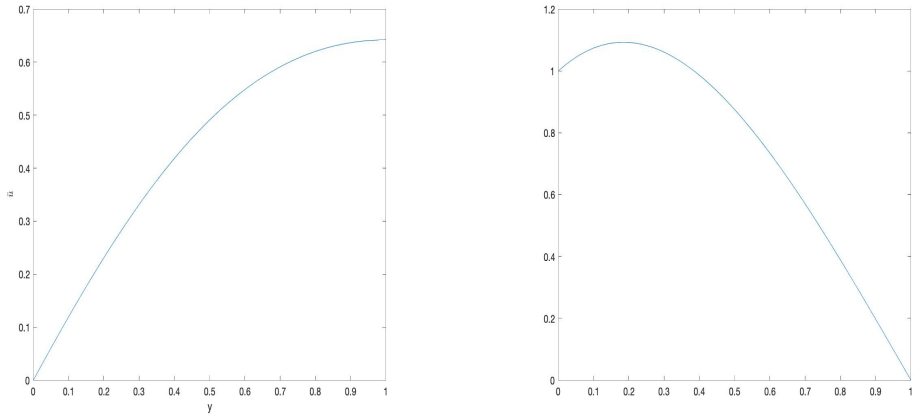
Substituting the approximations 5.9.0.1 into the eq.5.9.0.5 at the random point (i,j) where i and j is the coordinates at x and y directions, respectively, we have:

$$\Theta(i+1,j)\Big(\frac{1}{Dx^2}-\frac{\xi\bar{u}}{2Dx}\Big)+\Theta(i-1,j)\Big(\frac{1}{Dx^2}+\frac{\xi\bar{u}}{2Dx}\Big)+\Theta(i,j+1)\frac{1}{Dy^2}$$
$$\Theta(i,j-1)\frac{1}{Dy^2}+\Theta(i,j)\Big(-\frac{2}{Dx^2}-\frac{2}{Dy^2}-\lambda e^{-\beta\bar{\Theta}}\beta\bar{u}_y^2\Big)+\phi(i,j+1)\lambda e^{-\beta\bar{\Theta}}\frac{2\bar{u}_y}{Dy^2}$$
$$+\phi(i,j-1)\lambda e^{-\beta\bar{\Theta}}\frac{2\bar{u}_y}{Dy^2}+\phi(i+1,j)\Big(-\lambda e^{-\beta\bar{\Theta}}\frac{2\bar{u}_y}{Dx^2}+\frac{\xi\bar{\Theta}_y}{2Dx}\Big)$$
$$+\phi(i-1,j)\Big(-\lambda e^{-\beta\bar{\Theta}}\frac{2\bar{u}_y}{Dx^2}+\frac{-\xi\bar{\Theta}_y}{2Dx}\Big)+\phi(i,j)\Big(\lambda e^{-\beta\bar{\Theta}}4\bar{u}_y(\frac{1}{Dx^2}-\frac{1}{Dy^2})\Big)=0$$

We follow the same procedure as before, section 5.8, for the boundary conditions and ghost lines.

6.1 Numerical Experiments

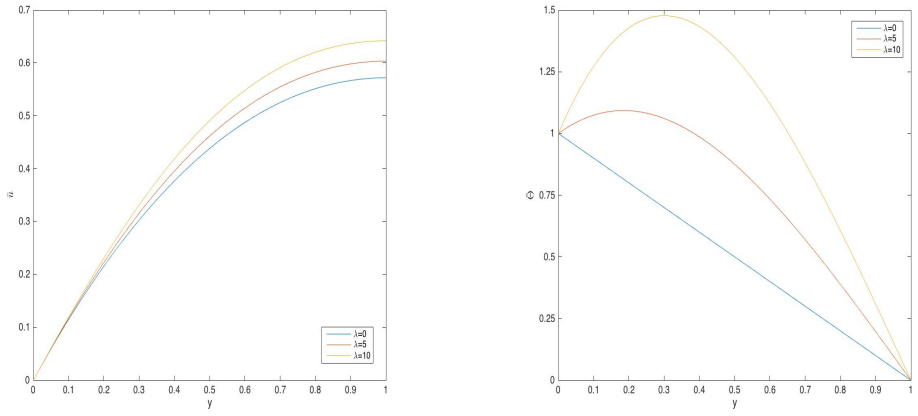
The base flow of the above system is solved numerically using a built-in routine in Matlab®. The dimensionless viscosity parameter, b, is 0.2, the dimensionless surface tension, Γ, is 10, Grashof number, ξ, is 0.7 and the Brinkman number λ is $O(1)$. Since the Brinkman number is equal to 5 the energy and momentum equations are coupled and must be solved numerically, and the solutions are displayed in the plots 6.1a and 6.1b.



(a) Velocity Profile **(b)** Temperature Profile

Figure 6.1: Base flow velocity and temperature where $\beta = 0.2$, $\Gamma = 10$, $\lambda = 5$, $\xi = 0.7$ and $\theta = 30^o$.

Increasing the Brinkman number we observe an increase in the temperature (6.2b) due to the higher viscous heating. This increase in temperature leads to a lower viscosity and so a higher base velocity (6.2a). These comparisons are displayed in the plots 6.2a and 6.2b. These increases in velocity and



(a) Velocity Profile **(b)** Temperature Profile

Figure 6.2: Comparison on Base Velocity and Temperature profiles regarding different Brinkman numbers where $\beta = 0.2$, $\Gamma = 10$, $\xi = 0.7$ and $\theta = 30^o$. An increase on Brinkman number leads to a higher temperature on the fluids, hence lower viscosity and a faster base flow.

temperature lead to higher surface instabilities, and we expect an increase in the altitude of the stationary waves (6.3).

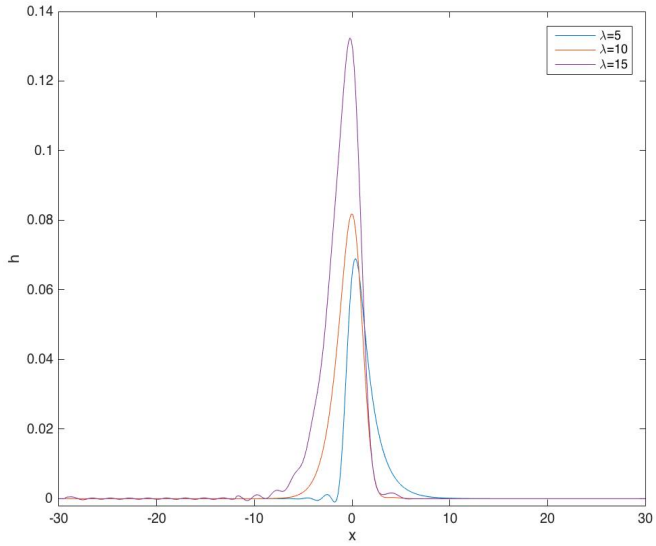
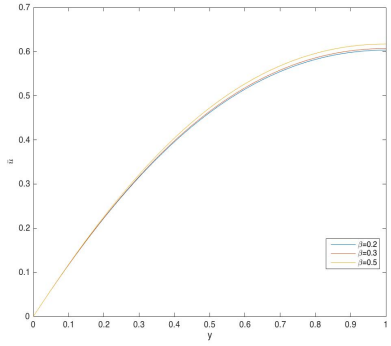
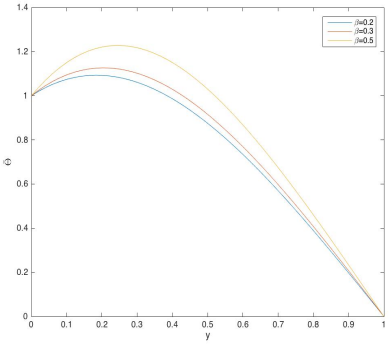


Figure 6.3: Deformation of the film surface regarding different λ, where $R = 1$, $\Gamma = 10$, $\xi = 0.7$, $\theta = 30^o$. The increase in λ increases the velocity and temperature that leads to higher surface deformation and shifts the peak point of the curve towards left.

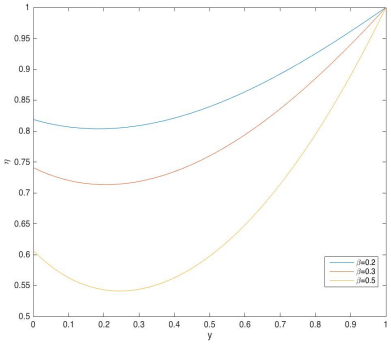
The other parameters were the subject of studies of the previous chapter (5.8). However, since the increase of the Brinkman number could effect the behavior of others, we include some characteristic plots such as the base flow velocity, temperature profiles and surface deformation for different values of the dimensionless viscosity parameter and surface tension. By increasing β, the viscosity increases (see plot 6.4c), and that leads to an increase in viscous heating (6.4b) and a higher base velocity (6.4a). What is follows is a increase in the altitude of the stationary waves on the free surface something is shown on the plot 6.4d. The decrease in Γ leads to an increase in surface deformation and in the altitude of the oscillations before the heating in comparison with the wavelength which decreases, similar as shown in paragraph (5.6). The Brinkman number magnitude the shift on the right of the surface deformation that the increase in Γ occurs.



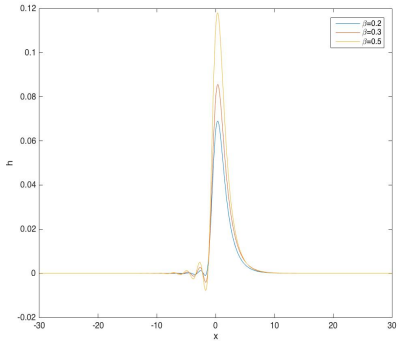
(a) Base Velocity Profile



(b) Base Temperature Profile



(c) Viscosity variation different β, $R = 1$,where $\mu = 1$.



(d) Deformation of the surface

Figure 6.4: Comparison on Velocity, Temperature and Viscosity profiles regarding different β where $\lambda = 5$, $\Gamma = 10$, $\xi = 0.7$ and $\theta = 30^o$.

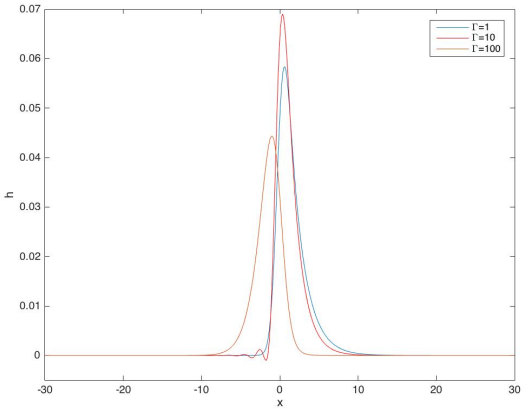


Figure 6.5: Deformation of the film surface regarding different Γ, where $R = 1$, $\lambda = 5$, $\xi = 0.7$, $\theta = 30^o$. The decrease in Γ leads to an increase in surface deformation and in the altitude of the oscillations before the heating in comparison with the wavelength which decreases. The Brinkman number magnitude the shift on the right of the surface deformation that the increase in Γ occurs.

7

Stability of Falling Film

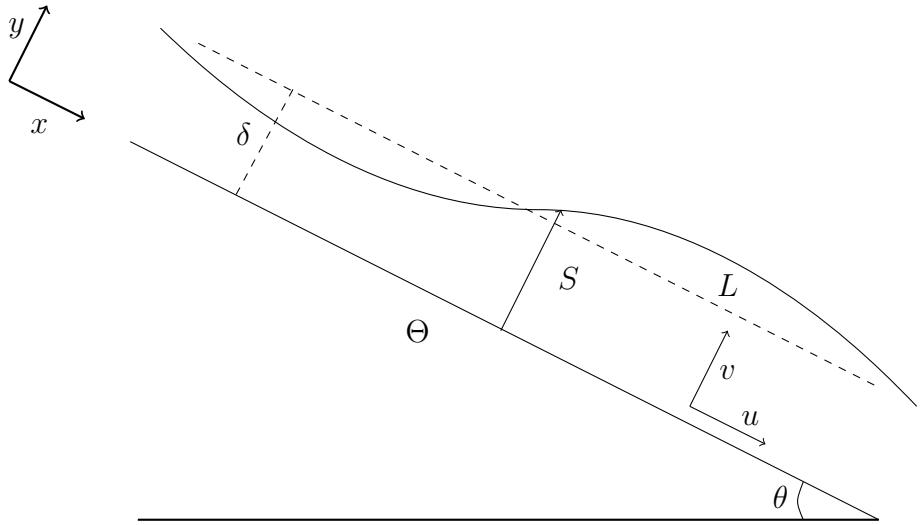
7.1 Introduction

Until now, this thesis has presented non-isothermal steady-state problems. The research presented in the following chapters focuses on the development of theoretical and numerical tools that allows us to study the linear stability of non-isothermal falling films in the presence of variable viscosity. In section 7.3, we solve the energy and analogue of the Orr-Sommerfeld equation and derive analytical expressions for the growth rates of disturbances to be used in verification of the method by extracting the isothermal solutions when the viscosity parameter tends to zero, section 7.4, and the validation of the numerical simulations, section 7.7.

7.1.1 Governing Equations

The aim of linear stability analysis is to predict whether or not a transition should happen for a particular flow, and how that flow changes. We shall use Cartesian coordinate system (x, y) and denote the corresponding components of velocity vector by $\boldsymbol{u}$ and $\boldsymbol{v}$ as well time by t, pressure by P, density by

ρ and viscosity by η. Once more, the density is considered constant and viscosity obeys Reynolds law Tanner (2000). The system of study depicted in Fig. 7.1.1.



Now, the governing equations, the energy (7.1.1.1), continuity (7.1.2.3), and Navier-Stokes (7.1.1.3,7.1.1.4) equations, for a Newtonian fluid, are written as follows

$$\rho\hat{C}_p\Big(T_t + uT_x + vT_y\Big) = \kappa\Big(T_{xx} + T_{yy}\Big) + \eta\left(2u_x^2 + (u_y + v_x)^2 + 2v_y^2\right) \quad (7.1.1.1)$$

$$u_x + v_y = 0 \quad (7.1.1.2)$$

$$\begin{aligned}\rho\Big(u_t + uu_x + vu_y\Big) = -P_x + 2\eta_x u_x + 2\eta u_{xx} + \eta_y(v_x + u_y) \\ + \eta(v_{yx} + u_{yy}) + \rho g \sin\theta\end{aligned} \quad (7.1.1.3)$$

$$\rho\Big(v_t + uv_x + vv_y\Big) = \eta_x(v_x + u_y) - P_y + \eta(v_{xx} + u_{xy}) - \rho g\cos\theta \quad (7.1.1.4)$$

where: $\hat{C_p}$ is the specific heat capacity at constant pressure, T the temperature, and k is the thermal conductivity.

7.1.2 Non-dimensionalization

We shall convert the governing equations (7.1.1.1 to 7.1.1.4) into dimensionless form. For this purpose, we use the characteristic thickness, δ. The non-dimensional independent and dependent variables are

$$\begin{aligned} &\boldsymbol{x} = \delta \boldsymbol{x}^*, \quad t = \frac{\mu}{\delta \rho g \sin\theta}, \quad \boldsymbol{u} = \frac{\delta^2 \rho g \sin\theta}{\mu} \boldsymbol{u^*}, \\ &P = P^* \delta \rho g \sin\theta, \quad \Theta = \frac{T - T_f}{T_0 - T_f}, \quad \beta = \alpha(T_0 - T_f) \end{aligned} \tag{7.1.2.1}$$

Substitution of 7.1.2.1 into the (7.1.1.1) to (7.1.1.4) and after dropping asterisks:

Energy Equation:

$$\Theta_{xx} + \Theta_{yy} + \lambda e^{-\beta\Theta} \left(2u_x^2 + (u_y + v_x)^2 + 2v_y^2 \right) = \xi \Big(\Theta_t + u\Theta_x + v\Theta_y \Big) \tag{7.1.2.2}$$

Continuity

$$u_x + v_y = 0 \tag{7.1.2.3}$$

Cauchy x-direction:

$$\begin{aligned} R\Big(u_t + uu_x + vu_y \Big) = -P_x + 2(e^{-\beta\Theta})_x u_x + e^{-\beta\Theta} u_{xx} + (e^{-\beta\Theta})_y (v_x + u_y) \\ + e^{-\beta\Theta} u_{yy} + 1 \end{aligned} \tag{7.1.2.4}$$

Cauchy y-direction:

$$\begin{aligned} R(v_t + uv_x + vv_y) =& (e^{-\beta\Theta})_x(u_y + v_x) + e^{-\beta\Theta}v_{xx} - P_y \\ &+ 2(e^{-\beta\Theta})_y v_y + e^{-\beta\Theta}v_{yy} - \cot\theta \end{aligned} \tag{7.1.2.5}$$

where: $\lambda = \frac{(\delta^2\rho g\sin\theta)^2}{\mu\kappa(T_0 - T_f)}$ is the Brinkman number, $R = \frac{\delta^3\rho^2 g\sin\theta}{\mu^2}$ is the Reynolds, and $\xi = \frac{\hat{C_p}\delta^3 g\rho^2\sin\theta}{\mu\kappa}$ is the Grashof number which is the Reynolds number times the ratio of the force due to differences in density and the viscous force.

7.1.3 Boundary Conditions

The corresponding boundary conditions to the system (7.1.2.2 to 7.1.2.5) are the temperature and the 2 no slip conditions on the bottom, and the kinematic, temperature, normal and tangential stress balance at the interface.

No-slip condition at the wall

$$u\Big|_{y=0} = v\Big|_{y=0} = 0 \tag{7.1.3.1}$$

Temperature Conditions

We assume that the temperature on the interface is equal to the ambient temperature T_f and T_0 on the lower wall. In dimensionless form the conditions are:

$$\Theta\Big|_{y=0} = 1, \qquad \Theta\Big|_{y=S} = 0 \tag{7.1.3.2}$$

Kinematic Condition

$$v = S_t + uS_x\Big|_{y=S} \tag{7.1.3.3}$$

Normal Stress Balance

$$\begin{aligned} -S_x\Big(\Big(-P + 2e^{-\beta\Theta}u_x\Big)(-S_x) + e^{-\beta\Theta}(u_y + v_x)\Big) + e^{-\beta\Theta}(u_y + v_x)(-S_x) \\ -P + 2e^{-\beta\Theta}v_y = -\gamma\frac{S_{xx}}{\Big(1 + (S_x)^2\Big)^{\frac{1}{2}}} \end{aligned} \tag{7.1.3.4}$$

Tangential Stress Balance

$$\begin{aligned} -S_x\Big(-P + e^{-\beta\Theta}u_x + e^{-\beta\Theta}\Big(u_y + v_x\Big)S_x\Big) + e^{-\beta\Theta}(u_y + v_x) \\ + \Big(-P + 2e^{-\beta\Theta}v_y\Big)S_x = 0 \end{aligned} \tag{7.1.3.5}$$

Note that on the interface, we use the basic Taylor series method for the denominator($u(x, t+\Delta) = u(x,t) + \Delta\frac{\partial u(x,t)}{\partial t} + \frac{\Delta^2}{2!}\frac{\partial^2 u(x,t)}{\partial t^2} + \cdots$) Fenton (1983). The interface is $S(x) = 1 + \epsilon h_1$, where $\epsilon h_1 << 1$.

7.2 Small Amplitude Perturbations And Normal Modes

We assume the above boundary value problem has a steady solution (basic state) like

$$u = \bar{u}, \qquad \Theta = \bar{\Theta}, \qquad P = \bar{P}, \qquad S = 1 \tag{7.2.0.1}$$

and then, we introduce small amplitude perturbations with small parameter ζ:

$$u = \bar{u}(y) + \zeta\tilde{u}(y,x,t), \qquad \Theta = \bar{\Theta}(y) + \zeta\tilde{\Theta}(y,x,t) \qquad P = \bar{P}(y) + \zeta\tilde{P}(y,x,t),$$
$$v = \zeta\tilde{v}(y,x,t) \qquad S = 1 + \zeta\tilde{S}(x,t) \tag{7.2.0.2}$$

Substituting (7.2.0.2) into the Energy (7.1.2.2), Continuity (7.1.2.3), and Navier-Stokes equations, the basic state and the equations for the perturbation functions are as follow:

Leading Order

$$\bar{\Theta}_{yy} + \lambda e^{-\beta\bar{\Theta}}\bar{u}_y^2 = 0, \tag{7.2.0.3}$$

$$\Big(e^{-\beta\bar{\Theta}}\bar{u}_y\Big)_y + 1 = 0, \tag{7.2.0.4}$$

$$\bar{P}_y + \cot\theta = 0, \tag{7.2.0.5}$$

and $\mathbf{O}(\zeta)$

$$\tilde{\Theta}_{xx} + \tilde{\Theta}_{yy} + \lambda e^{-\beta\bar{\Theta}}\Big(2\bar{u}_y(\tilde{u}_y + \tilde{v}_x) + \beta\tilde{\Theta}\bar{u}_y^2\Big) = \xi\Big(\tilde{\Theta}_t + \bar{u}\tilde{\Theta}_x + \tilde{v}\bar{\Theta}_y\Big), \tag{7.2.0.6}$$

$$\tilde{u}_x + \tilde{v}_y = 0 \tag{7.2.0.7}$$

$$\begin{aligned} R\Big(\tilde{u}_t + \bar{u}\tilde{u}_x + \tilde{v}\bar{u}_y\Big) &= -\tilde{P}_x \\ &+ e^{-\beta\bar{\Theta}}\Big(- \beta\bar{\Theta}_y(\tilde{v}_x + \tilde{u}_y + \beta\tilde{\Theta}\bar{u}_y) + \tilde{u}_{xx} + \tilde{u}_{yy} + \beta(\tilde{\Theta}_y\bar{u}_y + \tilde{\Theta}\bar{u}_{yy})\Big), \end{aligned} \tag{7.2.0.8}$$

$$R\Big(\tilde{v}_t + \bar{u}\tilde{v}_x\Big) = e^{-\beta\bar{\Theta}}\Big(\tilde{v}_{xx} + \beta\tilde{\Theta}_x\bar{u}_y + \tilde{v}_{yy}\Big) - \tilde{P}_y - 2e^{-\beta\bar{\Theta}}\beta\bar{\Theta}_y\tilde{v}_y \tag{7.2.0.9}$$

The corresponding boundary conditions are obtained be substituting (7.2.0.2) into (7.1.3)-(7.1.3.5)

No slip at the wall

$$\bar{u}\Big|_{y=0} = 0 \qquad \textbf{and} \quad \tilde{u}\Big|_{y=0} = \tilde{v}\Big|_{y=0} = 0 \tag{7.2.0.10}$$

Kinematic Condition:

$$\tilde{v} = \tilde{S}_t + \bar{u}\tilde{S}_x\Big|_{y=1} \tag{7.2.0.11}$$

Normal Stress Balance:

$$-\bar{P} = 0\Big|_{y=1} \tag{7.2.0.12}$$

$$-\tilde{P} - \tilde{S}\bar{P}_y + 2e^{-\beta\bar{\Theta}}\Big(- \tilde{S}_x\bar{u}_y + \tilde{v}_y\Big) = -\gamma\tilde{S}_{xx}\Big|_{y=1} \tag{7.2.0.13}$$

Tangential Stress Balance:

$$\bar{u}_y = 0\Big|_{y=1} \tag{7.2.0.14}$$

$$\tilde{u}_y + \tilde{S}\bar{u}_{yy} + \tilde{v}_x + \beta\tilde{\Theta}\bar{u}_y = 0\Big|_{y=1} \tag{7.2.0.15}$$

Temperature on the wall:

$$\bar{\Theta}\Big|_{y=0} = 1, and \quad \tilde{\Theta}\Big|_{y=0} = 0 \tag{7.2.0.16}$$

Temperature on the interface:

$$\Theta = 0\Big|_{y=1+\delta\hat{S}} \rightarrow \quad \bar{\Theta} = 0\Big|_{y=1}, \quad and \quad \tilde{S}\bar{\Theta}_y + \tilde{\Theta} = 0\Big|_{y=1} \tag{7.2.0.17}$$

These lead to:

$$\tilde{S} = -\frac{\tilde{\Theta}(1)}{\bar{\Theta}_y(1)} \tag{7.2.0.18}$$

We seek the solution for functions $\hat{\Theta}$, $\hat{u}$, $\hat{v}$, $\hat{P}$, and $\hat{S}$ in the normal mode form

$$\tilde{\Theta}(y,x,t) = \hat{\Theta}(y)e^{i\kappa(x-ct)}, \quad \tilde{u}(y,x,t) = \hat{u}(y)e^{i\kappa(x-ct)}, \quad \tilde{v}(y,x,t) = \hat{v}(y)e^{i\kappa(x-ct)},$$
$$\tilde{P}(y,x,t) = \hat{P}(y)e^{i\kappa(x-ct)}, \tilde{S}(x,t) = \hat{S}e^{i\kappa(x-ct)} \tag{7.2.0.19}$$

Where κ is the wave number and c a complex number, the phase velocity, defined as $c = c_r + ic_i$, $c * \kappa$ is the frequency of oscillations and c_i the amplifications rate. The instability of the flow develops when c_i becomes positive. Substituting (7.2.0.19) into (7.2.0.3)-(7.2.0.9):

$$-\kappa^2\hat{\Theta} + \hat{\Theta}_{yy} + \lambda e^{-\beta\bar{\Theta}}\Big(2\bar{u}_y(\hat{u}_y + i\kappa\hat{v}) + \beta\hat{\Theta}\bar{u}_y^2\Big) = \xi\Big(- i\kappa c\hat{\Theta} + i\kappa\bar{u}\hat{\Theta} + \hat{v}\bar{\Theta}_y\Big) \tag{7.2.0.20}$$

$$i\kappa\hat{u} + \hat{v}_y = 0 \tag{7.2.0.21}$$

$$R\Big(- i\kappa c\hat{u} + i\kappa\bar{u}\hat{u} + \hat{v}\bar{u}_y\Big) = -i\kappa\hat{P} \tag{7.2.0.22}$$
$$+ e^{-\beta\bar{\Theta}}\Big(- \kappa^2\hat{u} - \beta\bar{\Theta}_y(i\kappa\hat{v} + \hat{u}_y + \beta\hat{\Theta}\bar{u}_y) + \hat{u}_{yy} + \beta(\hat{\Theta}_y\bar{u}_y + \hat{\Theta}\bar{u}_{yy})\Big)$$

$$R\Big(- i\kappa c\hat{v} + i\kappa\bar{u}\hat{v}\Big) = e^{-\beta\bar{\Theta}}\Big(- \kappa^2\hat{v} + i\kappa\beta\hat{\Theta}\bar{u}_y + \hat{v}_{yy}\Big) - \hat{P}_y$$
$$- 2e^{-\beta\bar{\Theta}}\beta\bar{\Theta}_y\hat{v}_y \tag{7.2.0.23}$$

Substituting (7.2.0.19) into (7.2.0.11),(7.2.0.13), and(7.2.0.15)
Kinematic Condition:

$$\hat{v} = -i\kappa c\hat{S} + i\kappa\bar{u}\hat{S}\Big|_{y=1} \tag{7.2.0.24}$$

Normal Stress Balance:

$$-\hat{P} - \hat{S}\bar{P}_y + 2e^{-\beta\bar{T}}\Big(- i\kappa\hat{S}\bar{u}_y + \hat{v}_y\Big) = \kappa^2\gamma\hat{S}\Big|_{y=1} \tag{7.2.0.25}$$

Tangential Stress Balance:

$$\hat{S}\bar{u}_{yy} + \hat{u}_y + i\kappa\hat{v} + \beta\hat{T}\bar{u}_y = 0\Big|_{y=1} \tag{7.2.0.26}$$

We eliminate $\hat{S}$ and $\hat{u}$ by substituting the eq.(7.2.0.18) and 7.2.0.7 into the governing equations and boundary conditions and combining (7.2.0.8) with (7.2.0.9) we finally have the analogue of Orr-Sommerfeld equation for the non-isothermal problem. We decided to solve the above system using both analytical (7.3) and numerical (7.5) techniques.

7.3 Long Wave Analysis

We continue the analytic analysis by using the perturbation theory in order to lead us to an expression for the desired solution in terms of a formal power series in some small parameter Henry (2005). The wavelength of the perturbation is large compare to the thickness of the film, and so the wavenumber κ is small. We expand the $\hat{\Theta}$ and $\hat{v}$ functions as well as the constant c as follow

$$\hat{v} = \hat{v}_0(y) + \kappa\hat{v}_1(y) + \cdots, \quad \hat{\Theta} = \frac{1}{\kappa}\hat{\Theta}_0(y) + \hat{\Theta}_1(y) + \cdots, \quad \textit{and} \quad c = c_0 + \kappa c_1 + \cdots \tag{7.3.0.1}$$

Note we assume Θ is $O(\frac{1}{\kappa})$, because if we scale it as $O(1)$ this yields the isothermal problem. Substituting (7.3.0.1) into the governing equations and the corresponding boundary conditions we have

Leading Order

$$\hat{\Theta}_0'' + \lambda e^{-\beta\bar{\Theta}}\Big(2\bar{u}_y\hat{v}_0''i + \beta\hat{\Theta}_0\bar{u}_y^2\Big) = 0 \tag{7.3.0.2}$$

$$\begin{aligned}&-\beta\bar{\Theta}_y\Big(-\beta\bar{\Theta}_y(\hat{v}_0'' + \beta\hat{\Theta}_0\bar{u}_y) + \hat{v}_0''' + \beta(\hat{\Theta}_0'\bar{u}_y + \hat{\Theta}_0\bar{u}_{yy})\Big) - \beta\bar{\Theta}_{yy}(\hat{v}_0''i + \beta\hat{\Theta}_0\bar{u}_y)\\ &-\beta\bar{\Theta}_y\Big(\hat{v}_0'''i + \beta(\hat{\Theta}_0'\bar{u}_y + \hat{\Theta}_0\bar{u}_{yy})\Big) + \hat{v}_0^{(4)}i + \beta\Big(\bar{u}_y\hat{\Theta}_0'' + 2\hat{\Theta}_0'\bar{u}_{yy} + \hat{\Theta}_0\bar{u}_{yyy}\Big) = 0\end{aligned} \tag{7.3.0.3}$$

Boundary Conditions

Normal Stress:

$$\hat{v}_0''' - \beta\bar{\Theta}_y\hat{v}_0'' + \beta\hat{\Theta}_0 i = 0\Big|_{y=1} \tag{7.3.0.4}$$

Tangential Stress:

$$\frac{\hat{\Theta}_0(1)}{\bar{\Theta}_y(1)} + \hat{v}_0''i = 0\Big|_{y=1} \tag{7.3.0.5}$$

$\mathbf{O(\kappa)}$:

$$\hat{\Theta}_1'' + \lambda e^{-\beta\bar{\Theta}}\Big(2\bar{u}_y\hat{v}_1'' + \beta\hat{\Theta}_1\bar{u}_y^2\Big) = \xi\Big(-ic_0\hat{T}_0 + i\bar{u}\hat{\Theta}_0 + \hat{v}_0\bar{\Theta}_y\Big) \tag{7.3.0.6}$$

$$R\Big((c_0-\bar{u})\hat{v}_0''+\bar{u}_{yy}\hat{v}_0\Big)e^{\beta\bar{\Theta}}=\beta^2\bar{\Theta}_y^2 i\hat{v}_1''-\beta\bar{\Theta}_y\bar{u}_y\Big(\beta^2\bar{\Theta}_y\hat{\Theta}_1-\beta\hat{\Theta}_1'\Big)-\beta\bar{\Theta}_{yy}i\hat{v}_1''$$
$$-2\beta\bar{\Theta}_y i\hat{v}_1'''+\bar{u}_{yy}\Big(\beta^2\bar{\Theta}_y\hat{\Theta}_1-2\beta\hat{\Theta}_1'\Big)+\bar{u}_y\Big(\beta^2\bar{\Theta}_{yy}\hat{\Theta}_1+\beta^2\bar{\Theta}_y\hat{\Theta}_1'-\beta\hat{\Theta}_1''\Big)$$
$$+\beta^2\bar{\Theta}_y\hat{\Theta}_1\bar{u}_{yy}+\hat{v}_1''''i-\beta\hat{\Theta}_1\bar{u}_{yyy} \tag{7.3.0.7}$$

Boundary Conditions:
Normal Stress:

$$\frac{\hat{\Theta}_0(1)}{\bar{\Theta}_y(1)}\cot\theta i+R(c_0-\bar{u})\hat{v}_0'+\beta\bar{\Theta}_y i\hat{v}_1''-\hat{v}_1'''i+\beta\hat{\Theta}_1=0\Big|_{y=1}, \tag{7.3.0.8}$$

Tangential Stress:

$$\frac{\hat{\Theta}_1(1)}{\bar{\Theta}_y(1)}+\hat{v}_1''i=0\Big|_{y=1}, \tag{7.3.0.9}$$

Substituting tangential stress balance leading order into the normal stress balance leading order, we have:

$$\hat{v}_0'''+\beta\bar{\Theta}_y i\frac{\hat{\Theta}_0(1)}{\bar{\Theta}_y(1)}+\beta+\beta'\frac{\mu_p}{\mu_t}\hat{\Theta}_0 i=0\Big|_{y=1}\rightarrow\hat{v}_0'''\Big|_{y=1}=-2\beta\hat{\Theta}_0 i\Big|_{y=1}.$$

Similarly for the $O(\kappa)$:

$$\frac{\hat{\Theta}_0(1)}{\bar{\Theta}_y(1)}\cot\theta i+R\hat{v}_0'(c_0-\bar{u})-\beta\bar{\Theta}_y\frac{\hat{\Theta}_1(1)}{\bar{\Theta}_y(1)}-\hat{v}_1'''i+\beta\hat{\Theta}_1=0\Big|_{y=1}.$$

The problem at this stage has the same complexity as before (normal modes) since we have to solve like Orr-Sommerfeld (the analogue for non-isothermal) coupled with energy equations (7.3.0.3)-(7.3.0.2) and (7.3.0.7)-(7.3.0.6). To

move on with the analytic work, we make the assumption that Brinkman number is zero. This allows us to solve the basic flow analytically. The basic flow is

$$\bar{\Theta}_{yy} = 0 \rightarrow \hat{\Theta}_0 = a_1 y + a_2$$

with $\bar{\Theta}|_{y=0} = 1$ and $\bar{\Theta}_{y=1} = 0$. After finding the constants of integration we have

$$\bar{\Theta} = 1 - y \tag{7.3.0.10}$$

Substituting (7.3.0.10), (7.2.0.10), and (7.2.0.14) into (7.2.0.4)

$$\bar{u} = \frac{e^{-\beta(y-1)}(1 + \beta y - \beta)}{\beta^2} + \frac{e^{\beta}(\beta - 1)}{\beta^2} \tag{7.3.0.11}$$

And eq. (7.2.0.5) and (7.2.0.12) give

$$\bar{P} = \cot\theta(1 - y) \tag{7.3.0.12}$$

Eq. (7.3.0.2), and bc (7.2.0.17)

$$\hat{\Theta}_0 = A_1 y \tag{7.3.0.13}$$

where A_1 an arbitrary constant. Substituting (7.3.0.13) into (7.3.0.3) we have:

$$\hat{v}_0^{(4)} + 2\beta\hat{v}_0''' + \beta^2\hat{v}_0'' - 2\beta A_1 e^{-\beta(y-1)} i = 0 \tag{7.3.0.14}$$

The 4 boundary conditions of this fourth order ODE are:

$$\hat{v}_0''' + \beta\hat{v}_0'' + \beta A_1 i\Big|_{y=1} = 0 \tag{7.3.0.15}$$

$$\hat{v}_0'' + A_1 i\Big|_{y=1} = 0 \tag{7.3.0.16}$$

$$\hat{v}_0 + A_1(\bar{u} - c_0)i\Big|_{y=1} = 0 \tag{7.3.0.17}$$

$$\hat{v}\Big|_{y=0} = 0 \tag{7.3.0.18}$$

Solving the above ODE we have

$$\hat{v}_0 = \frac{A_1 i e^{-\beta(y-1)}}{\beta^3}\Big(-3\beta + 4\beta y - \beta^2 y + \beta^2 y^2 + 6\Big) + \frac{e^{\beta} A_1 i}{\beta^3}\Big(-6 + 3\beta - 2\beta^2 y + 2\beta y\Big) \tag{7.3.0.19}$$

and the eigenvalue c_0 is: $c_0 = \frac{e^{\beta}(6-6\beta+3\beta^2)-6}{\beta^3}$.
And the $O(\kappa)$ terms are:

$$\Theta_1'' = \xi\Big(\hat{\Theta}_0(\bar{u} - c_0)i - \hat{v}_0\Big) \tag{7.3.0.20}$$

and

$$\hat{v}_1'''' = -2\beta\hat{v}_1''' - \beta^2\hat{v}_1'' + \hat{\Theta}_1''(\beta\bar{u}_y)i + \hat{\Theta}_1' 2\beta e^{-\beta(y-1)}i + R\Big(\hat{v}_0''(\bar{u} - c_0) - \hat{v}_0\bar{u}_{yy}\Big)e^{-\beta\Theta_0}i \tag{7.3.0.21}$$

Since we found the analytical solutions for the perturbation function at leading order, we now can solve analytically the $O(k)$ equations 7.3.0.20 and 7.3.0.21 with the ultimate aim to express analytically the amplification rate

(the imaginary part of c_1)and predict the stability of the system.

$$\Theta_1 = \frac{e^{\beta(1-y)}(6A\xi - \frac{24A\xi}{\beta})i + 2C_{11}\beta^4 y - A\xi y e^{-\beta(y-1)}6i}{(2\beta^4)} \qquad (7.3.0.22)$$
$$+ \frac{A\beta\xi y^3(\beta e^{\beta} - 2e^{\beta} + 2)i - A\beta\xi y^2 e^{\beta}(\beta - 2)3i}{(2\beta^4)} - \frac{e^{\beta}(6A\xi - \frac{24A\xi}{\beta})i}{(2\beta^4)}$$

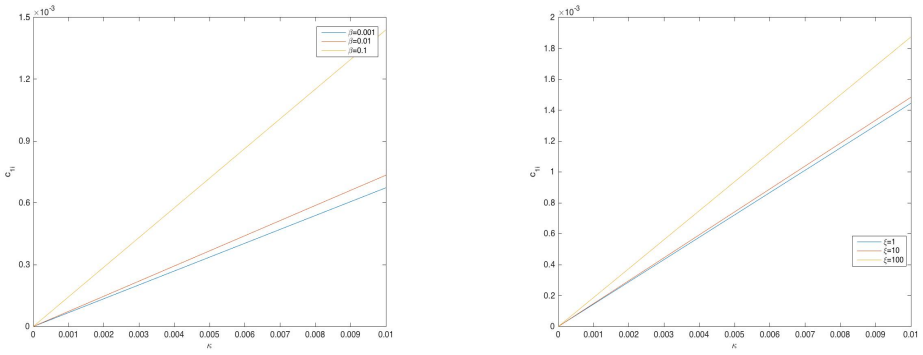
$v_1 = (25920A\xi e^{\beta} + 7776RAe^{-\beta(y-1)} - 3726RAe^{-2\beta(y-1)} - 12960RAe^{-\beta(y-2)} +$
$5184RAe^{-\beta(y-3)} - C_{11}\beta^5 e^{\beta}1296i + C_{11}\beta^6 e^{\beta}648i - 25920A\xi e^{-\beta(y-1)} + 25920A\xi e^{-\beta(y-2)} +$
$16686RAe^{2\beta} - 8910RAexp(3\beta) - 25920A\xi e^{2\beta} + C_{11}\beta^5 e^{-\beta(y-1)}1296i - C_{11}\beta^6 e^{-\beta(y-1)}648i +$
$3726RAexp(-\beta(2y-3)) - 7776RAe^{\beta} - 16524A\beta^2\xi e^{2\beta} + 1998A\beta^3\xi e^{2\beta} + 216A\beta^4\xi e^{2\beta} -$
$432A\beta^5 e^{\beta}\cot\theta + 216A\beta^6 e^{\beta}\cot\theta + 1728RA\beta^2 exp(-\beta(2y-3)) - 270RA\beta^3 exp(-\beta(2y-$
$3)) + C_{11}\beta^7 y^2 e^{-\beta(y-1)}216i - 1350RA\beta e^{\beta} + 432A\beta^5 e^{-\beta(y-1)}\cot\theta - 216A\beta^6 e^{-\beta(y-1)}\cot\theta -$
$2592A\beta\xi e^{\beta} + 1350RA\beta e^{-\beta(y-1)} + 1296RA\beta e^{-2\beta(y-1)} + 12528RA\beta e^{-\beta(y-2)} +$
$26RA\beta e^{-3\beta(y-1)} - 12096RA\beta e^{-\beta(y-3)} + 2592A\beta\xi e^{-\beta(y-1)} + 891A\beta\xi e^{-2\beta(y-1)} -$
$36288A\beta\xi e^{-\beta(y-2)} - 13824RA\beta e^{2\beta} + 16201RA\beta e^{3\beta} + C_{11}\beta^6 y e^{\beta}432i - C_{11}\beta^7 y e^{\beta}432i +$
$35397A\beta\xi e^{2\beta} - 216A\beta^3\xi e^{\beta} - 4131RA\beta e^{-\beta(2y-3)} - 3456RA\beta^2 e^{-\beta(y-2)} - 52RA\beta^2 e^{-3\beta(y-1)} +$
$10800RA\beta^2 e^{-\beta(y-3)} + 12RA\beta^3 e^{-3\beta(y-1)} - 4752RA\beta^3 e^{-\beta(y-3)} + 864RA\beta^4 e^{-\beta(y-3)} +$
$C_{11}\beta^6 y e^{-\beta(y-1)}864i - C_{11}\beta^7 y e^{-\beta(y-1)}216i - 972A\beta^2\xi e^{-2\beta(y-1)} + 17496A\beta^2\xi e^{-\beta(y-2)} +$
$216A\beta^3\xi e^{-\beta(y-1)} + 162A\beta^3\xi e^{-2\beta(y-1)} - 2160A\beta^3\xi e^{-\beta(y-2)} - 216A\beta^4\xi e^{-\beta(y-2)} +$
$3456RA\beta^2 e^{2\beta} - 12476RA\beta^2 e^{3\beta} + 5010RA\beta^3 e^{3\beta} - 864RA\beta^4 e^{3\beta} + 324RA\beta^2 y^2 e^{-\beta(2y-3)} -$
$162RA\beta^3 y^2 e^{-\beta(2y-3)} - 20736A\beta\xi y e^{-\beta(y-1)} + 20736A\beta\xi y e^{-\beta(y-2)} - 15876RA\beta y e^{2\beta} +$
$8100RA\beta y e^{3\beta} + 1350RA\beta^2 y e^{\beta} + 5184A\beta\xi y e^{2\beta} - 1296A\beta^2\xi y e^{\beta} + 216A\beta^4\xi y e^{\beta} +$
$1944RA\beta y e^{-\beta(2y-3)} + 324RA\beta^2 y e^{-2\beta(y-1)} + 2592RA\beta^2 y e^{-\beta(y-2)} + 52RA\beta^2 y e^{-3\beta(y-1)} -$
$4752RA\beta^2 y e^{-\beta(y-3)} - 24RA\beta^3 y e^{-3\beta(y-1)} + 3024RA\beta^3 y e^{-\beta(y-3)} - 864RA\beta^4 y e^{-\beta(y-3)} +$
$3888A\beta^2 xiy e^{-\beta(y-1)} + 972A\beta^2 xiy e^{-2\beta(y-1)} - 28512A\beta^2 xiy e^{-\beta(y-2)} - 324A\beta^3 xiy e^{-2\beta(y-1)} +$
$11016A\beta^3 xiy e^{-\beta(y-2)} - 1296A\beta^4 xiy e^{-\beta(y-2)} + 12204RA\beta^2 y e^{2\beta} - 13852RA\beta^2 y e^{3\beta} -$
$3456RA\beta^3 y e^{2\beta} + 10668RA\beta^3 y e^{3\beta} - 4392RA\beta^4 y e^{3\beta} + 864RA\beta^5 y e^{3\beta} - 6966A\beta^2 xiy e^{2\beta} +$
$4860A\beta^3 xiy e^{2\beta} - 540A\beta^4 xiy e^{2\beta} - 216A\beta^5 xiy e^{2\beta} + 216A\beta^6 y e^{\beta}\cot\theta - 216A\beta^7 y e^{\beta}\cot\theta -$
$1728RA\beta^2 y e^{-\beta(2y-3)} + 432RA\beta^3 y e^{-\beta(2y-3)} - 324RA\beta^2 y^2 e^{-2\beta(y-1)} + 12RA\beta^3 y^2 e^{-3\beta(y-1)} +$
$7776RA\beta y e^{\beta} + 216A\beta^6 y e^{-\beta(y-1)}\cot\theta - 7776A\beta^2\xi y^2 e^{-\beta(y-1)} + 7776A\beta^2\xi y^2 e^{-\beta(y-2)} +$
$1296A\beta^3\xi y^2 e^{-\beta(y-1)} + 162A\beta^3\xi y^2 e^{-2\beta(y-1)} - 9072A\beta^3\xi y^2 e^{-\beta(y-2)} - 1728A\beta^3\xi y^3 e^{-\beta(y-1)} +$
$1728A\beta^3\xi y^3 e^{-\beta(y-2)} + 3240A\beta^4\xi y^2 e^{-\beta(y-2)} + 216A\beta^4\xi y^3 e^{-\beta(y-1)} - 1728A\beta^4\xi y^3 e^{-\beta(y-2)} -$
$216A\beta^4\xi y^4 e^{-\beta(y-1)} - 324A\beta^5\xi y^2 e^{-\beta(y-2)} + 216A\beta^4\xi y^4 e^{-\beta(y-2)} + 432A\beta^5\xi y^3 e^{-\beta(y-2)} -$

$108A\beta^5\xi y^4 e^{-\beta(y-2)} - 5184A\beta\xi y e^{\beta} - 1944RA\beta y e^{-2\beta(y-1)} - 2592RA\beta y e^{-\beta(y-2)} + 2592RA\beta y e^{-\beta(y-3)})/(216\beta^8)$.

And the amplification rate is:

$c_1 = \Big(\Big(4050 * R - 41472\xi + 728R\beta - 19845\beta\xi - 17010Re^{\beta} - 2592\beta^2\xi + 82944\xi e^{\beta} + 21870Re^{2\beta} - 8910Re^{3\beta} + 432\beta^5\cot(\theta) - 41472\xi e^{2\beta} - 37584\beta\xi e^{\beta} - 39204R\beta e^{2\beta} + 24301R\beta e^{3\beta} + 810R\beta^2 e^{\beta} + 57429\beta\xi e^{2\beta} + 1296\beta^2\xi e^{\beta} + 1512\beta^3\xi e^{\beta} - 216\beta^4\xi e^{\beta} + 21708R\beta^2 e^{2\beta} - 26328R\beta^2 e^{3\beta} - 5184R\beta^3 * e^{2\beta} + 15678R\beta^3 e^{3\beta} - 5256R\beta^4 e^{3\beta} + 864R\beta^5 e^{3\beta} - 34506\beta^2\xi e^{2\beta} + 11610\beta^3\xi e^{2\beta} - 2268\beta^4\xi e^{2\beta} + 216\beta^5\xi e^{2\beta} - 432\beta^5 e^{\beta}\cot(\theta) + 432\beta^6 e^{\beta}\cot(\theta) - 216\beta^7 e^{b}\cot(\theta) + 14175R\beta e^{\beta}\Big) * 1i\Big)/(216 * b^8)$

In the chapter 7.5 we compare the analytical results with the numerical.



(a) c_{1i} regarding different β **(b)** c_{1i} regarding different ξ

Figure 7.1: The amplification rate increases with the increase in β and ξ, where R=3, and $\theta = 45^o$. The flow is unstable since the critical Reynolds is $R_c = 2.5$

7.4 Validation Of Model

In order to examine the above data we attempt a direct comparison with a similar problem. Yih in 1962 investigated the stability of a liquid flow down an inclined plane under isothermal conditions. After derived the Orr-Sommerfeld equation, he assumed that the wavelength of the perturbation is large compare to the depth of the film, the wavenumber ,in his case α, is small, and it was used to as scaling for the stream-function ϕ and the eigenvalue c such as $\phi = \phi_0 + \alpha\phi_1$ and $c = c_0 + \alpha c_1$. The results he came up with were $c_0 = 3$ and $c_1 = \frac{6\alpha R}{5} - \frac{\alpha\cot\theta}{3}$. In that thesis different scaling was

used on the average velocity and Reynolds number. The scaling for Yih was $\bar{u_a} = \frac{gd^2 \sin\theta}{3\nu}$,where ν the kinematic viscosity and defined Reynolds number as $R = \frac{\bar{u_a}}{\nu}$. Adjusting the above according to the scaling of that thesis the values are: $c_0 = 1$ and $c_{1i} = \frac{2\alpha R}{15} - \frac{\alpha \cot\theta}{3}$. In order to compare these results with our data, we have to modified the problem properly. Grashof number set to zero and Taylor approximations are used. More specific, $e^{\beta} = 1 + \beta + \frac{\beta^2}{2!} + \cdots + \frac{\beta^{\nu}}{\nu!}$. Substituting the above expansion into the c_0 we have: $c_0 = \frac{(1+\beta+\frac{\beta^2}{2}+\frac{\beta^3}{6})(6-6\beta+3\beta^2)-6}{\beta^3} = 1+O(\beta)$ ad the limit when β goes to zero is 1. Since the denominator of the polynomial of c_1 is β^8 the above approximations should be taken up to eighth order and indeed it is in line with Yih's results.

7.5 Arbitrary Wavenumber - Numerical Analysis

In this section, unlike the 7.3, the wavenumber κ is $O(1)$. The governing equations (eq. 7.2.0.20-7.2.0.23) with the corresponding boundary conditions (7.2.0.24-7.2.0.26) were displayed in the previous chapter. We eliminate $\hat{S}$ and $\hat{u}$ by substituting the eq.(7.2.0.18) and 7.2.0.7 into the governing equations and boundary conditions and combining (7.2.0.8) with (7.2.0.9), and we finally derived the analogue of Orr-Sommerfeld equation for the non-isothermal flow. At this point we assume that Brinkman number is zero.

$$\hat{\Theta}'' - \kappa^2\hat{\Theta} = \xi\Big(\hat{\Theta}i\kappa(\bar{u}-c) + \hat{v}\bar{\Theta}_y\Big) \tag{7.5.0.1}$$

$$\begin{aligned}
&\kappa R\Big(\hat{v}\bar{u}_{yy} + (\hat{v}'' - k^2\hat{v})(c-\bar{u})\Big)e^{\beta\bar{\Theta}} = \hat{v}''''i - 2\beta\bar{\Theta}_y i\hat{v}''' + \hat{v}''\Big((\beta\bar{\Theta}_y)^2 i - 2\kappa^2 i\Big)\\
&+ \hat{v}'\Big(2\beta\kappa^2 i\bar{\Theta}_y + 2\kappa^2\beta\bar{\Theta}_y i - \beta\bar{\Theta}_y\kappa^2 i - \beta\bar{\Theta}_y\kappa^2 i\Big) + \hat{v}\Big(\kappa^4 i + (\beta\bar{\Theta}_y)^2 i\kappa^2\Big)\\
&+ \hat{\Theta}''(-\beta\bar{u}_y\kappa) + \hat{\Theta}'\Big(\beta^2\bar{u}_y\kappa\bar{\Theta}_y - \beta\kappa\bar{u}_{yy} + \beta^2\kappa\bar{\Theta}_y\bar{u}_y - \beta\kappa\bar{u}_{yy}\Big)\\
&+ \hat{\Theta}\Big(-\beta\kappa^3\bar{u}_y - \beta^3\bar{\Theta}_y^2\bar{u}_y\kappa + \beta^2\bar{\Theta}_y\bar{u}_{yy}\kappa + \bar{\Theta}_y\bar{u}_{yy}\kappa\beta^2 - \beta\kappa\bar{u}_{yyy} + \beta^2\bar{\Theta}_{yy}\bar{u}_y\Big)
\end{aligned} \tag{7.5.0.2}$$

with the corresponding boundary conditions:

No Slip: $$\hat{v}\Big|_{y=0} = \hat{v}'\Big|_{y=0} = 0 \tag{7.5.0.3}$$

Modified Normal Stress Balance: $$\begin{aligned}
&\hat{v}''' + \hat{v}''\Big(\frac{-\bar{P}_y\kappa e^{\beta\bar{\Theta}}}{\bar{u}_{yy}} - \beta\bar{\Theta}_y - \frac{\gamma\kappa^3 e^{\beta\bar{\Theta}}i}{\bar{u}_{yy}}\Big)\\
&+ \hat{v}'\Big(R(c-\bar{u})e^{\beta\bar{\Theta}}\kappa i - 3\kappa^2\Big) + \hat{v}\Big(-\frac{P_y\kappa^{\bar{3}}e^{\beta}\bar{\Theta}i}{\bar{u}_{yy}}\Big) + \hat{\Theta}\kappa\beta\bar{u}_{yy}i\Big|_{y=1} = 0
\end{aligned} \tag{7.5.0.4}$$

$$\text{Tangential Stress Balance:} \quad (\hat{v}'' - \kappa^2 \hat{v})(c - \bar{u}) + \hat{v}\bar{u}_{yy}\Big|_{y=1} = 0 \tag{7.5.0.5}$$

The basic flow can now be solved analytically like in previous chapters. After solving the ODEs for the basic flow we have: $\bar{\Theta} = 1 - y$, $\bar{P} = \cot\theta(1 - y)$ and $\bar{u} = \frac{e^{-\beta(y-1)}}{\beta^2}\Big(1 - \beta + \beta y\Big) + \frac{e^{\beta}}{\beta^2}\Big(\beta - 1\Big)$

The eigenvalue problem (7.5.0.1-7.5.0.2) is not possible to be solved analytically, so the problem has to be tackled numerically. From a numerical point of view, there are to general methods for finding the eigenvalues; the local method and the global method. The first one requires initial guesses which are modified until satisfy the boundary conditions. The global method uses the fully discretized stability operator and supplies it to a matrix eigenvalue solver which results in the spectrum. Hence, the global methods overweight the local by delivering the full spectrum instead of one, but very accurate, eigenvalue. However, direct methods could be prohibitively expensive or impossible, even with the best available computing power [Schmid (2000), Amritkar et al. (2015)]. A global approach for that system is chosen. We use a finite differences code specifically designed for this particular problem. Central finite difference method is used, with second order accuracy.

Using the five-point stencil, we need to extend the boarders over the wall and the free surface using ghost points. Since momentum equation is a fourth order ODE and the normal stress balance is third order we need to create two more ghost lines above the free surface and one below the wall. For the last one the boundary condition $\hat{v}'\Big|_{y=0} = 0$ is applied. To create and evaluate the ghost points above the free surface we use the momentum equation on the surface accompanied with the normal stress balance (7.5.0.4). By doing that we are able to construct a generalized eigenvalue problem of the form of $\bar{\boldsymbol{A}} \cdot \boldsymbol{X} = c\bar{\boldsymbol{B}} \cdot \boldsymbol{X}$, where: $\boldsymbol{X}$ is the vector of unknowns, $\bar{\boldsymbol{A}}$, $\bar{\boldsymbol{B}}$ are the matrices of the finite difference approximations for the energy and momentum equations and boundary conditions, respectively, and c the eigenvalue. Unfortunately, the no slip condition creates a serious problem, since this condition doesn't contain the eigenvalue and is represented with a zero row on

the matrix $\bar{B}$, that makes it singular. To overtake this obstacle we modify the first rows of both $\bar{\boldsymbol{A}}$ and $\bar{\boldsymbol{B}}$. In the $\bar{\boldsymbol{B}}$ we add 1 and in the $\bar{A}$ row we include a large arbitrary complex number that sends the spurious eigenvalue due to the condition far away, in the negative complex plane and it doesn't interfere with the rest eigenvalues [Schmid et al. (2002)].

7.6 Numerical Experiment

We carry out numerical experiment of the above eigenvalue problem (7.3.0.20-7.3.0.21). The dimensionless viscosity parameter β destabilizes the system and increases the growth rate rapidly. The same effect produces the increase of the Reynolds number. Furthermore, the increase in Grashof number increases the growth rate, only slightly and it's more obvious in the analytical solutions. On the other hand, the increase in the value of the dimensionless surface tension decreases the growth rate substantially.

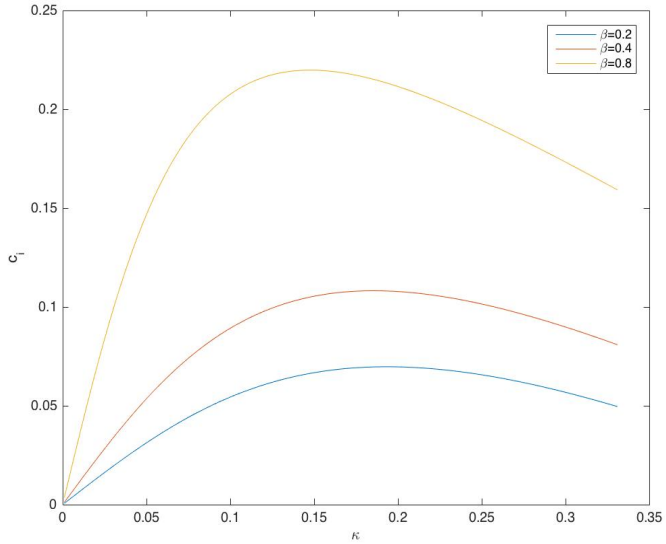


Figure 7.2: Growth rate over wavenumber regarding different values of β, where: $\beta = 0.5$, $\xi = 1$, $R = 5$, and $\theta = 45^o$. The dimensionless viscosity parameter β increases the growth rate rapidly.

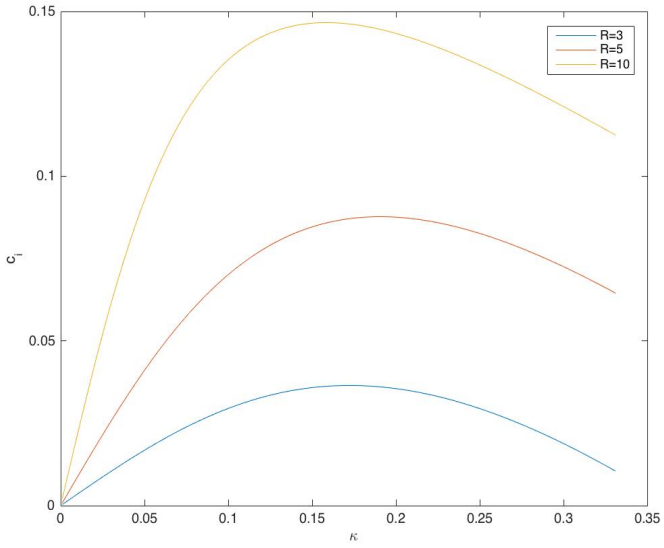


Figure 7.3: Growth rate over wavenumber regarding different Reynolds numbers, where: $\beta = 0.5$, $\xi = 1$, $R = 5$, and $\theta = 45^o$. When R increases, the growth rate increases substantially.

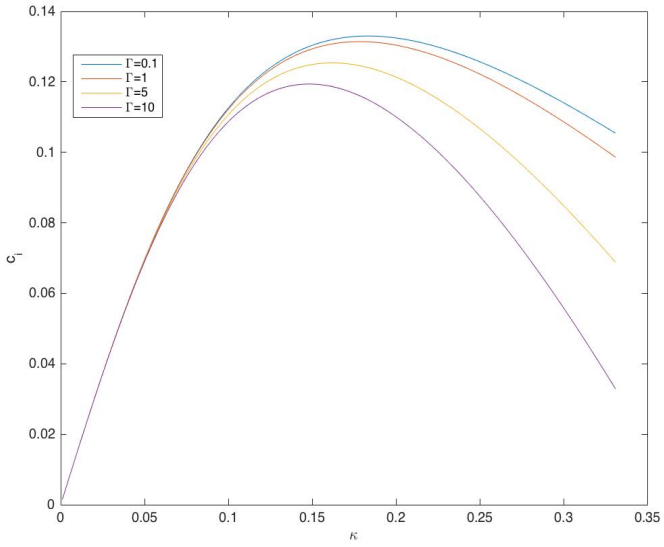


Figure 7.4: Growth rate over wavenumber regarding different values of the dimensioless surface tension, where: $\beta = 0.5$, $\xi = 1$, $R = 5$, and $\theta = 45^o$. The increase in Γ decreases the growth rate.

7.7 Verification of the numerical Methods

The global method is a well establish numerical process with remarkable accuracy. However, the code was designed for this specific eigenvalue problem (7.5.0.1-7.5.0.2) and requires validation. To do that, we are using the exact solutions of the long wave analysis for the linear stability of isothermal (7.4) and the non-isothermal flow (7.3). For small values of κ the growth rate should reach the c_{1i} in section 7.3 with arbitrary β. When the dimensionless viscosity parameter reaches zero then the growth rate should reach the accurate solution for the isothermal flow $c_{1i} = \frac{2}{15}R - \frac{1}{3}\cot\theta$ (section 7.4).

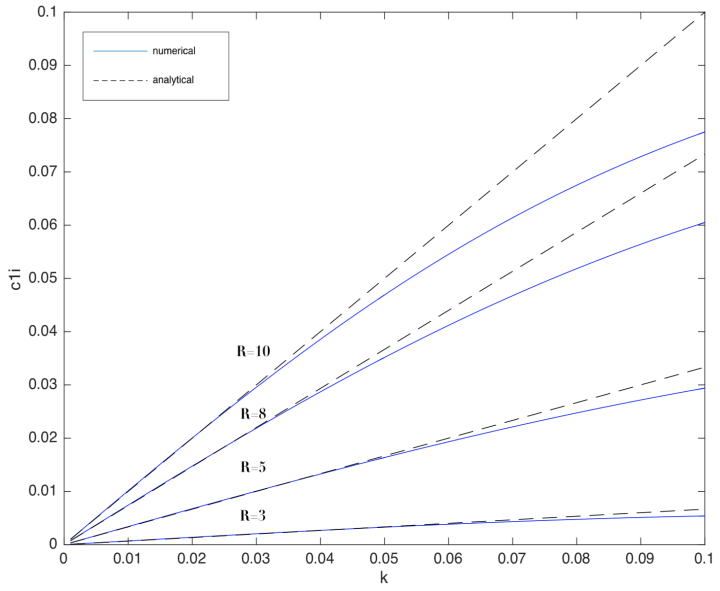


Figure 7.5: Comparison between long wave exact solutions and the non-isothermal plots, where: $\beta = 0.01$,$\xi = 1$, $\Gamma = 0.1$, and $\theta = 45^o$. For small values of wavenumber, the analytical and numerical solutions match.

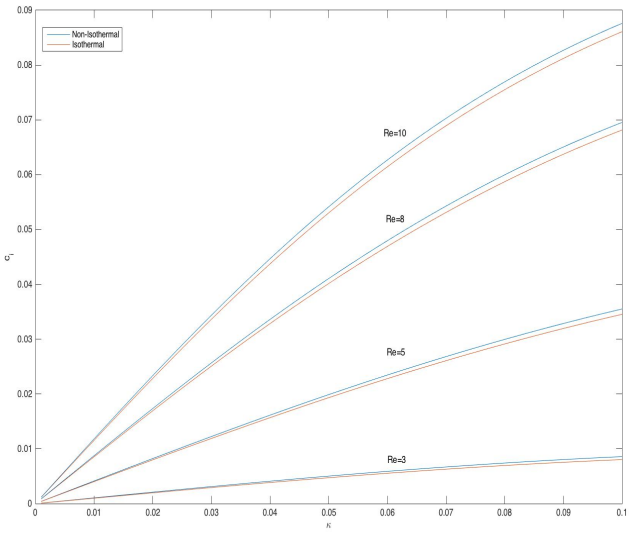


Figure 7.6: Comparison between isothermal and non-isothermal flow where: $\beta = 0.01$, $\xi = 1$ and $\Gamma = 0.1$. The uniform heating creates a slightly higher growth rate.

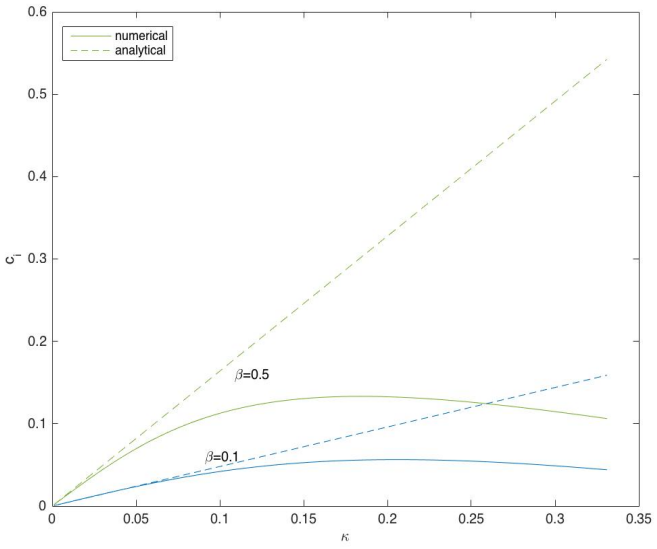


Figure 7.7: Comparison of long wave exact solutions with the non-isothermal plots regarding different value of Grashof number, where: $\beta = 0.01$, $R = 5$, $\Gamma = 0.1$, and $\theta = 45^o$. The numerical solutions match the analytical for small wavenumbers. Increasing β we notice a rapidly increase in the growth rate.

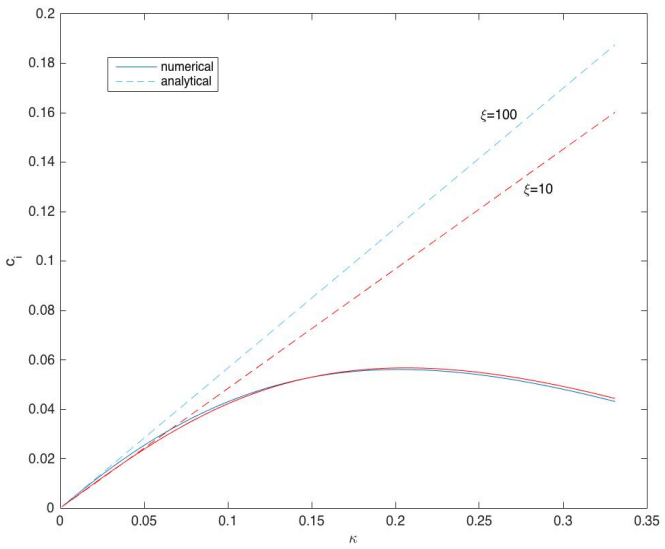


Figure 7.8: Comparison of long wave exact solutions with the non-isothermal plots regarding different value of Grashof number, where: $\beta = 0.01$, $R = 5$, $\Gamma = 0.1$, and $\theta = 45^o$. The numerical solutions match the analytical for small wavenumbers. An increase in Grashof increase the growth rate which is very noticeable especially in the exact solutions.

8

Conclusions

We have analyzed the dynamics of a film falling with variable viscosity down an inclined, heated wall. We considered two types of wall heating: uniform and non-uniform. Firstly, we investigated the heat transfer of viscoelastic fluid flows down an inclined, uniformly heated plate. The Oldroyd-B model was used to describe the polymeric part of viscosity. Using a combination of a boundary value problem solver and an ODE solver, we obtained the velocity and temperature profiles. We continued with problems regarding Newtonian fluid and non-uniform heating. The flow and heat transport was modeled with a long-wave theory for small Brinkman numbers and zero Grashof numbers. These assumptions led to the analytic solutions of energy and momentum equations for the basic flow and first-order ϵ. We examined the analytical solitary-wave solution of the long-wave theory for different values of the surface tension and predicted the general shape. We carried out extensive numerical experiments and revealed the contribution of each parameter in the velocity, temperature profile, as well as in the deformation of the surface, for even and odd heating conditions. The Brinkman and Reynolds number affected greatly the temperature and velocity profile, while they had zero effects in the stationary waves of the surface. On the

other hand, the increase in surface tension decreases the amplitude of the deformation of the surface while increasing the wavelength of it. An increase in the viscosity parameter increases, hugely, the deformation of the surface, the velocity, and temperature. We continued with a non-uniformly weakly heated falling film. Due to the nonlinear nature of the temperature field in the energy equation (5.4.1.1), it was convenient to take a power series expansion. Substituting the solution series into the energy and momentum equations, we modeled the basic flow, as a system of ODEs with the analytical solution for zero Brinkman number, and the $O(\epsilon)$ as a system of coupled PDEs, which had to be tackled numerically. A finite-difference code was designed for a specific problem. The numerical experiments showed the effect of each parameter in the velocity, temperature profile, and surface deformation. Quitting the zero Brinkman assumption, we faced a system of coupled ODEs for the basic flow and coupled PDEs for the next order. Using a boundary value problem solver as well as an ODE solver in Matlab, we were able to solve the basic flow accurately. Re-designed the code from the previous section (5.8), we highlighted the importance and effects of each parameter. Reynolds and Grashof numbers affected the system similarly like before (sections 5.7 and 5.8). While the increase in surface tension decreases the deformation of the surface, as expected, it also shifts the plot towards right. However, the increasing of Brinkman number increases the amplitude of the deformation and shifts the plot toward left. The linear stability of a non-isothermal uniformly heated inclined plane was the system of study for chapter 7. We started with a steady solution and introduced a small amplitude perturbation (ζ). Due to the nonlinear nature of the temperature field in the energy equation, we used power series expansions. We seek the solution in the form of the normal mode, which leads to the non-isothermal analogue of the Orr -Sommerfeld equation along with the energy equation. At this point, we wanted to carry out an analytical as well as numerical solution. To solve analytically the above systems of ODEs, basic flow and $O(\zeta)$, we incorporated in our analysis the small wavenumber theory. That reduced the complexity of the above problem by creating two more ODEs that can be solved analytically. That allowed us to find the analytical solutions for velocity, temperature, phase speed, and amplification rate up to order ζ and

κ. In what follows, we calculated the effect of the viscosity parameter and Grashof number on the critical Reynolds number. Also, we verified the results by deriving the isothermal model and compared it with Yih's results with remarkable accuracy. To continue without the small wavenumber assumption, we designed a finite-difference code to solve the specific problem, following a global approach. We carried out numerical experiments where the parameters vary. That showed the destabilizing behavior of the increasing β, R, and Grashof number, while the increase of the surface tension tended to stabilize the system. To verify the numerical method, we directly compare these results with the analytical ones from section (7.3), which presented perfect matching for small wavenumber.

9

Future Work

In this section, we will set directions for future work regarding this research, which can be classified into two categories: steady states and stability.
Firstly, we will study the steady states of a viscoelastic falling film with variable viscosity over a non-uniformly heated pate. In particular, we will extend the work of chapters 5 and 6 by deriving analogous governing systems which will additionally include the polymeric viscosity. For those calculations, the relaxation time will vary while the shear modulus remains constant. A first attempt can be found in the appendix A where we derive the governing equation for a non-uniformly heated viscoelastic falling film after assuming that the thickness of the film is very small compared to the length of it (section A.2.2), and in section A.2.3 we present the governing equations for weakly heated falling films.

In chapter 7, we carried out a linear stability analysis to determine growth rates in the presence of variable viscosity. We derived analytical expressions and performed numerous numerical simulations to examine the effects of the variable viscosity. It was proven to destabilize the system severely. The interesting part is what happens when the Reynolds number tends to the critical value ($R_c = \frac{5}{2}\cot\theta$). A falling film with the same properties, but

with constant viscosity, will be stable for all Reynolds numbers below the critical. However, a falling film with variable viscosity will remain unstable even for Reynolds below, but near, the critical value, depending on β. We calculated the exact expression in section 5.5 for small wavenumber. More research needs to be done to evaluate the effect of the viscosity parameter and the Grashof number on the critical Reynolds for $O(1)$ wavenumber. We are planning to achieve that by "silhouetting" and comparing the neutral curves between falling films with and without variable viscosity.

In addition, we want to extend the research of section 7.5 by studying the linear stability of non-isothermal falling films with variable viscosity and $O(1)$ Brinkman number. Also, we like to investigate further the above problem in the presence of a temperature gradient along the heated wall.

Finally, the work of chapter 7 provides an excellent ground for future research on the linear stability of non-uniformly heated viscoelastic falling films. We chose to solve the stability problem using a global approach. Using the fully discretized stability operator and supplying it to a matrix eigenvalue solver results in the full spectrum. Although this method does not require any initial guesses, it challenged even the best available computational power and was extremely time-consuming. After carrying extensively numerical experiments for the chapter 7, we conclude that a global approach would be challenging for the viscoelastic stability of the falling films with variable viscosity, so the results of the Newtonian flow can be used as initial guess for a local-method. The first step is the investigation of the linear stability of a Newtonian falling film with variable viscosity over a non-uniformly heated plane, where the results of chapter 7 will be the initial guesses for an iterative method.

Bibliography

Amritkar, A., de Sturler, E., Świrydowicz, K., Tafti, D., and Ahuja, K. (2015). Recycling krylov subspaces for cfd applications and a new hybrid recycling solver. *Journal of Computational Physics*, 303:222–237.

Bejan, A. (2016). *Advanced engineering thermodynamics*. John Wiley & Sons.

Benjamin, T. B. (1957). Wave formation in laminar flow down an inclined plane. *Journal of Fluid Mechanics*, 2(6):554–573.

Benney, D. (1966). Long waves on liquid films. *Studies in Applied Mathematics*, 45(1-4):150–155.

Blyth, M. G., Hall, P., and Papageorgiou, D. T. (2003). Chaotic flows in pulsating cylindrical tubes: a class of exact navier–stokes solutions. *Journal of Fluid Mechanics*, 481:187–213.

Borsoff, V. (1959). On the mechanism of gear lubrication. *Journal of Basic Engineering*, 80:79–93.

Davalos-Orozco, L. A. (2013). Stability of thin liquid films falling down isothermal and nonisothermal walls. *Interfacial Phenomena and Heat Transfer*, 1(2).

Dowson, D. and Higginson, G. R. (1966). *Elasto-hydrodynamic lubrication: the fundamentals of roller and gear lubrication*, volume 23. Pergamon Press.

Fenton, J. (1983). A taylor series method for numerical fluid mechanics. In *8th Australasian Fluid Mech Conf. Newcastle*.

Frank, A. (2006). Suppression of thermocapillary instability in a falling film. *Physics of Fluids*, 18(7):078106.

Green, D. W. and Perry, R. H. (1973). *Perry's Chemical Engineers' Handbook 8th edition Don W. Green y Robert H. Perry.* Number C 660.28 P47 2008.

Henry, D. (2005). *Perturbation of the boundary in boundary-value problems of partial differential equations*, volume 318. Cambridge University Press.

Jones, L. O. and Whitaker, S. (1966). An experimental study of falling liquid films. *AIChE Journal*, 12(3):525–529.

Joo, S., Davis, S., and Bankoff, S. (1991). Long-wave instabilities of heated falling films: two-dimensional theory of uniform layers. *Journal of Fluid Mechanics*, 230:117–146.

Kalliadasis, S. (2007). Falling films under complicated conditions. In *Thin Films of Soft Matter*, pages 137–190. Springer.

Kalliadasis, S., Kiyashko, A., and Demekhin, E. (2003). Marangoni instability of a thin liquid film heated from below by a local heat source. *Journal of Fluid Mechanics*, 475:377–408.

Karapantsios, T., Paras, S. t., and Karabelas, A. (1989). Statistical characteristics of free falling films at high reynolds numbers. *International Journal of Multiphase Flow*, 15(1):1–21.

Keenan, J. H., Keyes, F. G., Hill, P. G., and Moore, J. G. (1969). *Steam tables: thermodynamic properties of water including vapor, liquid, and solid phases*, volume 24. John Wiley Hoboken, NJ.

Kelly, R., Davis, S., and Goussis, D. (1986). On the instability of heated film flow with variable surface tension. *Heat Transfer*, pages 1937–1942.

Khani, F., Darvishi, M., and Gorla, R. S. R. (2011). Analytical investigation for cooling turbine disks with a non-newtonian viscoelastic fluid. *Computers & Mathematics with Applications*, 61(7):1728–1738.

Kierzenka, J. and Shampine, L. F. (2001). A bvp solver based on residual control and the maltab pse. *ACM Transactions on Mathematical Software*, 27(3):299–316.

Lawrence, C. (1988). The mechanics of spin coating of polymer films. *The Physics of fluids*, 31(10):2786–2795.

Makinde, O. (2010). Thermodynamic second law analysis for a gravity-driven variable viscosity liquid film along an inclined heated plate with convective cooling. *Journal of Mechanical Science and Technology*, 24(4):899–908.

Makinde, O. D. (2006). Laminar falling liquid film with variable viscosity along an inclined heated plate. *Applied Mathematics and Computation*, 175(1):80–88.

Marrucci, G. (1972). The free energy constitutive equation for polymer solutions from the dumbbell model. *Transactions of The Society of Rheology (1957-1977)*, 16(2):321–330.

Matthews, G. (1982). Brownian motion: An undergraduate laboratory experiment. *J. Chem. Educ*, 59(3):246.

Nóbrega, J., Pinho, F. T. d., Oliveira, P., and Carneiro, O. (2004). Accounting for temperature-dependent properties in viscoelastic duct flows. *International journal of heat and mass transfer*, 47(6):1141–1158.

Prilutski, G., Gupta, R., Sridhar, T., and Ryan, M. (1983). Model viscoelastic liquids. *Journal of Non-Newtonian Fluid Mechanics*, 12(2):233–241.

Pumir, A., Manneville, P., and Pomeau, Y. (1983). On solitary waves running down an inclined plane. *Journal of Fluid Mechanics*, 135:27–50.

Reisfeld, B. and Bankoff, S. (1990). Nonlinear stability of a heated thin liquid film with variable viscosity. *Physics of Fluids A: Fluid Dynamics*, 2(11):2066–2067.

Salamon, T. R., Armstrong, R. C., and Brown, R. A. (1994). Traveling waves on vertical films: Numerical analysis using the finite element method. *Physics of Fluids*, 6(6):2202–2220.

Schmid, P. J. (2000). Linear stability theory and bypass transition in shear flows. *Physics of Plasmas*, 7(5):1788–1794.

Schmid, P. J., Henningson, D. S., and Jankowski, D. (2002). Stability and transition in shear flows. applied mathematical sciences, vol. 142. *Appl. Mech. Rev.*, 55(3):B57–B59.

Shampine, L. F., Kierzenka, J., and Reichelt, M. W. (2000). Solving boundary value problems for ordinary differential equations in matlab with bvp4c. *Tutorial notes*, 2000:1–27.

Shortland, A. (2009). Glass production.

Sibgatullin, N. and Sibgatullina, A. (2003). Longwave approximation in film flow theory. *Fluid dynamics*, 38:601–611.

Sreenivasan, S. and Lin, S. (1978). Surface tension driven instability of a liquid film flow down a heated incline. *International Journal of Heat and Mass Transfer*, 21(12):1517–1526.

Tanner, R. I. (2000). *Engineering rheology*, volume 52. OUP Oxford.

Tarhan, M. O. (1983). *Catalytic reactor design*. McGraw-Hill Companies.

Wapperom, P. and Hassager, O. (1999). Numerical simulation of wire-coating: The influence of temperature boundary conditions. *Polymer Engineering & Science*, 39(10):2007–2018.

Winkler, R. G. (2016). Dynamics of flexible active brownian dumbbells in the absence and the presence of shear flow. *Soft matter*, 12(16):3737–3749.

Yih, C.-S. (1963). Stability of liquid flow down an inclined plane. *The physics of Fluids*, 6(3):321–334.

Zhang, F., Tang, D.-L., Geng, J., Wang, Z.-X., and Zhang, Z.-B. (2008). Study on the temperature distribution of heated falling liquid films. *Physica D: Nonlinear Phenomena*, 237(7):867–872.

A

Appendix

A.1 Introduction

We study the steady states of a viscoelastic falling film with variable viscosity over a non-uniformly heated pate. We extend the work of chapters 5 and 6 by deriving analogous systems inclouding the polymeric viscosity. As we saw in chapter 3.2.3, the polymeric viscosity introduce extra stress in the fluid, $\bar{\boldsymbol{\sigma}}^p = G\bar{\boldsymbol{A}}$.(equation 3.2.3.13). The polymeric viscosity is defined as $\eta_p = G\tau$. Both of those terms, shear modulus and relaxation time, are temperature-dependent variables. However, the relaxation time changes with a much faster rate than the shear modulus, allows us to assume constant shear modulus Nóbrega et al. (2004). In what follows, section A.2, we present the governing equations and boundary conditions and non-dimensionalize them, A.2.1. In chapter A.2.2 we derive the governing equation for a non-uniformly heated viscoelastic falling film after assuming that the thickness of the film is very small compared to the length of it. In section A.2.3 we present the governing equations for weakly heated falling films. Both systems will be tackled numerically.

A.2 Falling Film

Imagine a two-dimensional flow of an incompressible viscoelastic fluid of density ρ and variable viscosity η_t driven by gravity along an inclined, at an angle θ to the horizontal, channel, as shown in figure 5.1. In this report, we assume the angle θ does not impose any instability. A Cartesian frame of reference (x, y) is adopted with x and y measuring distances down and perpendicular to the wall, respectively. The assumption of steady state is used. The Oldroyd-B model is selected to describe the polymeric stress. The wall is smooth and heated non-uniformly. The upper surface of the liquid film is considered free with uniform temperature (T_f).

We use the 2-D version of equations 4.0.0.1 to 4.0.0.5.

Energy Equation:

$$\rho\hat{C_p}\Big(u_x\frac{\partial T}{\partial x}+u_y\frac{\partial T}{\partial y}\Big)=\kappa\Big(\frac{\partial^2 T}{\partial x^2}+\frac{\partial^2 T}{\partial y^2}\Big)+\eta_s\Bigg(2\Big(\frac{\partial u_x}{\partial x}\Big)^2+\Big(\frac{\partial u_x}{\partial y}+\frac{\partial u_y}{\partial x}\Big)+2\Big(\frac{\partial u_y}{\partial y}\Big)^2\Bigg) \tag{A.2.0.1}$$

Cauchy x-direction:

$$\rho\Big(u_x\frac{\partial u_x}{\partial x}+u_y\frac{\partial u_x}{\partial y}\Big)=\frac{\partial \sigma_{xx}}{\partial x}+\frac{\partial \sigma_{xy}}{\partial y}+\rho g\sin\theta \tag{A.2.0.2}$$

Cauchy y-direction:

$$\rho\Big(u_x\frac{\partial u_y}{\partial x}+u_y\frac{\partial u_y}{\partial y}\Big)=\frac{\partial \sigma_{xy}}{\partial x}+\frac{\partial \sigma_{yy}}{\partial y}+\rho g\cos\theta \tag{A.2.0.3}$$

where: $\hat{C_p}$ is the specific heat capacity at constant pressure, T the temperature, k is the thermal conductivity, u_x and u_y are the velocity in x and y

direction, respectively, ρ density, $\bar{\boldsymbol{\sigma}}$ the stress tensor with $\bar{\boldsymbol{\sigma}} = \begin{bmatrix} \sigma_{xx} & \sigma_{xy} \\ \sigma_{yx} & \sigma_{yy} \end{bmatrix}$, p the pressure, η_s the solvent viscosity, and g the gravity acceleration. The stress and conformation tensor can be evaluated from equations 4.0.1.2 and 4.0.1.3.

$$\sigma_{xx} = -p + 2\eta_s \frac{\partial u_x}{\partial x} + GA_{xx} \tag{A.2.0.4}$$

$$u_x \frac{\partial A_{xx}}{\partial x} + u_y \frac{\partial A_{xx}}{\partial y} - A_{xx} \frac{\partial u_x}{\partial x} - A_{xy} \frac{\partial u_x}{\partial y} - A_{xx} \frac{\partial u_x}{\partial x} - A_{yx} \frac{\partial u_x}{\partial y} = - \frac{1}{\tau}(A_{xx} - 1) \tag{A.2.0.5}$$

$$u_x \frac{\partial A_{xy}}{\partial x} + u_y \frac{\partial A_{xy}}{\partial y} - A_{xx} \frac{\partial u_y}{\partial x} - A_{xy} \frac{\partial u_y}{\partial y} - A_{xy} \frac{\partial u_x}{\partial x} - A_{yy} \frac{\partial u_x}{\partial y} = - \frac{1}{\tau} A_{xy} \tag{A.2.0.6}$$

$$u_x \frac{\partial A_{yy}}{\partial x} + u_y \frac{\partial A_{yy}}{\partial y} - A_{yx} \frac{\partial u_x}{\partial x} - A_{yy} \frac{\partial u_y}{\partial y} - A_{xy} \frac{\partial u_y}{\partial x} - Ayy \frac{\partial u_y}{\partial y} = -\frac{1}{\tau}(A_{yy} - 1) \tag{A.2.0.7}$$

$$\sigma_{yx} = \eta_s (\frac{\partial u_x}{\partial y} + \frac{\partial u_y}{\partial x}) + GA_{yx} \tag{A.2.0.8}$$

$$\sigma_{yy} = -p + 2\eta_s \frac{\partial u_y}{\partial y} + GA_{yy} \tag{A.2.0.9}$$

where, $\bar{\boldsymbol{A}}$ is the conformation tensor with $\bar{\boldsymbol{A}} = \begin{bmatrix} A_{xx} & A_{xy} \\ A_{yx} & A_{yy} \end{bmatrix}$, τ the relaxation time and G the shear modulus. Substituting equations A.2.0.4 to A.2.0.9 into

A.2.0.2 and A.2.0.3, we get the dimensional system of governing equations:

Energy:

$$\rho\hat{C_p}\Big(u_x\frac{\partial T}{\partial x}+u_y\frac{\partial T}{\partial y}\Big)=\kappa\Big(\frac{\partial^2 T}{\partial x^2}+\frac{\partial^2 T}{\partial y^2}\Big) + \eta_s\left(2\Big(\frac{\partial u_x}{\partial x}\Big)^2+\Big(\frac{\partial u_x}{\partial y}+\frac{\partial u_y}{\partial x}\Big)+2\Big(\frac{\partial u_y}{\partial y}\Big)^2\right) \tag{A.2.0.10}$$

Cauchy x-direction:

$$\rho\Big(u_x\frac{\partial u_x}{\partial x}+u_y\frac{\partial u_x}{\partial y}\Big)=2\frac{\partial \eta_s}{\partial x}\frac{\partial u_x}{\partial x}+\eta_s\frac{\partial^2 u_x}{\partial x^2}+\frac{\partial G}{\partial x}A_{xx}+G\frac{\partial A_{xx}}{\partial x} + \frac{\partial \eta_s}{\partial y}\Big(\frac{\partial u_y}{\partial x}+\frac{\partial u_x}{\partial y}\Big)+\eta_s\frac{\partial^2 u_x}{\partial y^2}+\frac{\partial G}{\partial y}A_{xy}+G\frac{\partial A_{xy}}{\partial y}+\rho g\sin\theta \tag{A.2.0.11}$$

Cauchy y-direction:

$$\rho\Big(u_x\frac{\partial u_y}{\partial x}+u_y\frac{\partial u_y}{\partial y}\Big)=\frac{\partial \eta_s}{\partial x}\Big(\frac{\partial u_y}{\partial x}+\frac{\partial u_x}{\partial y}\Big)+\eta_s\frac{\partial^2 u_y}{\partial x^2}+\frac{\partial G}{\partial x}A_{xy} + G\frac{\partial A_{xy}}{\partial x}-\frac{\partial p}{\partial y}+2\frac{\partial \eta_s}{\partial y}\frac{\partial u_y}{\partial y}+\eta_s\frac{\partial^2 u_y}{\partial y^2}+\frac{\partial G}{\partial y}A_{yy}+G\frac{\partial A_{yy}}{\partial y}+\rho g\cos\theta \tag{A.2.0.12}$$

where:

$$u_x\frac{\partial A_{xx}}{\partial x}+u_y\frac{\partial A_{xx}}{\partial y}-A_{xx}\frac{\partial u_x}{\partial x}-A_{xy}\frac{\partial u_x}{\partial y}-A_{xx}\frac{\partial u_x}{\partial x} - A_{yx}\frac{\partial u_x}{\partial y}=-\frac{1}{\tau}(A_{xx}-1) \tag{A.2.0.13}$$

$$u_x\frac{\partial A_{xy}}{\partial x}+u_y\frac{\partial A_{xy}}{\partial y}-A_{xx}\frac{\partial u_y}{\partial x}-A_{xy}\frac{\partial u_y}{\partial y}-A_{xy}\frac{\partial u_x}{\partial x} - A_{yy}\frac{\partial u_x}{\partial y}=-\frac{1}{\tau}A_{xy} \qquad \text{(A.2.0.14)}$$

$$u_x\frac{\partial A_{yy}}{\partial x}+u_y\frac{\partial A_{yy}}{\partial y}-A_{yx}\frac{\partial u_x}{\partial x}-A_{yy}\frac{\partial u_y}{\partial y}-A_{xy}\frac{\partial u_y}{\partial x} - Ayy\frac{\partial u_y}{\partial y}=-\frac{1}{\tau}(A_{yy}-1) \qquad \text{(A.2.0.15)}$$

The fact that the lower surface has a non-uniform temperature, imposes an non-uniformity on the flow. Because of the steady state assumption the interface is located at $y = h(x)$ and the following boundary conditions need to be imposed.

- 2 Boundary Conditions: At the lower surface the average temperature is T_0 and the free surface, located at $y = h(x)$, has a uniform temperature T_f.
- No slip condition at the wall: $u_x\Big|_{y=0} = u_y\Big|_{y=0} = 0$.
- Force Balance on the interface that gives the kinematic and dynamic boundary conditions, equations 4.0.1.4, 4.0.1.6 and 5.4.2.2. The kinematic boundary Condition that dictates the velocity of the fluid normal to the boundary must equal the velocity of the boundary normal to itself, while the dynamic boundary Condition implies that the pressure must be continuous at the free surface.

Normal Stress Balance

$$\frac{-h'}{\Big(1+(h')^2\Big)^{\frac{1}{2}}}\Bigg(\Big(-p+2\eta_s\frac{\partial u_x}{\partial x}+GA_{xx}\Big)\cdot\frac{-h'}{\Big(1+(h')^2\Big)^{\frac{1}{2}}}+\Big(\eta_s(\frac{\partial u_x}{\partial y}+\frac{\partial u_y}{\partial x})$$
$$+GA_{xy}\Big)\cdot\frac{1}{\Big(1+(h')^2\Big)^{\frac{1}{2}}}\Bigg)+\frac{1}{\Big(1+(h')^2\Big)^{\frac{1}{2}}}\Bigg(\Big(\eta_s(\frac{\partial u_x}{\partial y}+\frac{\partial u_y}{\partial x})+GA_{xy}\Big)\cdot\frac{-h'}{\Big(1+(h')^2\Big)^{\frac{1}{2}}}$$
$$+\Big(-p+2\eta_s\frac{\partial u_y}{\partial y}+GA_{yy}\Big)\cdot\frac{1}{\Big(1+(h')^2\Big)^{\frac{1}{2}}}\Bigg)=-\sigma\frac{h"}{\Big(1+(h')^2\Big)^{\frac{3}{2}}} \tag{A.2.0.16}$$

Tangential Stress Balance

$$\frac{-h'}{\Big(1+(h')^2\Big)^{\frac{1}{2}}}\Bigg(\Big(-p+2\eta_s\frac{\partial u_x}{\partial x}+GA_{xx}\Big)\frac{1}{\Big(1+(h')^2\Big)^{\frac{1}{2}}}$$
$$+\Big(\eta_s(\frac{\partial u_x}{\partial y}+\frac{\partial u_y}{\partial x})+GA_{xy}\Big)\frac{h'}{\Big(1+(h')^2\Big)^{\frac{1}{2}}}\Bigg)+\frac{1}{\Big(1+(h')^2\Big)^{\frac{1}{2}}}\Bigg(\Big(\eta_s(\frac{\partial u_x}{\partial y}+\frac{\partial u_y}{\partial x})$$
$$+GA_{xy}\Big)\frac{1}{\Big(1+(h')^2\Big)^{\frac{1}{2}}}+\Big(-p+2\eta_s\frac{\partial u_y}{\partial y}+GA_{yy}\Big)\frac{h'}{\Big(1+(h')^2\Big)^{\frac{1}{2}}}\Bigg)=0 \tag{A.2.0.17}$$

A.2.1 Non-dimensionalization

We non-dimensionalize the governing equations. We assume that the solvent and polymeric viscosities obey an Arrhenius type equation, $\eta_s = \mu_s e^{\alpha(T-T_f)}$ and $\eta_p = \mu_p e^{\alpha(T-T_f)}$ where μ_s and μ_p are positive constants. We introduce the constant μ_t defined like $\mu_t = \mu_s + \mu_p$. Also we assume that the lower surface has an average temperature T_0. After that the dimensionless variables are:

$$x = \delta x^*, \qquad y = \delta y^*, \qquad \boldsymbol{u} = \frac{\delta^2 \rho g \sin\theta}{\mu_t}\boldsymbol{u^*} \qquad p = p^* \delta \rho g \sin\theta$$

$$\Theta = \frac{T - T_0}{T_f - T_0}, \qquad G = G^* \delta \rho g \sin\theta, \qquad \tau = e^{-\beta\Theta}\frac{\mu_p}{\delta \rho g \sin\theta}, \qquad \beta = \alpha(T_0 - T_f)$$

After dropping the asterisks:

Energy Equation:

$$\frac{\partial^2\Theta}{\partial x^2}+\frac{\partial^2\Theta}{\partial y^2}+\lambda e^{-\beta\Theta}\left(2\Big(\frac{\partial u_x}{\partial x}\Big)^2+\Big(\frac{\partial u_x}{\partial y}+\frac{\partial u_y}{\partial x}\Big)^2+2\Big(\frac{\partial u_y}{\partial y}\Big)^2\right) = \xi\Big(u_x\frac{\partial\Theta}{\partial x}+u_y\frac{\partial\Theta}{\partial y}\Big) \tag{A.2.1.1}$$

Cauchy x-direction:

$$R\Big(u_x\frac{\partial u_x}{\partial x}+u_y\frac{\partial u_x}{\partial y}\Big) = -\frac{\partial p}{\partial x}+2\beta'\frac{\partial e^{-\beta\Theta}}{\partial x}\frac{\partial u_x}{\partial x}+\beta' e^{-\beta\Theta}\frac{\partial^2 u_x}{\partial x^2}+\frac{\partial G}{\partial x}A_{xx}+G\frac{\partial A_{xx}}{\partial x}$$
$$+\beta'\frac{\partial e^{-\beta\Theta}}{\partial y}\Big(\frac{\partial u_y}{\partial x}+\frac{\partial u_x}{\partial y}\Big)+\beta' e^{-\beta\Theta}\frac{\partial^2 u_x}{\partial y^2}+\frac{\partial G}{\partial y}A_{xy}+G\frac{\partial A_{xy}}{\partial y}+1 \tag{A.2.1.2}$$

Cauchy y-direction:

$$R\Big(u_x\frac{\partial u_y}{\partial x}+u_y\frac{\partial u_y}{\partial y}\Big) = \beta'\frac{\partial e^{-\beta\Theta}}{\partial x}\Big(\frac{\partial u_x}{\partial y}+\frac{\partial u_y}{\partial x}\Big)+\beta' e^{-\beta\Theta}\frac{\partial^2 u_y}{\partial x^2}$$
$$+\frac{\partial G}{\partial x}A_{xy}+G\frac{\partial A_{xy}}{\partial x}-\frac{\partial p}{\partial y}+2\beta'\frac{\partial e^{-\beta\Theta}}{\partial y}\frac{\partial u_y}{\partial y}+\beta' e^{-\beta\Theta}\frac{\partial^2 u_y}{\partial y^2}+\frac{\partial G}{\partial y}A_{yy}$$
$$+G\frac{\partial A_{yy}}{\partial y}+\cot\theta = 0 \tag{A.2.1.3}$$

where: $\lambda = \frac{(\delta^2\rho g\sin\theta)^2}{\mu_o\kappa(T_0-T_f)}$ is the Brinkman number, $R = \frac{\delta^3\rho^2 g\sin\theta}{\mu_t^2}$ is the Reynolds, $\xi = \frac{\hat{C_p}\delta^3 g\rho^2\sin\theta}{\mu_t\kappa}$ is the Grashof number which is the Reynolds number times the ratio of the force due to differences in density and the viscous force [Wapperom and Hassager (1999)], and $\beta' = \frac{\mu_0}{\mu_t}$ is the retardation parameter.

Then we non-dimensionalize the $\bar{\boldsymbol{A}}$:

That leads to:

$$u_x\frac{\partial A_{xx}}{\partial x}+u_y\frac{\partial A_{xx}}{\partial y}-A_{xx}\frac{\partial u_x}{\partial x}-A_{xy}\frac{\partial u_x}{\partial y}-A_{xx}\frac{\partial u_x}{\partial x}-A_{yx}\frac{\partial u_x}{\partial y}= -\frac{\mu_t}{\mu_p}e^{\beta\Theta}(A_{xx}-1) \qquad \text{(A.2.1.4)}$$

$$u_x\frac{\partial A_{xy}}{\partial x}+u_y\frac{\partial A_{xy}}{\partial y}-A_{xx}\frac{\partial u_y}{\partial x}-A_{xy}\frac{\partial u_y}{\partial y}-A_{xy}\frac{\partial u_x}{\partial x}-A_{yy}\frac{\partial u_x}{\partial y}= -\frac{\mu_t}{\mu_p}e^{\beta\Theta}A_{xy} \qquad \text{(A.2.1.5)}$$

$$u_x\frac{\partial A_{yy}}{\partial x}+u_y\frac{\partial A_{yy}}{\partial y}-A_{yx}\frac{\partial u_x}{\partial x}-A_{yy}\frac{\partial u_y}{\partial y}-A_{xy}\frac{\partial u_y}{\partial x}-Ayy\frac{\partial u_y}{\partial y}= -\frac{\mu_t}{\mu_p}e^{\beta\Theta}(A_{yy}-1) \qquad \text{(A.2.1.6)}$$

A.2.2 Non-uniformly heated Plane - Long wave Analysis

In this section we investigate a problem of weakly heated falling films, and we use the long wave assumption. Also, I would like to remind you, I have assumed that shear modulus G is constant and only relaxation time τ is a function of x and y, for more see Nóbrega et al. (2004). As a result of the complexity of this problems, it is convenient to use expansions of dimension-

less variables as follow:

$$\Theta = \Theta_0(y) + \epsilon\Theta_1(x,y) + \cdots + \epsilon^\nu\Theta_\nu(\epsilon x, y) + \cdots$$
$$u_x = u_{xo}(y) + \epsilon u_{\epsilon x1}(\epsilon x, y) + \cdots + \epsilon^\nu u_{x\nu}(\epsilon x, y) + \cdots$$
$$u_y = 0 + \epsilon u_{y1}(\epsilon x, y) + \cdots + \epsilon^\nu u_{y\nu}(\epsilon x, y) + \cdots$$
$$A_{ij} = A_{ij}(y) + \epsilon A_{ij1}(\epsilon x, y) + \cdots + \epsilon^\nu A_{ij\nu}(\epsilon x, y) + \cdots$$
$$h(x) = 1 + \epsilon h_1(\epsilon x) + \cdot\cdot + \epsilon^\nu h_\nu(\epsilon x) + \cdots$$
$$p = p_0(y) + \epsilon p_1(\epsilon x, y) + + \cdots + \epsilon^\nu p_\nu(\epsilon x, y) + \cdots$$

To the leading order:

$O(1)$

$$\frac{\partial^2\Theta_0}{\partial y^2} + \lambda e^{-\beta\Theta_0}\Big(\frac{\partial u_{x0}}{\partial y}\Big)^2 = 0$$
$$-\beta\beta' e^{-\beta\Theta_0}\frac{\partial\Theta_0}{\partial y}\frac{\partial u_{x0}}{\partial y} + \beta' e^{-\beta\Theta_0}\frac{\partial^2 u_{x0}}{\partial y^2} + G\frac{\partial A_{xy0}}{\partial y} + 1 = 0$$
$$-\frac{\partial p_0}{\partial y} + G\frac{\partial A_{yy0}}{\partial y} + \cot\theta = 0$$

$O(\epsilon)$

$$\frac{\partial^2\Theta_1}{\partial y^2} + \lambda e^{-\beta\Theta_0}\left(2\frac{\partial u_{x0}}{\partial y}\frac{\partial u_{x1}}{\partial y} - \beta\Theta_1\Big(\frac{\partial u_{x0}}{\partial y}\Big)^2\right) = \xi u_{y1}\frac{\partial\Theta_0}{\partial y}$$

$$Ru_{y1}\frac{\partial u_{x0}}{\partial y} = -\beta'\beta e^{-\beta\Theta_0}\frac{\partial\Theta_1}{\partial y}\frac{\partial u_{x0}}{\partial y} - \beta\beta' e^{-\beta\Theta_0}\frac{\partial\Theta_0}{\partial y}\frac{\partial u_{x1}}{\partial y}$$
$$+\beta^2\beta' e^{-\beta\Theta_0}\Theta_1\frac{\partial\Theta_0}{\partial y}\frac{\partial u_{x0}}{\partial y} + \beta' e^{-\beta\Theta_0}\frac{\partial^2 u_{x1}}{\partial y^2} - \beta\beta' e^{-\beta\Theta_0}\Theta_1\frac{\partial^2 u_{x0}}{\partial y^2} + G\frac{\partial A_{xy1}}{\partial y}$$

$$-\frac{\partial p_1}{\partial y} - 2\beta\beta' e^{-\beta\Theta_0}\frac{\partial\Theta_0}{\partial y}\frac{\partial u_{y1}}{\partial y} + 2\beta' e^{-\beta\Theta_0}\frac{\partial^2 u_{y1}}{\partial y^2} + G\frac{\partial A_{yy1}}{\partial y} = 0$$

The configuration tensor:

$$
\begin{aligned}
&u_x\frac{\partial A_{xx}}{\partial x}+u_y\frac{\partial A_{xx}}{\partial y}-2\Big(A_{xx}\frac{\partial u_x}{\partial x}+A_{xy}\frac{\partial u_x}{\partial y}\Big)=--\frac{\mu_t}{\mu_p}e^{\beta\Theta}(A_{xx}-1)\\
&\rightarrow\Big(u_{x0}+\epsilon u_{x1}\Big)\epsilon^2\frac{\partial A_{xx1}}{\partial x}+\epsilon u_{y1}\Big(\frac{\partial A_{xx0}}{\partial y}+\epsilon\frac{\partial A_{xx1}}{\partial y}\Big)\\
&-2\bigg((A_{xx0}+\epsilon A_{xx1})\epsilon\frac{\partial u_{x1}}{\partial x}+(\frac{\partial A_{xy0}}{\partial y}+\epsilon A_{xy1})\Big(\frac{\partial u_{x0}}{\partial y}+\epsilon\frac{\partial u_{x1}}{\partial y}\Big)\bigg)\\
&=-\frac{\mu_t}{\mu_p}e^{\beta\Theta_0}(1+\epsilon\beta\Theta_1)(A_{xx0}+\epsilon\frac{\partial A_{xx1}}{\partial x}-1)
\end{aligned}
$$

That leads to:

$$O(1)$$

$$
\begin{aligned}
&2A_{xy0}\frac{\partial u_x}{\partial y}=\frac{\mu_t}{\mu_p}e^{-\beta\Theta_0}(A_{xx0}-1) \qquad A_{xx0}=1+2\Big(\frac{\mu_p}{\mu_t}\Big)^2e^{-2\beta\Theta_0}\Big(\frac{\partial u_{x0}}{\partial y}\Big)^2\\
&A_{yy0}\frac{\partial u_x}{\partial y}=\frac{\mu_t}{\mu_p}e^{-\beta\Theta_0}A_{xy0} \qquad A_{xy0}=\frac{\mu_p}{\mu_t}e^{-\beta\Theta_0}\frac{\partial u_x}{\partial y}\\
&\frac{\mu_t}{\mu_p}e^{-\beta\Theta_0}(A_{yy0}-1)=0 \qquad A_{yy0}=1
\end{aligned}
$$

$$O(\epsilon)$$

$$
\begin{aligned}
&\frac{\partial A_{xx0}}{\partial y}u_{y1}-\frac{\partial u_{y1}}{\partial x}A_{xx0}-2A_{xy1}\frac{\partial u_{x0}}{\partial y}=-\frac{\mu_t}{\mu_p}e^{\beta\Theta_0}\Big(\frac{\partial A_{xx1}}{\partial x}+\beta\Theta_1A_{xx0}-1\Big)\Rightarrow\\
&u_{y1}\bigg(1+2\Big(\frac{\mu_p}{\mu_t}\Big)^2e^{-2\beta\Theta_0}\Big(\frac{\partial u_{x0}}{\partial y}\Big)^2\bigg)-\frac{\partial u_{y1}}{\partial x}\bigg(1+2\Big(\frac{\mu_p}{\mu_t}\Big)^2e^{-2\beta\Theta_0}\Big(\frac{\partial u_{x0}}{\partial y}\Big)^2\bigg)\\
&-2A_{xy1}\frac{\partial u_{x0}}{\partial y}=-\frac{\mu_t}{\mu_p}e^{\beta\Theta_0}\Big(\frac{\partial A_{xx1}}{\partial x}+\beta\Theta_1\Big(1+2\Big(\frac{\mu_p}{\mu_t}\Big)^2e^{-2\beta\Theta_0}\Big(\frac{\partial u_{x0}}{\partial y}\Big)^2\Big)-1\Big)
\end{aligned}
$$

$$u_{y1}\Big(\frac{\mu_t}{\mu_p}e^{-\beta\Theta_0}\frac{\partial u_{x0}}{\partial y}\Big)-\frac{\partial u_{y1}}{\partial y}\Big(\frac{\mu_t}{\mu_p}e^{-\beta\Theta_0}\frac{\partial u_{x0}}{\partial y}\Big)-\frac{\partial u_{x1}}{\partial y}-\frac{\partial u_{x0}}{\partial y}\Big(1-\beta\Theta_1+2\frac{\mu_p}{\mu_t}e^{-\beta\Theta_0}\frac{\partial u_{y1}}{\partial y}\Big)=$$
$$\frac{\mu_t}{\mu_p}e^{\beta\Theta_0}\bigg(A_{xy1}+\beta\Theta_1\Big(\frac{\mu_t}{\mu_p}e^{-\beta\Theta_0}\frac{\partial u_{x0}}{\partial y}\Big)\bigg)$$

$$\frac{\partial A_{xy0}}{\partial y}u_{y1}\quad-\frac{\partial u_{y1}}{\partial y}A_{xy0}\quad-\frac{\partial u_{x1}}{\partial y}A_{yy0}-A_{yy1}\frac{\partial u_{x0}}{\partial y}=\quad\frac{\mu_t}{\mu_p}e^{\beta\Theta_0}\Big(A_{xy1}+\beta\Theta_1A_{xy0}\Big)\Rightarrow$$
$$u_{y1}\frac{\mu_t}{\mu_p}e^{-\beta\Theta_0}\frac{\partial u_{x0}}{\partial y}-\frac{\mu_t}{\mu_p}e^{-\beta\Theta_0}\frac{\partial u_{x0}}{\partial y}\frac{\partial u_{y1}}{\partial y}-\frac{\partial u_{x1}}{\partial y}-\frac{\partial u_{x0}}{\partial y}\Big(1-\beta\Theta_1+2\frac{\mu_p}{\mu_t}e^{-\beta\Theta_0}\frac{\partial u_{y1}}{\partial y}\Big)=$$
$$\frac{\mu_t}{\mu_p}e^{\beta\Theta_0}\Big(A_{xy1}+\beta\Theta_1\frac{\mu_t}{\mu_p}e^{-\beta\Theta_0}\frac{\partial u_{x0}}{\partial y}\Big)$$

$$\frac{\partial A_{yy0}}{\partial y}u_{y1}-2A_{yy0}\frac{\partial u_{y1}}{\partial y}=-\frac{\mu_t}{\mu_p}e^{\beta\Theta_0}\Big(A_{yy1}+\beta\Theta_1A_{yy0}-1\Big)$$
$$\Rightarrow-2\frac{\partial u_{y1}}{\partial y}=-\frac{\mu_t}{\mu_p}e^{\beta\Theta_0}\Big(A_{yy1}+\beta\Theta_1-1\Big)$$

$$\frac{\partial A_{xy0}}{\partial y}u_{y1}\quad-\frac{\partial u_{y1}}{\partial y}A_{xy0}\quad-\frac{\partial u_{x1}}{\partial y}A_{yy0}-A_{yy1}\frac{\partial u_{x0}}{\partial y}=\quad\frac{\mu_t}{\mu_p}e^{\beta\Theta_0}\Big(A_{xy1}+\beta\Theta_1A_{xy0}\Big)\Rightarrow$$
$$\frac{\mu_t}{\mu_p}e^{-\beta\Theta_0}\frac{\partial u_{x0}}{\partial y}u_{y1}-\frac{\partial u_{y1}}{\partial y}\frac{\mu_t}{\mu_p}e^{-\beta\Theta_0}\frac{\partial u_{x0}}{\partial y}-\frac{\partial u_{x1}}{\partial y}-\Big(1-\beta\Theta_1+2\frac{\mu_p}{\mu_t}e^{-\beta\Theta_0}\frac{\partial u_{y1}}{\partial y}\Big)\frac{\partial u_{x0}}{\partial y}=$$
$$\frac{\mu_t}{\mu_p}e^{\beta\Theta_0}\Big(A_{xy1}+\beta\Theta_1\frac{\mu_t}{\mu_p}e^{-\beta\Theta_0}\frac{\partial u_{x0}}{\partial y}\Big)$$

$$\frac{\partial A_{yy0}}{\partial y}u_{y1} - 2A_{yy0}\frac{\partial u_{y1}}{\partial y} = -\frac{\mu_t}{\mu_p}e^{\beta\Theta_0}\Big(A_{yy1} + \beta\Theta_1 A_{yy0} - 1\Big) \Rightarrow$$
$$-2\frac{\partial u_{y1}}{\partial y} = -\frac{\mu_t}{\mu_p}e^{\beta\Theta_0}\Big(A_{yy1} + \beta\Theta_1 - 1\Big)$$

Summarizing the $O(\epsilon)$ is:

$$A_{xx1} = -2\beta\Theta_1\Big(\frac{\mu_p}{\mu_t}\Big)^2 e^{-2\beta\Theta_0}\Big(\frac{\partial u_{x0}}{\partial y}\Big)^2 + 4\Big(\frac{\mu_p}{\mu_t}\Big)^3 e^{-3\beta\Theta_0}\Big(\beta\frac{\partial\Theta_0}{\partial y}\Big(\frac{\partial u_{x0}}{\partial y}\Big)^2 - \frac{\partial u_{x0}}{\partial y}\frac{\partial^2 u_{x0}}{\partial y^2}\Big)u_{y1}$$
$$+ 2\frac{\mu_p}{\mu_t}e^{-\beta\Theta_0}\Big(1 + 2\Big(\frac{\mu_p}{\mu_t}\Big)^2 e^{-2\beta\Theta_0}\Big(\frac{\partial u_{x0}}{\partial y}\Big)^2\Big)\frac{\partial u_{y1}}{\partial x}$$
$$+ 2\frac{\mu_p}{\mu_t}e^{-\beta\Theta_0}\Big(-\beta\Theta_1\frac{\mu_p}{\mu_t}e^{-\beta\Theta_0}\frac{\partial u_{x0}}{\partial y} - \Big(\frac{\mu_p}{\mu_t}\Big)^2 e^{-2\beta\Theta_0}\Big(-\beta\frac{\partial\Theta_0}{\partial y}\frac{\partial u_{x0}}{\partial y} + \frac{\partial^2 u_{x0}}{\partial y^2}\Big)u_{y1}$$
$$+ \Big(\frac{\mu_p}{\mu_t}\Big)^2 e^{-2\beta\Theta_0}\frac{\partial u_{x0}}{\partial y}\frac{\partial u_{y1}}{\partial y} + \frac{\mu_p}{\mu_t}e^{-\beta\Theta_0}\frac{\partial u_{x1}}{\partial y} + 2\Big(\frac{\mu_p}{\mu_t}\Big)^2 e^{-2\beta\Theta_0}\frac{\partial u_{y1}}{\partial y}\frac{\partial u_{x0}}{\partial y}\Big)$$

$$A_{xy1} = -\beta\Theta_1\frac{\mu_p}{\mu_t}e^{-\beta\Theta_0}\frac{\partial u_{x0}}{\partial y} - \Big(\frac{\mu_p}{\mu_t}\Big)^2 e^{-2\beta\Theta_0}\Big(-\beta\frac{\partial\Theta_0}{\partial y}\frac{\partial u_{x0}}{\partial y} + \frac{\partial^2 u_{x0}}{\partial y^2}\Big)u_{y1}$$
$$+ \Big(\frac{\mu_p}{\mu_t}\Big)^2 e^{-2\beta\Theta_0}\frac{\partial u_{x0}}{\partial y}\frac{\partial u_{y1}}{\partial y} + \frac{\mu_p}{\mu_t}e^{-\beta\Theta_0}\frac{\partial u_{x1}}{\partial y} + 2\Big(\frac{\mu_p}{\mu_t}\Big)^2 e^{-2\beta\Theta_0}\frac{\partial u_{y1}}{\partial y}\frac{\partial u_{x0}}{\partial y}$$

$$A_{yy1} = 2\frac{\mu_p}{\mu_t}e^{-\beta\Theta_0}\frac{\partial u_{y1}}{\partial y}$$

As a result of the complexity of the above system, it is reasonable to begin with the Newtonian problem section 5.5. We are going to use the Newtonian results as initial guesses for a iteration numerical method.

A.2.3 Non-uniformly heated plane - Weakly Heating

In this section we consider a weakly heated plane like before. This time we don't use the long wave assumption. Because of the nonlinear behavior of the temperature field equation in (A.2.1.1), (A.2.1.2) and (A.2.1.3), it is convenient to take asymptotic expansions in the dimensionless variables as follow:

$$
\begin{aligned}
&\Theta = \Theta_0(y) + \epsilon\Theta_1(x,y) + \cdots + \epsilon^{\nu}\Theta_{\nu}(x,y) + \cdots \\
&u_x = u_{xo}(y) + \epsilon u_{x1}(x,y) + \cdots + \epsilon^{\nu} u_{x\nu}(x,y) + \cdots \\
&u_y = 0 + \epsilon u_{y1}(x,y) + \cdots + \epsilon^{\nu} u_{y\nu}(x,y) + \cdots \\
&A_{ij} = A_{ij}(y) + \epsilon A_{ij1}(x,y) + \cdots + \epsilon^{\nu} A_{ij\nu} + \cdots \\
&S(x) = 1 + \epsilon h_1(x) + \cdot\cdot + \epsilon^{\nu} h_{\nu}(x) + \cdots \\
&p = p_0(y) + \epsilon p_1(x,y) + + \cdots + \epsilon^{\nu} p_{\nu}(x,y) + \cdots
\end{aligned}
$$

So the governing equations become:

Energy

$$
\begin{aligned}
&\epsilon\frac{\partial^2\Theta_1}{\partial x^2} + \frac{\partial^2\Theta_0}{\partial y^2} + \epsilon\frac{\partial^2\Theta_1}{\partial y^2} + \lambda e^{-\beta(\Theta_0+\epsilon\Theta_1)}\left(2\epsilon^2\Big(\frac{\partial u_{x1}}{\partial x}\Big)^2\right. \\
&\left. + \Big(\epsilon\frac{\partial u_{y1}}{\partial x} + \frac{\partial u_{x0}}{\partial y} + \epsilon\frac{\partial u_{x1}}{\partial y}\Big)^2 + 2\epsilon^2\Big(\frac{\partial u_{y1}}{\partial y}\Big)^2\right) = \\
&\xi\Big(\epsilon u_{x0}\frac{\partial\Theta_1}{\partial x} + \epsilon^2 u_{x1} + \epsilon u_{y1}\frac{\partial\Theta_0}{\partial y} + \epsilon^2 u_{y1}\frac{\partial\Theta_1}{\partial y}\Big)
\end{aligned}
$$

Similarly for the other equations and summarizing to the leading order:

O(1):

$$\frac{\partial^2\Theta_0}{\partial y^2} + \lambda e^{-\beta\Theta_0}\Big(\frac{u_{x0}}{\partial y}\Big)^2 = 0$$
$$-\beta'\beta e^{-\beta\Theta_0}\frac{\partial\Theta_0}{\partial y}\frac{\partial u_{x0}}{\partial y} + \beta' e^{-\beta\Theta_0}\frac{\partial^2 u_{x0}}{\partial y^2} + G\frac{\partial A_{xy0}}{\partial y} + 1 = 0$$
$$-\frac{\partial p_0}{\partial y} + G\frac{\partial A_{yy0}}{\partial y} + \cot\theta = 0$$

O(ϵ):

$$\frac{\partial^2\Theta_1}{\partial x^2} + \frac{\partial^2\Theta_1}{\partial y^2} + \lambda e^{-\beta\Theta_0}\Big(2\Big(\frac{\partial u_{y1}}{\partial x}\frac{\partial u_{x0}}{\partial y} + \frac{\partial u_{x0}}{\partial y}\frac{\partial u_{x1}}{\partial y}\Big) - \beta\Theta_1\Big(\frac{\partial u_{x0}}{\partial y}\Big)^2\Big) = \xi\Big(\frac{\partial u_x}{\partial t}\frac{\partial\Theta_1}{\partial x} + u_{y1}\frac{\partial\Theta_0}{\partial y}\Big)$$

$$R\Big(u_{x0}\frac{\partial u_{x1}}{\partial x} + u_{y1}\frac{\partial u_{x0}}{\partial y}\Big) = -\frac{\partial p_1}{\partial x} + 2\beta' e^{-\beta\Theta_0}\frac{\partial^2 u_{x1}}{\partial x^2} + G_0\frac{\partial A_{xx1}}{\partial x}$$
$$-\beta\beta' e^{-\beta\Theta_0}\Big(\frac{\partial\Theta_0}{\partial y}\Big(\frac{\partial u_{y1}}{\partial x} + \frac{\partial u_{x1}}{\partial y}\Big) - \beta\Theta_1\frac{\partial\Theta_0}{\partial y}\frac{\partial u_{x0}}{\partial y} + \frac{\partial\Theta_1}{\partial y}\frac{\partial u_{x0}}{\partial y}\Big)$$
$$+\beta' e^{-\beta\Theta_0}\Big(\frac{\partial^2 u_{y1}}{\partial y\partial x} + \frac{\partial^2 u_{x1}}{\partial y^2} - \beta\Theta_1\frac{\partial^2 u_{x0}}{\partial y^2}\Big) + G\frac{\partial A_{xy1}}{\partial y}$$

$$Ru_{x0}\frac{\partial u_{y1}}{\partial x} = \beta\beta' e^{-\beta\Theta_0}\frac{\partial u_{x0}}{\partial y}\frac{\partial\Theta_1}{\partial y} + \beta' e^{-\beta\Theta_0}\Big(\frac{\partial^2 u_{x1}}{\partial x\partial y} + \frac{\partial^2 u_{y1}}{\partial x^2}\Big) + G_0\frac{\partial A_{xy1}}{\partial x} - \frac{\partial p_1}{\partial y}$$
$$-2\beta\beta' e^{-\beta\Theta_0}\frac{\partial\Theta_0}{\partial y}\frac{\partial u_{y1}}{\partial y} + 2\beta' e^{-\beta\Theta_0}\frac{\partial^2 u_{x1}}{\partial y^2} + G\frac{\partial A_{yy1}}{\partial y}$$

$$u_x\frac{\partial A_{xx}}{\partial x}+u_y\frac{\partial A_{xx}}{\partial y}-2\Big(A_{xx}\frac{\partial u_x}{\partial x}+A_{xy}\frac{\partial u_x}{\partial y}\Big)=--\frac{\mu_t}{\mu_p}e^{\beta\Theta}(A_{xx}-1)$$
$$\rightarrow\Big(u_{x0}+\epsilon u_{x1}\Big)\epsilon^2\frac{\partial A_{xx1}}{\partial x}+\epsilon u_{y1}\Big(\frac{\partial A_{xx0}}{\partial y}+\epsilon\frac{\partial A_{xx1}}{\partial y}\Big)-2\Bigg((A_{xx0}+\epsilon A_{xx1})\epsilon\frac{\partial u_{x1}}{\partial x}$$
$$+(\frac{\partial A_{xy0}}{\partial y}+\epsilon A_{xy1})\Big(\frac{\partial u_{x0}}{\partial y}+\epsilon\frac{\partial u_{x1}}{\partial y}\Big)\Bigg)=-\frac{\mu_t}{\mu_p}e^{\beta\Theta_0}(1+\epsilon\beta\Theta_1)(A_{xx0}+\epsilon\frac{\partial A_{xx1}}{\partial x}-1)$$

That leads to:

$$O(1)$$

$$2A_{xy0}\frac{\partial u_x}{\partial y}=\frac{\mu_t}{\mu_p}e^{-\beta\Theta_0}(A_{xx0}-1)\qquad A_{xx0}=1+2\Big(\frac{\mu_p}{\mu_t}\Big)^2e^{-2\beta\Theta_0}\Big(\frac{\partial u_{x0}}{\partial y}\Big)^2$$
$$A_{yy0}\frac{\partial u_x}{\partial y}=\frac{\mu_t}{\mu_p}e^{-\beta\Theta_0}A_{xy0}\qquad A_{xy0}=\frac{\mu_p}{\mu_t}e^{-\beta\Theta_0}\frac{\partial u_x}{\partial y}$$
$$\frac{\mu_t}{\mu_p}e^{-\beta\Theta_0}(A_{yy0}-1)=0\qquad A_{yy0}=1$$

$$O(\epsilon)$$

$$u_{x0}\frac{\partial A_{xx1}}{\partial x}+u_{y1}\frac{\partial A_{xx0}}{\partial y}-2A_{xx0}\frac{\partial u_{x1}}{\partial x}-2A_{xy1}\frac{\partial u_{x0}}{\partial y}-2A_{xy0}\frac{\partial u_{x1}}{\partial y}=$$
$$-\frac{\mu_t}{\mu_p}e^{\beta\Theta_0}\Big(A_{xx1}+\beta\Theta_1(A_{xx0}-1)\Big)$$

$$u_{x0}\frac{\partial A_{xy1}}{\partial x}+u_{y1}\frac{\partial A_{xy0}}{\partial y}-A_{xx0}\frac{\partial u_{y1}}{\partial x}-A_{xy0}\frac{\partial u_{y1}}{\partial y}-A_{xy0}\Big(\frac{\partial u_{x1}}{\partial x}\frac{\partial u_{y1}}{\partial y}\Big)$$
$$-A_{yy0}\frac{\partial u_{x1}}{\partial y}-A_{yy1}\frac{\partial u_{x0}}{\partial y}=-\frac{\mu_t}{\mu_p}e^{\beta\Theta_0}\Big(A_{xy1}+\beta\Theta_1 A_{xy0}\Big)$$

$$u_{x0}\frac{\partial A_{yy1}}{\partial x}+u_{y1}\frac{\partial A_{yy0}}{\partial y}-2A_{xy0}\frac{\partial u_{y1}}{\partial x}-1A_{yy0}\frac{\partial u_{y1}}{\partial y}=-\frac{\mu_t}{\mu_p}e^{\beta\Theta_0}\Big(A_{yy1}-\epsilon\beta\Theta_1(A_{yy0}-1)\Big)$$

Summarizing, we have:

$$O(\epsilon)$$

$$u_{x0}\frac{\partial A_{xx1}}{\partial x}+u_{y1}\bigg(-4\Big(\frac{\mu_p}{\mu_t}\Big)^2e^{-2\beta\Theta_0}\Big(\beta\frac{\partial\Theta_0}{\partial y}\Big(\frac{\partial u_{x0}}{\partial y}\Big)^2\Big)-\frac{\partial u_{x0}}{\partial y}\frac{\partial^2u_{x0}}{\partial y^2}\bigg)\frac{\partial u_{y1}}{\partial x}$$
$$-2A_{xy1}\frac{\partial u_{x0}}{\partial y}-2\beta e^{-\beta\Theta_0}\frac{\mu_p}{\mu_t}\frac{\partial u_{x0}}{\partial y}\frac{\partial u_{x1}}{\partial y}=-\frac{\mu_t}{\mu_p}e^{\beta\Theta_0}\bigg(A_{xx1}+2\beta\Theta_1\Big(\frac{\mu_p}{\mu_t}\Big)^2e^{-2\beta\Theta_0}\Big(\frac{\partial u_{x0}}{\partial y}\Big)^2\bigg)$$

$$u_{x0}\frac{\partial A_{xy1}}{\partial x}+u_{y1}\frac{\mu_p}{\mu_t}e^{-\beta\Theta_0}\frac{\partial u_{x0}}{\partial y}e^{-\beta\Theta_0}\Big(-\beta\frac{\partial\Theta_0}{\partial y}\frac{\partial u_{x0}}{\partial y}+\frac{\partial^2u_{x0}}{\partial y^2}\Big)$$
$$-\bigg(1+2\Big(\frac{\mu_p}{\mu_t}\Big)^2e^{-2\beta\Theta_0}\Big(\frac{\partial u_{x0}}{\partial y}\Big)^2\bigg)\frac{\partial u_{y1}}{\partial x}-\frac{\mu_p}{\mu_t}e^{-\beta\Theta_0}\frac{\partial u_{x0}}{\partial y}\Big(\frac{\partial u_{x1}}{\partial x}+\frac{\partial u_{y1}}{\partial y}\Big)$$
$$\frac{\partial u_{x1}}{\partial y}-A_{yy1}\frac{\partial u_{x0}}{\partial y}=-\frac{\mu_t}{\mu_p}e^{\beta\Theta_0}\Big(A_{xy1}+\beta\Theta_1\frac{\mu_p}{\mu_t}e^{-\beta\Theta_0}\frac{\partial u_{x0}}{\partial y}\Big)$$

$$\frac{\partial A_{yy1}}{\partial x}u_{x0}+A_{yy1}\frac{\mu_t}{\mu_p}e^{\beta\Theta_0}-2\Big(\frac{\mu_p}{\mu_t}e^{-\beta\Theta_0}\frac{\partial u_{x0}}{\partial y}\frac{\partial u_{y1}}{\partial x}+\frac{\partial u_{y1}}{\partial y}\Big)=0$$

As a result of the complexity of the above system, it is reasonable to begin with the Newtonian problem as it will simplify the elastic terms, and then consider the non-Newtonian. The Newtonian problem is the subject of study of the section 5.8.